Democratic and People's Republic of Algeria
Ministry of Higher Education and Scientific Research
Abbes Laghrour University of Khenchela
Faculty of Science and Technology
Department of Science of Matter

Thesis

Presented to Obtain a Doctoral Degree in Chemistry

Specialty: Physical Chemistry

By:

Rim Imen

Entitled:

Improving the effectiveness of clay minerals for the removal of heavy metals

Graduation Committee:

Messai Amel	**Prof**	**Abbes Laghrour Khenchela University**	**President**
Hezil Naouel	**Prof**	**Abbes Laghrour Khenchela University**	**Superviser**
Fellah Mamoun	**Prof**	**Abbes Laghrour Khenchela University**	**Co-superviser**
Farh Hichem	**Prof**	**Larbi Ben M'hidi University of Oum Bouaghi**	**Reviewer**
Bouakkadia Amel	**Dr**	**Abbes Laghrour Khenchela University**	**Reviewer**
Benmahdi Fatiha	**Dr**	**Hadj Lakhdar University of Batna 1**	**Reviewer**

2024/2025

DEDICATE

I dedicate this dissertation to my dear father, who has always been my greatest source of inspiration, strength, and unwavering support throughout this academic journey. His boundless encouragement and unconditional love have been the driving force behind my perseverance, and his kind words have been a guiding light in moments of doubt and exhaustion. He never hesitated to give, never wavered in his support, and always stood by my side with his presence, wisdom, and prayers. For all this and so much more, I extend my deepest gratitude, appreciation, and love. I pray that Allah blesses him with good health, grants him a long and fulfilling life, and rewards him abundantly for all the sacrifices he has made for me.

I also dedicate this dissertation to my beloved mother, the heart that beats with love and kindness, and the soul that has given me strength and patience through every stage of my life. She has always been by my side, supporting me with her love, praying for me every step of the way, and surrounding me with her endless care and generosity. She endured hardships and sleepless nights for my sake, becoming the light that guided me, my pillar in times of weakness, and my refuge in moments of struggle. No words can truly express my gratitude, but from the depths of my heart, I pray that Allah blesses her with a long and healthy life, grants her endless happiness, and rewards her abundantly for all the sacrifices she has made for me.

I dedicate this dissertation to my beloved husband, my life partner and unwavering support, who has been my strength in the most challenging times. He has been my rock when I felt exhausted, the hand that lifted me in moments of doubt, and the voice that always reassured me that I could overcome any obstacle. His support was never just words—it was a constant presence, an unshakable belief in me that gave me the determination to move forward. I am deeply grateful for his patience, understanding, and the countless ways he stood by my side throughout this journey. I pray that Allah protects him, blesses his life and work, and grants him happiness and success, just as he has always been a source of joy and strength for me.

And finally, I dedicate this dissertation to my dear sisters, my lifelong companions, and cherished confidantes, who have always stood by my side with their unconditional love and unwavering support. They have been my source of joy, my strength, and a guiding light in difficult times. With them, I have never felt alone; instead, I have always been surrounded by love and encouragement that gave me the strength to keep going. From the depths of my heart, I thank them for every word of support and every moment of joy we have shared. I pray that Allah protects them, blesses their lives, and grants them happiness and success in every step they take.

ACKNOWLEDGMENTS

At the end of this thesis, I would like to take a moment to express my deepest gratitude to **Allah** Almighty, who granted me the strength, determination, and patience to overcome all the challenges I faced throughout the journey of completing this dissertation. Without His guidance, I would not have been able to keep striving despite the obstacles.

I would like to extend my deepest gratitude, utmost appreciation, and sincere thanks to my esteemed supervisor, **Professor HEZIL Naouel**, who has been a guiding light throughout this academic journey. She has given me her time, effort, and wisdom without hesitation, serving as both a mentor and an academic mother, always ensuring my success and pushing me to achieve my best. Words fall short of expressing my gratitude, but I will always hold her in the highest regard and pray for her continued success and well-being as a token of my appreciation.

My heartfelt gratitude also goes to my co-supervisor, **Professor FELLAH Mamoun**, for his invaluable support and insightful guidance, which played a crucial role in the completion of this thesis. He has been a true example of a dedicated professor, always generous with his knowledge and expertise, and ever willing to provide advice and direction with patience and care. I am truly grateful for his efforts, and I wish him continued success and prosperity.

I extend my sincere gratitude to the members of the Jury, Professor **Messai Amel**, Doctor **Bouakkadia Amel**, Doctor **Benmahdi Fatiha**, and Professor **Farh Hichem**, for their valuable time, insightful feedback, and constructive guidance, which have greatly contributed to enriching this dissertation. Their contributions were instrumental in enhancing the quality of this work, and I truly appreciate their efforts in evaluating it with such precision and objectivity.

Finally, I am deeply grateful to every teacher who has guided me, from my very first letter to the completion of this dissertation. To all those who played a role in my education, from my early school days to my university years, I sincerely thank you for your efforts, your knowledge, and your unwavering support. May Allah bless those who are still with us and grant His infinite mercy to those who have departed, making their knowledge a lasting source of light and a continuous charity for them.

ABSTRACT

The discharge of heavy metals into the environment represents a significant threat to ecosystems and human health. Among the available strategies, adsorption is widely considered to be the most promising due to its clarity, affordability, and high efficiency in eliminating metal ions, even in small amounts.

The objective of this thesis is to enhance the adsorbent capacity of kaolin-type (from Guelma, east of Algeria) clays through chemical means, with the subsequent intention of utilizing these materials to remove heavy metals from an aqueous phase.

The initial modification entailed the use of diphenylamine to synthesize DPA-Kaolin, with the objective of efficiently removing lead (II) and copper (II) from aqueous solutions. The subsequent modification involved the modification of kaolin with surfactants (SLS, SDBS, and their mixture), with the aim of efficiently removing mercury (II) from aqueous solutions.

The characterization of the samples was conducted through a range of analytical methodologies, encompassing X-ray diffraction (XRD) and Fourier-transform infrared spectroscopy (FTIR) to ascertain their structural composition. In addition, scanning electron microscopy (SEM), energy dispersive X-ray (EDX) and Brunauer-Emmett-Teller (BET) analysis were employed to determine their morphological characteristics.

The findings showed an increase in the BET specific surface area of kaolin by nearly 25% (from 66.69 $m^2.g^{-1}$ to 71.35 $m^2.g^{-1}$) after DPA modification, and this increase demonstrated significantly greater maximum adsorption capacities for Pb(II) and Cu(II) on DPA-kaolin than on Nat-kaolin, with values of 151 $\mu mol.g^{-1}$ and 134 $\mu mol.g^{-1}$, respectively, suggesting an enhanced adsorption capacity, which confirmed the successful modification of kaolin using DPA.

Conversely, the specific surface area of kaolin increased significantly with the addition of surfactants, reaching 38.3%, 31.9%, and 17.5% for K-SLS, K-SDBS, and K-M, respectively. This finding indicates that the mercury adsorption capacity of kaolin modified with anionic surfactant SLS surpasses that of kaolin modified with a mixture of surfactants (SLS+SDBS) and finally kaolin modified with anionic surfactant SDBS. The corresponding values for mercury adsorption capacity were determined to be 17.77$mg.g^{-1}$, 15.77$mg.g^{-1}$, and 13.45 $mg.g^{1}$, respectively.

Keywords: *Kaolin; Surfactants; heavy metals; Water treatment; Adsorption; Chemical modification.*

RESUME

Le rejet de métaux lourds dans l'environnement représente une menace importante pour les écosystèmes et la santé humaine. Parmi les stratégies disponibles, l'adsorption est largement considérée comme la plus prometteuse en raison de sa clarté, de son coût abordable et de sa grande efficacité dans l'élimination des ions métalliques, même en petites quantités.

L'objectif de cette thèse est d'améliorer la capacité d'adsorption des argiles de type kaolin (de Guelma, à l'est de l'Algérie) par des moyens chimiques, avec l'intention ultérieure d'utiliser ces matériaux pour éliminer les métaux lourds d'une phase aqueuse.

La première modification a consisté à utiliser de la diphénylamine pour synthétiser le DPA-Kaolin, dans le but d'éliminer efficacement le plomb (II) et le cuivre (II) des solutions aqueuses. La modification suivante a consisté à modifier le kaolin avec des surfactants (SLS, SDBS et leur mélange), dans le but d'éliminer efficacement le mercure (II) des solutions aqueuses.

La caractérisation des échantillons a été effectuée à l'aide d'une série de méthodologies analytiques, comprenant la diffraction des rayons X (XRD) et la spectroscopie infrarouge à transformée de Fourier (FTIR) pour vérifier leur composition structurelle. En outre, la microscopie électronique à balayage (MEB), les rayons X à dispersion d'énergie (EDX) et l'analyse Brunauer-Emmett-Teller (BET) ont été utilisés pour déterminer leurs caractéristiques morphologiques.

Les résultats ont montré une augmentation de la surface spécifique BET du kaolin de près de 25 % (de 66,69 $m^2.g^{-1}$ à 71,35 $m^2.g^{-1}$) après modification par DPA, et cette augmentation a démontré des capacités maximales d'adsorption de Pb(II) et Cu(II) significativement plus importantes sur le kaolin DPA que sur le kaolin Nat, avec des valeurs de 151 $\mu mol.g^{-1}$ et 134 $\mu mol.g^{-1}$, respectivement, suggérant une capacité d'adsorption améliorée, ce qui a confirmé la réussite de la modification du kaolin par DPA.

Inversement, la surface spécifique du kaolin a augmenté de manière significative avec l'ajout de tensioactifs, atteignant 38,3 %, 31,9 % et 17,5 % pour K-SLS, K-SDBS et K-M, respectivement. Cette constatation indique que la capacité d'adsorption du mercure du kaolin modifié avec le tensioactif anionique SLS dépasse celle du kaolin modifié avec un mélange de tensioactifs (SLS+SDBS) et enfin celle du kaolin modifié avec le tensioactif anionique SDBS. Les valeurs correspondantes pour la capacité d'adsorption du mercure ont été déterminées comme étant respectivement de 17,77 $mg.g^{-1}$, 15,77 $mg.g^{-1}$, et 13,45 $mg.g^{-1}$.

***Mots-clés** : Kaolin ; Surfactants ; métaux lourds ; Traitement de l'eau ; Adsorption ; Modification chimique.*

ملخص

يمثل رمي المعادن الثقيلة في البيئة تهديداً كبيراً للنظم الإيكولوجية وصحة الإنسان. ومن بين الاستراتيجيات المتاحة، يُعتبر الامتزاز على نطاق واسع أكثر الاستراتيجيات الواعدة نظرًا لوضوحه وقدرته على تحمل التكاليف وكفاءته العالية في إزالة أيونات المعادن حتى بكميات صغيرة.

الهدف من هذه الأطروحة هو تحسين قدرة امتزاز الطين من نوع الكاولين (من قالمة في شرق الجزائر) بالوسائل الكيميائية، بهدف استخدام هذه المواد لإزالة المعادن الثقيلة من الوسط اللمائي.

تم إجراء التعديل الأول باستخدام ثنائي الفينيل أمين (DPA) لإنشاء كاولين DPAبهدف إزالة أيونات الرصاص(II)والنحاس (II)بكفاءة من المحاليل المائية، بينما تم تعديل الكاولين في التجربة الثانية باستخدام مواد خافضة للتوتر السطحي (SLS، SDBS، SLS+SDBS) لإزالة أيونات الزئبق (II) بكفاءة.

تمت دراسة جميع العينات باستخدام طرق تحليلية مختلفة، بما في ذلك حيود الأشعة السينية (XRD) وقياس الطيف بالأشعة تحت الحمراء (FTIR)لتحديد البنية التركيبية، بالإضافة إلى الفحص المجهري الإلكتروني الماسح(SEM) ، وتحليل الأشعة السينية المشتتة للطاقة(EDX) ، وتحليل برونور-إيميت-تيلر (BET) لدراسة البنية السطحية والمورفولوجية.

أظهرت النتائج زيادة في المساحة السطحية النوعية للكاولين بنسبة تقارب 25% بعد التعديل بـ DPA (من 66.69 م²/غ إلى 71.35 م²/غ)، مما أدى إلى ارتفاع ملحوظ في سعات الامتصاص القصوى لأيونات الرصاص (II) والنحاس (II) على كاولين المعدل بـ DPAمقارنة بالكاولين الطبيعي، حيث بلغت القيم 151 ميكرومول/غ و134 ميكرومول/غ على التوالي، مما يشير إلى زيادة قدرة الامتصاص وهو ما يؤكد نجاح تعديل الكاولين باستخدام.DPA

من ناحية أخرى، ازدادت المساحة السطحية النوعية للكاولين بشكل ملحوظ مع إضافة المواد الخافضة للتوتر السطحي، حيث بلغت الزيادة 38.3% و31.9% و17.5% لكل من كاولين المعدل بـSLS، كاولين المعدل بـSDBS، كاولين المعدل بـ (SLS+SDBS) على التوالي. مما أدى إلى ارتفاع امتصاص الزئبق في الكاولين المعدل بالمادة الخافضة للتوتر السطحي الأيونية SLS أكثر من الكاولين المعدل بمزيج (SLS+SDBS)، وأخيرًا الكاولين المعدل بالمادة الخافضة للتوتر السطحي الأيونية SDBS ، حيث بلغت القيم 17.77، 15.77، و13.45 ملغ/غ على التوالي.

الكلمات المفتاحية :الكاولين؛ المواد الخافضة للتوتر السطحي؛ المعادن الثقيلة؛ معالجة المياه؛ الامتصاص؛ التعديل الكيميائي.

TABLE OF CONTENT

LIST OF TABLES

CHAPTER I

CHAPTER II

CHAPTER III

CHAPTER IV

LIST OF FIGURES

CHAPTER I

CHAPTER II

CHAPTER III

CHAPTER IV

LIST OF ABBREVIATIONS

Pb:	Lead
Cu:	Copper
Hg:	Mercury
SEM:	Scanning electron microscopy
EDS:	Energy dispersive spectroscopy
XRD:	X-ray diffraction
FTIR:	Fourier Transform Infrared Spectroscopy
TGA:	Gravitational Thermal Analysis
BET:	Brunauer-Emmett-Teller method
DPA:	Diphenylamine
SLS:	Sodium Lauryl Sulfate
SDBS:	Sodium Dodecyl Benzene Sulfonate
HTDMA:	Hexadecyl Trimethyl Ammonium bromide
DTAC:	Dodecyl Trimethyl Ammonium Chloride
Cr:	Chromium
Cd:	Cadmium
Ni:	Nickel
O:	Oxygen
Si:	Silicon
Mg:	Magnesium
Al:	Aluminium
Na:	Sodium
Ca:	Calcium
K:	potassium
pH:	Hydrogen Potential
CEC:	Cationic Exchange Capacity

SSA: Specific Surface Area

Q_{ads}: Amount of adsorption

C_e: Equilibrium concentration of solute

C_i: Initial concentration of solute

V: Volume of solute

m: Masse of adsorbent

K_F: Freundlich constant

1/n: Freundlich constant that reflects adsorption intensity

Q_m: Maximum adsorption capacity

K_L: Langmuir constant

R_L: Dimensionless separation factor

Q_s: The highest possible adsorption level

K_s: Sips constant

n_s: The constant related to the heterogeneity of adsorbent without unit.

R: The universal constant of perfect gas

T: Temperature

K_T: The equilibrium binding constant

Q_t: Amount adsorbed at time t

Q_e: Equilibrium adsorbed amount

K_1: First order speed constant

K_2: Second order speed constant

K_{ID}: The interparticle diffusion constant

ΔG: Gibbs free energy

ΔH: Enthalpy Variation

ΔS: Entropy Variation

WHO: World Health Organization

IARC: International Agency for Research on Cancer

MCL: The Maximum Contaminant Level

EPA: Environmental Protection Agency

S_{BET}: BET surface area

v_m: monolayer volume

s: Surface area occupied by an adsorbate molecule

N: Avogadro number

V: The molar volume of the adsorbate gas

m: masse of the sample

P: Pressure

P_0 : Saturation pressure at the adsorption temperature.

C: BET constant.

Nat: Natural

d_{hkl}: The interplanar distance

θ: The diffraction angle

n: The order of reflection

λ: Wavelength of radiation used

DTA: Differential Thermal Analysis

C°: Celsius

NaOH: Sodium hydroxide

HCl: Hydrochloric acid

$HgSO_4$: Mercuric sulfate

CMC: The Critical Micelle Concentration

C: Carbon

N: Nitrogen

Q: Quartz

M:	Mica
ICCD:	International Centre for Diffraction Data
Å:	Angström
CTAB:	Cetyl Trimethyl Ammonium bromide
IUPAC:	International Union of Pure and Applied Chemistry's
OH:	Hydroxide
N_2:	Nitrogen gas
R^2:	The correlation coefficients
PFO:	Pseudo-First-Order
PSO:	Pseudo-Second-Order

GENERAL INTRODUCTION

GENERAL INTRODUCTION

Water is the quintessence of life, an irreplaceable resource that supports the survival and well-being of all living organisms on Earth. It is the primary component of cells, making up 60-70% of the human body, and is essential for physiological processes such as digestion, nutrient transport, temperature regulation, and the elimination of toxins. For plants, water facilitates photosynthesis and nutrient absorption, forming the basis of all terrestrial and aquatic ecosystems [1, 2].

Beyond its biological role, water sustains communities and economies; it is crucial for agriculture (providing irrigation for crops that feed billions of people), for industry (powering it, driving energy production), and for sanitation and public health (in fact, access to clean water is directly linked to improved living standards and reduced mortality rates worldwide [3].

The accelerated processes of industrialization and urbanization that are characteristic of modern society have resulted in the pervasive contamination of water resources by heavy metals, thereby posing a considerable threat to ecosystems and human health. Among the most hazardous pollutants are lead (Pb), copper (Cu), and mercury (Hg), which are characterized by their non-degradable nature and bioaccumulative potential [4, 5]. The elimination of such pollutants poses a considerable challenge, and the effective remediation of this critical issue necessitates the development of efficient, cost-effective, and sustainable technologies. Adsorption has emerged as a promising method for heavy metal removal, offering advantages such as simplicity, scalability, and the ability to utilize natural or modified adsorbents [6].

Kaolin, a naturally occurring aluminosilicates clay mineral, has attracted attention as a potential adsorbent due to its abundance, low cost, and inherent ion-exchange properties. Nevertheless, the adsorption capacity of raw kaolin is frequently constrained by its surface area, porosity, and chemical reactivity [7, 8]. In order to overcome these limitations, chemical modifications such as surfactant intercalation and organic molecule modification have been explored with a view to enhancing its physicochemical properties [9, 10].

The objective of this research endeavor is twofold: firstly, to devise a novel adsorbent, modified with diphenylamine, derived from kaolin and treated with acid, for the efficient

removal of Pb(II) and Cu(II) from aqueous solutions; and secondly, to enhance the efficiency of kaolin using two surfactants and their mixture for the removal of Hg(II) from wastewater. This thesis is organized into five chapters:

The initial chapter comprises a bibliographic study. This study commences with a review of fundamental notions of clay minerals, including their chemical composition, structural properties, classification, and industrial applications. It then progresses to a discussion of heavy metals, addressing their sources, applications, and toxicities. The chapter concludes with an examination of the phenomenon of adsorption, encompassing its definition, types, influencing factors, and practical applications.

The second chapter details the experimental methods employed for the characterization of clay minerals (kaolin) such as: scanning electron microscopy (SEM), energy-dispersive X-ray spectroscopy (EDX), X-ray diffraction (XRD), Fourier-transform infrared spectroscopy (FTIR), thermogravimetric and differential thermal analyses (ATG), and Brunauer-Emmett-Teller (BET) analysis.

The third chapter of this study presents the adsorption capacities of natural kaolin (Nat-kaolin) and modified kaolin (DPA-kaolin) for the removal of lead (Pb) and copper (Cu) ions from aqueous solutions. Furthermore, a comprehensive analysis of the kinetics, thermodynamics, isothermal absorption lines, and adsorption mechanisms of Pb(II) and Cu(II) on both types of kaolin is conducted. The study places particular emphasis on understanding how diphenylamine alteration affects adsorption efficiency and the impact of factors including temperature, pH, contact time, and metal ion concentration.

The fourth chapter focuses on the detailed characterization of natural kaolin (K) and its modifications using two anionic surfactants, sodium lauryl sulfate (SLS) and sodium Dodecylbenzene sulfonate (SDBS), as well as their mixture (K-M). A range of analytical techniques have been employed to evaluate the structural, thermal, and textural properties of these kaolin samples. Contact time analysis, adsorption kinetics, and equilibrium models, employing Langmuir, Freundlich, and Sips models.

Finally, we will end with a general conclusion and the perspectives to give to this work.

REFERENCES

[1] Khilchevskyi, V., & Karamushka, V. (2021). Global Water Resources: distribution and demand. In Encyclopedia of the UN sustainable development goals (pp. 1–11). https://doi.org/10.1007/978-3-319-70061-8_101-1.

[2] Maduelosi, J. N., & Ezuluofor, M. U. (2023). Education as a vaccine against girl child bullying. British Journal of Multidisciplinary and Advanced Studies, 4(3), 1–8. https://doi.org/10.37745/bjmas.2022.0207.

[3] Knorr, D., & Augustin, M. A. (2023). Vanishing Water: Rescuing the neglected food resource. Food Engineering Reviews, 15(4), 609–624. https://doi.org/10.1007/s12393-023-09349-z.

[4] Zhang, P., Yang, M., Lan, J., Huang, Y., Zhang, J., Huang, S., Yang, Y., & Ru, J. (2023). Water quality degradation due to Heavy metal contamination: Health impacts and Eco-Friendly Approaches for Heavy Metal Remediation. Toxics, 11(10), 828. https://doi.org/10.3390/toxics11100828.

[5] Jadaa, W., & Mohammed, H. (2023). Heavy Metals – Definition, Natural and Anthropogenic Sources of Releasing into Ecosystems, Toxicity, and Removal Methods – An Overview Study. Journal of Ecological Engineering, 24(6), 249–271. https://doi.org/10.12911/22998993/162955.

[6] Chai, W.S., Cheun, J.Y., Kumar, P.S., Mubashir, M., Majeed, Z., Banat, F., Ho, S., & Show, P.L. (2021). A review on conventional and novel materials towards heavy metal adsorption in wastewater treatment application. Journal of Cleaner Production. 296, 126589.

[7] Anam, A., Gamit, N., Prajapati, V., & Dholakiya, B. Z. (2023). An overview of kaolin and its potential application in thermosetting polymers. Materials Today Communications, 36, 106827. https://doi.org/10.1016/j.mtcomm.2023.106827.

[8] Ochieng, O. (2016). Characterization and classification of clay minerals for potential applications in Rugi Ward, Kenya. African Journal of Environmental Science and Technology, 10(11), 415–431. https://doi.org/10.5897/ajest2016.2184.

[9] Putra, A., hwati, Z., Syahyadi, R., Rihaya, T., & Aidy, N. (2021). Removal of Hg(II) metal ions using kaolin adsorbents modified with anionic surfactant and efficient ultrasonic assisted. International Journal of Research –Granthaalayah. 9, 72-84. https://doi.org/10.29121/granthaalayah.v9.i11.2021.4379.

[10] Liang, X., Li, Q., & Fang, Y. (2023). Preparation and characterization of modified kaolin by a mechanochemical method. Materials, 16(8), 3099. https://doi.org/10.3390/ma16083099.

LITERATURE REVIEW

Kaolin clay has attracted considerable attention for applications in water purification due to its abundance and affordability. However, the effectiveness of kaolin in adsorbing contaminants is limited by its relatively small surface area and cation exchange capacity. Previous studies have indicated that these restrictions can be overcome by alterations including thermal treatment, chemical modification, acid activation, cation exchange, etc…to enhance the adsorption properties of the clay mineral (Kaolin).

For instance, when *Dinh et al.*, [1] created HTDMA-modified Bentonite clay to effectively remove Pb (II) from the aqueous solution. According to the Langmuir model, the maximum adsorption capacity of this modified clay was approximately 36.5% higher than the value obtained for the unmodified sample.

In another study reported by *Hezil et al.*, [2] where they employed modified kaolin with dodecyl trimethyl ammonium chloride (DTAC) to adsorb Cr (VI) in water, they discovered that the adsorption capacity increased from 48.75 m^2/g to 63.7 m^2/g.

One effective way to increase kaolin's adsorption and cation exchange capacity was to activate it with Humic acid *Al-Essa and Khalili.*, [3] discovered that whereas modified kaolin clay adsorbed roughly 22 mg/g of Cd (II), or nearly twenty times more than that of natural clay, it was only 1 mg/g of Cd (II) was adsorbed by natural clay. Following chemical treatment with sulfuric acid.

Chai et al., [4] observed an increase of 84.58% in the specific surface area and a rise of 3.57% in the pore volume of Malaysian kaolin clay after the treatment.

Belachew and Hinsene., [5] observed that the removal of Cr (VI) from aqueous solution reached 99% after the modification of Ethiopian kaolin by cationic surfactant (cetyl trimethyl ammonium Bromide).

In another research reported by *Putra et al.*, [6] they modified kaolin with Hexadecyl trimethyl ammonium bromide anionic surfactant for the removal of mercury ions from water

where they found the maximum adsorption of mercury on modified kaolin is better than on natural with 94.57% and 73.83% respectively. In addition, *Merrikhpour et al*., [7] mentioned that using SDS to modify bentonite to remove Cd^{2+}, Cu^{2+}, and Ni^{2+} from water demonstrated a notable increase in adsorption efficiency compared to Na-Bentonite.

Mudzielwana et al., [8] mentioned that the intercalation of HDTMA-Br surfactant onto natural kaolin successfully increased the pore diameter from 9.53 to 20.41 nm and decreasing the total surface area from 18.61 to 3.39 m^2/g thus improving the adsorption of As(III) and As(V) from groundwater the same author *Mudzielwana et al*., [9] showed that the pore volume and specific surface area increased from 0.04 to 0.083 cc/g and 19.02 m^2/g to 29.8 m^2/g, respectively. This might be explained by the parent clay mineral interlayer structure being propped up during alteration. Following alteration, the pore diameter dropped from 9.54 to 8.5 nm. The reduction in pore diameter would suggest that during modification, the Fe and Mn oxides permeated into RK's pores. The clay can be categorized as a mesoporous material based on the range of average pore diameters.

REFERENCES

[1] Dinh, V., Nguyen, P., Tran, M., Luu, A., Hung, N. Q., Luu, T., Kiet, H. T., Mai, X., Luong, T., Nguyen, T., Ho, H. T., Nguyen, D., Pham, D., Hoang, A., Le, V., & Nguyen, T. (2021). HTDMA-modified bentonite clay for effective removal of Pb(II) from aqueous solution. Chemosphere, 286, 131766. https://doi.org/10.1016/j.chemosphere.2021.131766.

[2] Hezil, N., Fellah, M., Assala, O., Touhami, M. Z., & Guerfi, K. (2018). Elimination of Chromium (VI) by Adsorption onto Natural and/or Modified Kaolinite. Diffusion Foundations, 18, 106–112. https://doi.org/10.4028/www.scientific.net/df.18.106.

[3] Al-Essa, K. (2018). Heavy Metals Adsorption from Aqueous Solutions onto Unmodified and Modified Jordanian Kaolinite Clay: Batch and Column Techniques. American Journal of Applied Chemistry, 6(1), 25. https://doi.org/10.11648/j.ajac.20180601.14.

[4] Chai, J., Au, P., Mubarak, N. M., Khalid, M., Ng, W. P., Jagadish, P., Walvekar, R., & Abdullah, E. C. (2020). Adsorption of heavy metal from industrial wastewater onto low-cost Malaysian kaolin clay–based adsorbent. Environmental Science and Pollution Research, 27(12), 13949–13962. https://doi.org/10.1007/s11356-020-07755-y.

[5] Belachew, N., & Hinsene, H. (2019). Preparation of cationic surfactant-modified kaolin for enhanced adsorption of hexavalent chromium from aqueous solution. Applied Water Science, 10(1). https://doi.org/10.1007/s13201-019-1121-7.

[6] Putra, A., Zaimahwati, N., Syahyadi, R., Rihayat, T., & Aidy, N. (2021). Removal of Hg(II) metal ions using kaolin adsorbents modified with anionic surfactant and efficient ultrasonic assisted. International Journal of Research -GRANTHAALAYAH, 9(11), 72–84. https://doi.org/10.29121/granthaalayah.v9.i11.2021.4379.

[7] Merrikhpour, H., Mobarakpour, S., & Azimi, S. B. (2022). Adsorption of Cd2+, Cu2+, and Ni2+ onto surfactant modified bentonite. Desalination and Water Treatment, 271, 157–165. https://doi.org/10.5004/dwt.2022.28768.

[8] Mudzielwana, R., Gitari, M. W., & Ndungu, P. (2019). Performance evaluation of surfactant modified kaolin clay in As(III) and As(V) adsorption from groundwater: adsorption kinetics, isotherms and thermodynamics. Heliyon, 5(11), e02756. https://doi.org/10.1016/j.heliyon.2019.e02756.

[9] Mudzielwana, R., Gitari, M. W., & Ndungu, P. (2019). Uptake of As(V) from Groundwater Using Fe-Mn Oxides Modified Kaolin Clay: Physicochemical Characterization and Adsorption Data Modeling. Water, 11(6), 1245. https://doi.org/10.3390/w11061245.

CHAPTER I

BIBLIOGRAPHIC STUDY

INTRODUCTION

Clay minerals have long been recognized as essential components of the Earth's crust and are pivotal to human civilization and industry. The term "clay," which originates from the Greek word "Argilos," reflects the historical and scientific significance of the material. Over the centuries [1], clay has evolved from a basic building material for bricks and ceramics to an indispensable resource in advanced applications such as wastewater treatment and environmental remediation [2-5]. Among these applications, the ability of clay to adsorb various contaminants plays a crucial role in environmental sustainability and industrial processes.

The adsorption phenomenon, first identified in the late 19th century, is a critical process in both natural and industrial systems. Initially distinguished from absorption by Kayser in 1881 and later expanded upon by McBain in 1909 [6], adsorption is now recognized as one of the most effective separative technologies. Its simplicity and efficiency have made it particularly appealing in water treatment, where it serves as a powerful tool for removing pollutants such as heavy metals. In this context, clay minerals, due to their high surface area and unique structural properties, exhibit remarkable adsorption capacities, making them highly effective materials for capturing and immobilizing toxic metal ions from contaminated water sources.

Heavy metals, owing to their non-degradable and accumulative nature, have become a critical environmental concern. These elements, widely present in both natural and anthropogenic sources, can have severe consequences for both ecosystems and human health. While some heavy metals, such as iron, zinc, and copper, are essential in trace amounts for biological processes, others, like arsenic, lead, and mercury, poses significant toxicity risks even at low concentrations. Given their persistent nature, the removal of these pollutants from water bodies is imperative, further highlighting the significance of adsorption-based treatment methods using clay minerals. This part aims to explore the characteristics, sources, applications, and toxicities of various heavy metals, emphasizing their impact on the environment and public health [7].

The first chapter is a bibliographic study, which is divided into three parts. In the first part, we described Clay minerals (exploring their chemical composition, structural properties,

classification, and industrial applications…). The second part consists of some notions about the adsorption phenomenon and their Factors influencing. The final section provides an overview of Heavy metals, a description of their Utilization and toxicity.

I.1 CLAY MINERALS

I.1.1 Definition

The term “clay” applies to the materials having a particle size of less than 2 micrometers, and also to the family of minerals having similar chemical compositions and common crystal structural characteristics [8].

Hydrated alumina silicates make up the majority of the chemical components of clays, with some related minerals like iron oxides and hydroxides, carbonates, quartz, etc., also present [9].

I.1.2 Chemical composition of clay minerals

Clay, as a raw material, is a mixture of clay minerals (kaolinite, montmorillonite, etc.) and crystalline impurities, in the form of rock debris of infinitely diverse composition [10].

Impurities consist of:

- Silicon oxides and hydroxides: (quartz and cristobalite).
- Ferriferous minerals: Fe_2O_3 hematite, Fe_3O_4 magnetite.
- Carbonates: $CaCO_3$ calcite, CaMg dolomite $(CO_3)_2$.
- Aluminum oxides and hydroxides: Gibbsite $Al(OH)_3$.
- Organic matter.

I.1.3 Structure of clay minerals

Clay minerals are mainly characterized by a leaf structure in most cases, hence their designation of phyllosilicates. These sheets consist of two types of layers, octahedral and tetrahedral, the vertices of which are occupied by the O^{2-} and OH^- ions. These negatively charged ions tend to repel and form a structure where cations can be lodged that ensure the electrostatic stability of the entire structure [1, 11]. The structural representation of clay minerals can be

schematized as a unit that combines a sheet and an interfoliar space. Generally, the sheet is formed by two types of layers.

I.1.3.1 The tetrahedral layer

Four oxygen atoms (O) surround a silicon atom (Si) to form a tetrahedron. These tetrahedrons combine to form hexagonal meshes by sharing oxygens; this gives rise to a tetrahedral layer as shown in Figure I.1.

I.1.3.2 The octahedral layer

Metal cations like Mg^{+2} and $Al^{+3}$are surrounded by six oxygen atoms to form an octahedron (O). A chain of octahedrons makes up the octahedral layer as shown in Figure I.1.

I.1.3.3 Interfoliar space

Interfoliar space refers to the gap between two parallel primary sheets in the structure of clays. Every clay has a unique interfoliar area.

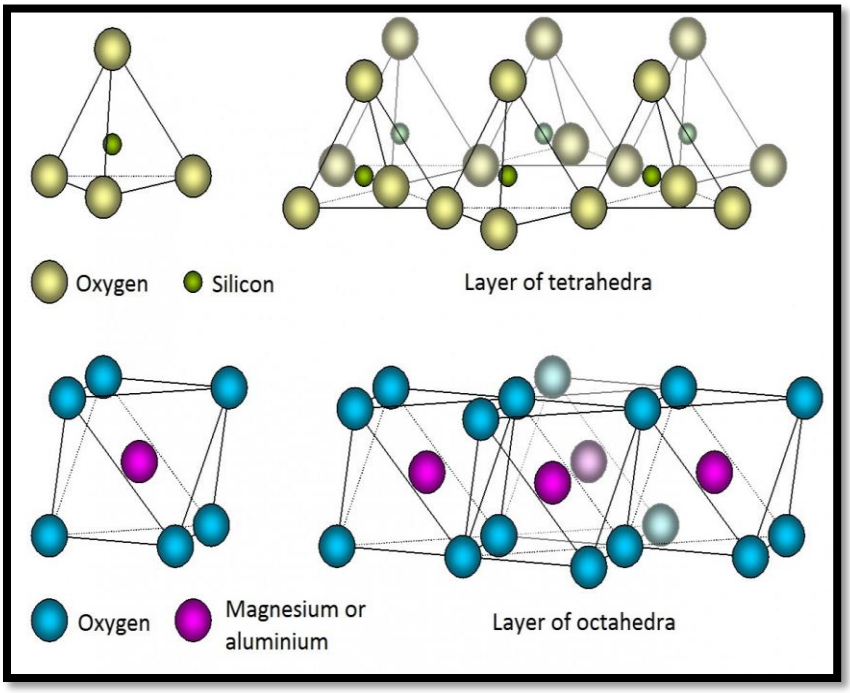

Figure I.1: Representation of tetrahedral and octahedron layers.

I.1.4 Classification of clay minerals

The following two criteria are typically used to categorize clay minerals [1]:

Type of sheet

- Total charge of sheets

We divide the clay into three main families according to the constitution or thickness of the sheet.

I.1.4.1 Minerals T/O or type 1/1 of 7 Å

The combination of a tetrahedral layer and an octahedral layer (T/O or 1/1) defines this mineral group. It consists of nacrite, halloysite, and kaolinite. Kaolinites have a limited number of cationic substitutions and have the chemical formula $Al_2Si_2O_5(OH)_4$ [12].

a. Kaolinite

The Chinese Kao-Ling site, where this clay rock was found, is where it gets its name. Its name is a corruption of the Chinese word "gao ling," which means "high hills." It is also known as kaolinite clay mineral and kaolin rock, its structure is represented in Figure I.2.

This white clay is refractory, soft, and friable [13]. It is used to make porcelain and ceramics because it is high in silica and low in mineral salt concentration. One of the rare clays that are chemically inert is this one [14].

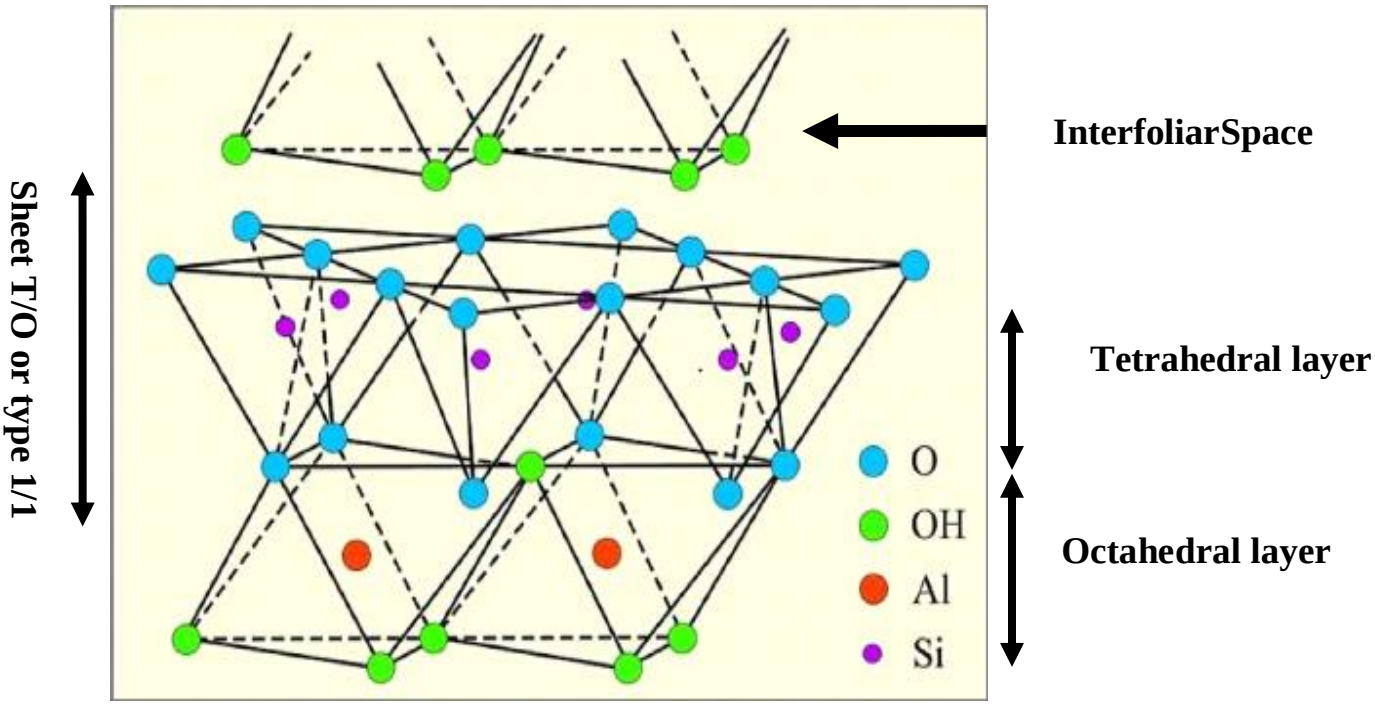

Figure I.2: Schematic representation of a kaolinite sheet [11, 15].

I.1.4.2 Minerals T/O/Tor type 2/1 of 10Å

The T/O/T series of three-layer minerals is also known as the 10Å series. The sheets are composed of two tetrahedral layers and one octahedral layer with the second tetrahedral layer reversed from the first. The sheet's thickness can range from 9.3 to 15.

a. Illite

The term illite was proposed by *Grim et al*., [16]. As a general term and not as a specific clay name. The name was derived from the abbreviation for the state of Illinois in the USA. The structure of illite is a combination of an octahedral layer and two tetrahedral layers (T/O/T or 2/1 diocesan or trioctahedral). Cations (K+) are adsorbed into the interfacial space to compensate for the imbalance of charges. These ions fit tightly into the bases of the silica layer and are therefore fixed and not exchangeable [17]. The general formula for illite is $K_yAl_4\,(Si_{8-y},Al_y)O_{20}(OH)_4$, the value of y usually between 1 and 1.5. Illites are non-inflating clays due to the presence of intercalary cations (K^+) that prevent the intrusion of water molecules into the structure as shown in (Figure. I.3) [18].

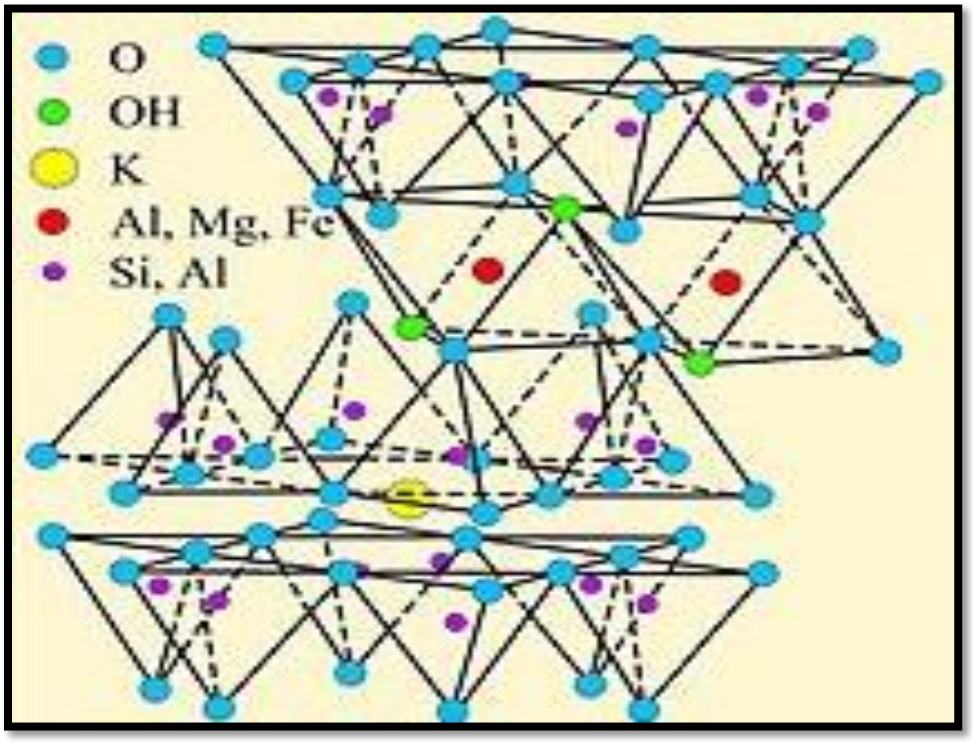

Figure I.3: Schematic representation of an illite sheet [19].

b. Vermiculites

Vermiculites Figure I.4 are clays of volcanic origin, rich in magnesium [20]. They are formed by the hydrothermal modification of mica minerals. When heated, it experiences a phenomenon of expansion, making it particularly useful as thermal insulation for constructions, this material has a low mass, an inability to burn, and is imputrescible and unalterable [21].

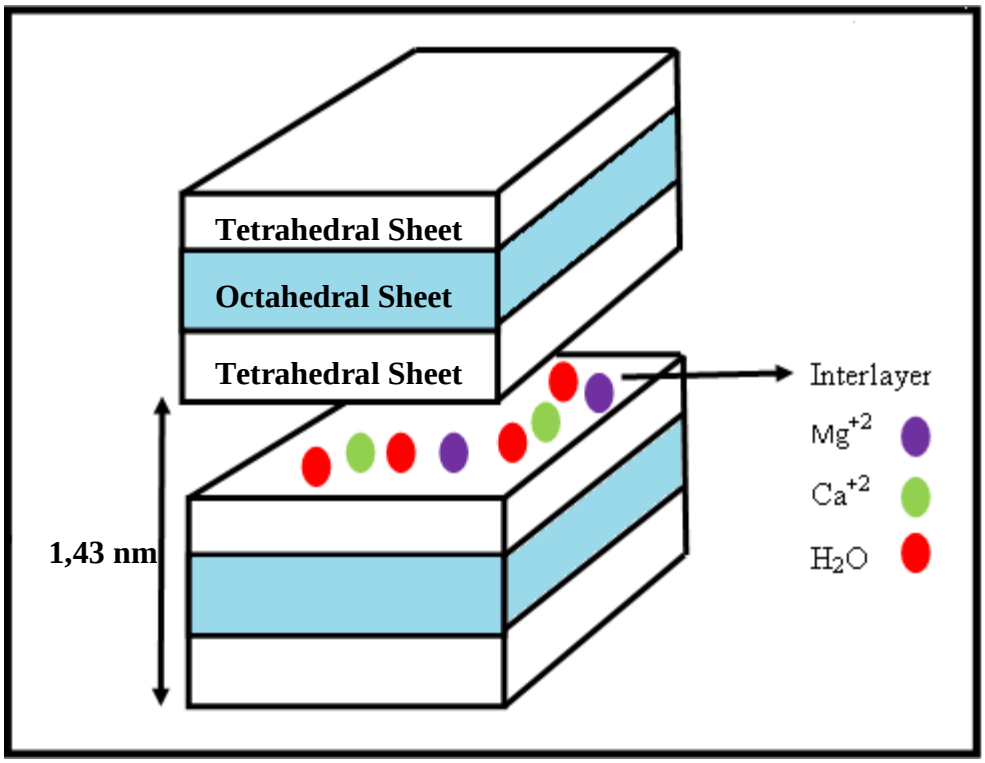

Figure I.4: Schematic representation of a vermiculites sheet.

c. Smectites

These different clays are known for their ability to trap water molecules. They are called inflating clays. Under the action of water, they can increase their volume by up to 30%. By trapping water, they also fix cations allowing exchanges by adsorption. They take a gel-like texture, able to carry ions or active molecules; this property is the basis of dressing technologies for the digestive tract [22]. Montmorillonites, bentonites, saponites, nontronites, and beidelites are members of this clay family.

d. Montmorillonite

Clay most commonly harvested, it is usually sold green but can be found in other colors: gray, white, bluish. Its name comes from its original town, Montmorillon in Vienna [23]. It has a high concentration of silica, minerals including potash, oxides of magnesium, iron, manganese, aluminum, soda, etc as shown in Figure I.5.

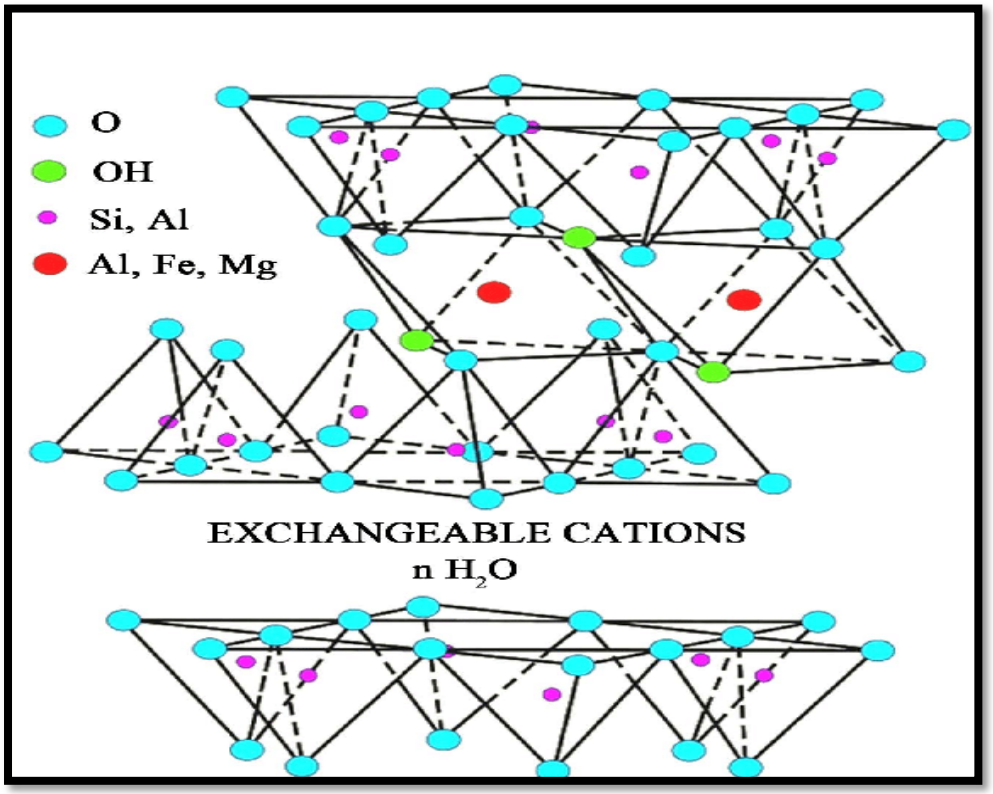

Figure I.5: Schematic representation of a montmorillonite sheet [19].

I.1.4.3 Minerals T/O/T/O or type 2/1/1 of 14 Å

The 2:1:1 sheet consists of the alternating T-O-T sheet and an interfoliar octahedral layer. The characteristic equidistance is about 14 Å. This type of mineral belongs to the chlorite family [24].

a. Chlorites

This term, derived from the Greek word "chloros" for green, was given to them because of their greenish color. There are other chlorites that are yellow, red, or white, similar to Illites and Smectites in structure [25]; they have an extra layer of magnesium hydroxide, iron, aluminum, etc. between their leaves as shown in Figure I.6.

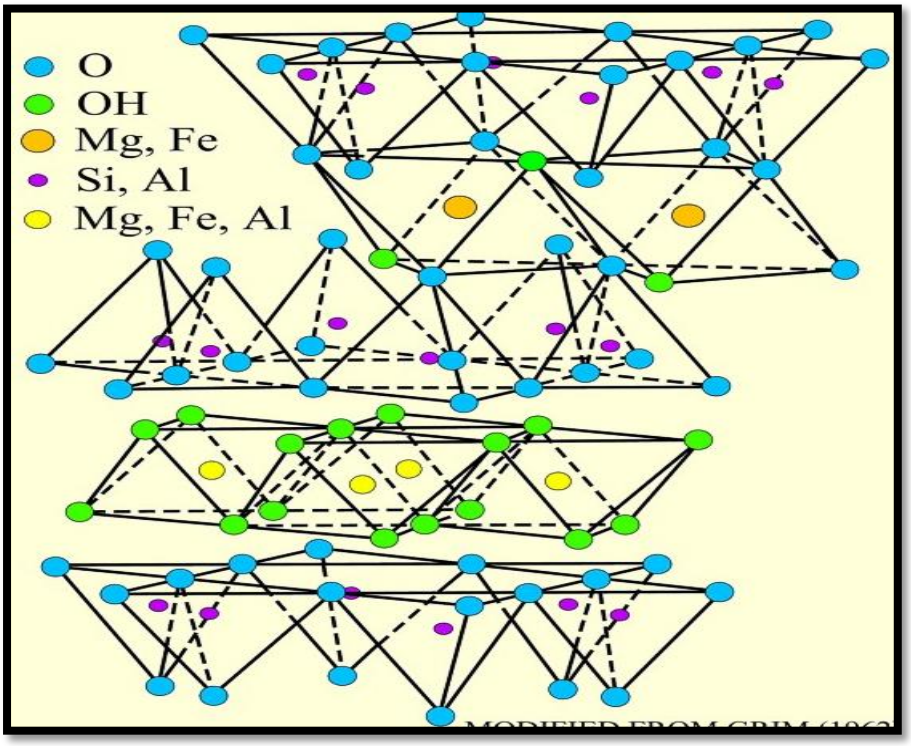

Figure I.6: Schematic representation of a chlorites sheet [19].

I.1.4.4 Interstratified clay minerals

Interstratified minerals are characterized by a vertical stacking of two (or more) types of sheets. These minerals are common in the natural environment [26].

These minerals are formed by the superposition of sheets that are either:

- Of a different nature (illite-smectite, vermiculite-smectite, etc.);
- Of the same nature but which differ by their interfoliar fillings (case of the hydrated Montmorillonite where the interfoliar space may contain one, two, three or four layers of water)
- By nature, and interfoliar filling: illite-smectite with Smectite sheets in varying states of hydration

Of these minerals, illite/Smectite interstratifies are the most studied, if we consider an interstratified mineral that contains two types of A and B sheets, we can consider essentially three types of interstratified [26].

1-segregated: a given particle has AAABBB sequences;

2- regular: a given particle then has sequences ABABAB… AB;

3- Random: all intermediate cases, between the first two described above, are represented in Figure I.7.

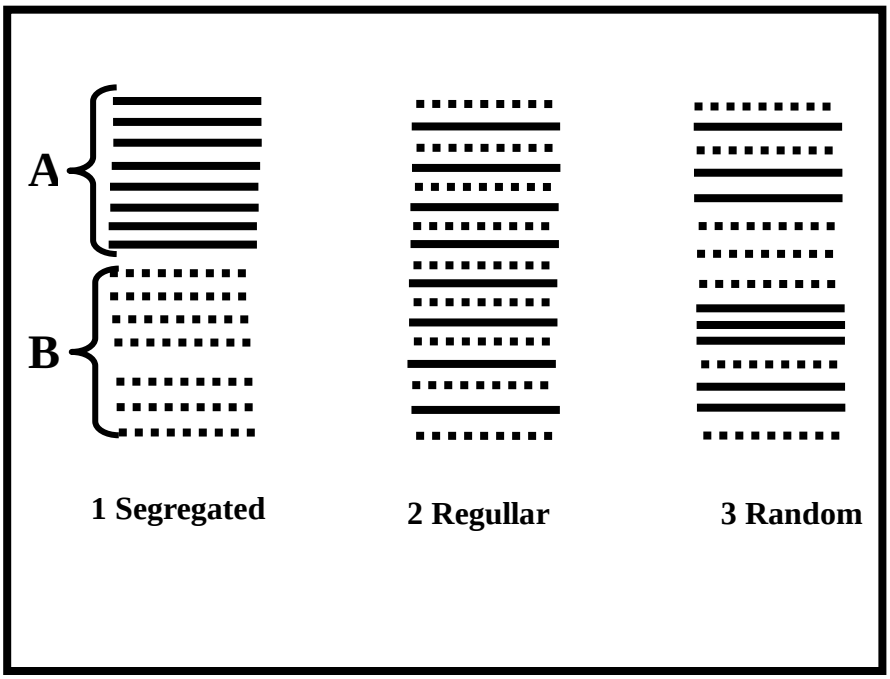

Figure I.7: Different modes of leaf succession within an interstratified unit.

I.1.5 Properties of clay minerals

Clay minerals are characterized by several main properties such as:

- Charge of clay surfaces
- The specific surface area
- Water adsorption capacity (swelling)
- Cation exchange capacity

I.1.5.1 Charge of clay surfaces

Most clay has an electric, non-neutral surface that results from isomorphic replacements as well as the environment.There are two categories of charges.

- **permanent charge**

It is mainly negative and located on the surface. It comes from isomorphic substitutions within the sheet, resulting from the replacement of metal cations by those of another metal of lower valence. It therefore leads to a deficit in the surface of the slips, offset by the presence of compensating cations such as Na^{+},Ca^{2+}, K^{+}, or Mg^{+2}

- **The variable charge**

It can be positive or negative and is located at the edges of the sheets. It only appears in suspension. This is a charge dependent on the pH of the solution. In acidic medium, the positively charged species is predominant, while in basic environment, it is the negatively charged species that is the majority.

Clay has a high anionic exchange capacity at low pH levels: Compared to OH^{-}ions, H^{+} ions bind more frequently, and a positive charge results Figure I.8.

A cationic exchange capacity (CEC) emerges at high pH. More OH^{-} than H^{+} ions bind, indicating a growing negative charge Figure I.9.

There is no exchange capability in a state of balance Figure I.10.

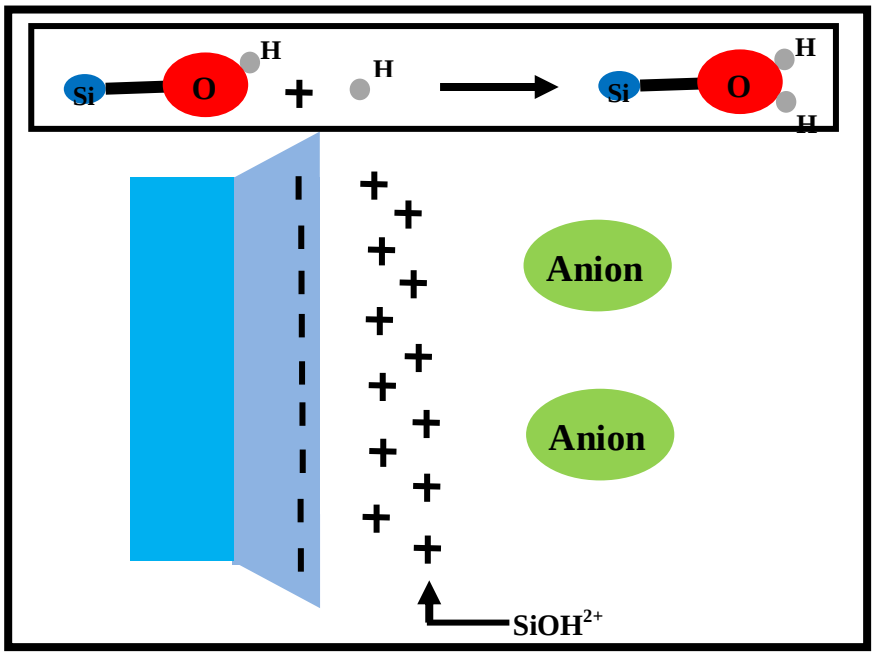

Figure I.8: Clay surface charge at low pH.

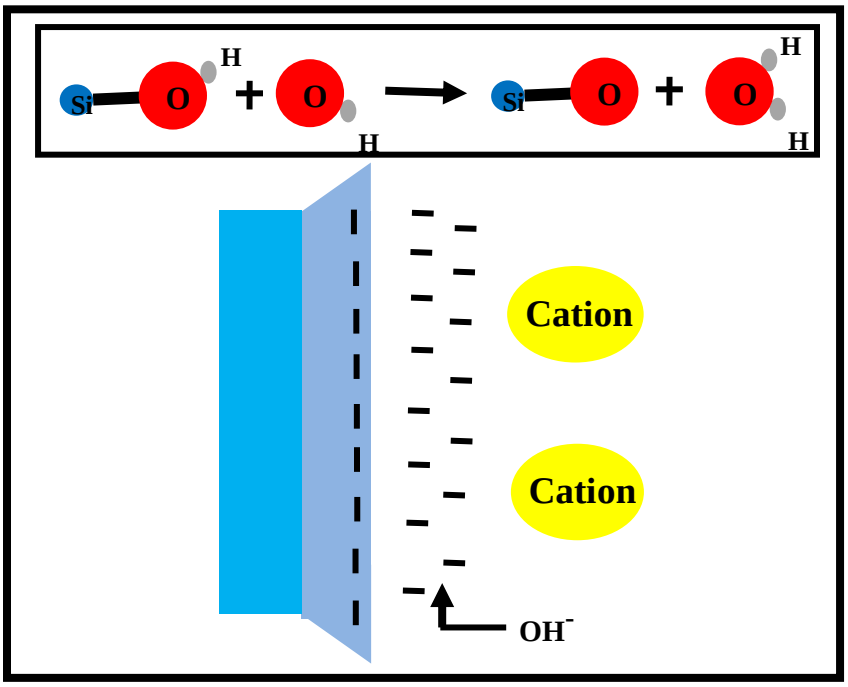

Figure I.9: Clay surface charge at high pH.

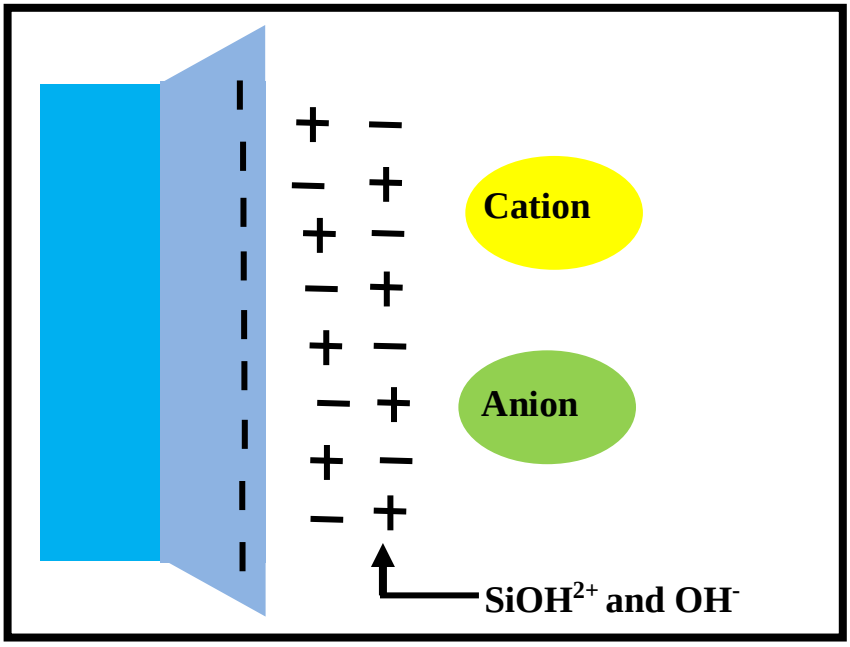

Figure I.10: Clay surface charge at neutral pH.

I.1.5.2 The specific surface area

Clays have a substantial specific surface area despite their small size. The characteristic surface values of the major clay families are provided in Table I.1. The inner surface corresponding to the interfoliar gap and the outer surface between the clayey particles make up the overall surface area [27].

Table I.1: Specific surface area of some clay minerals [28].

Mineral	Inner surface (m^2/g)	External surface (m^2/g)	Total surface (m^2/g)
Kaolinite	0	10-30	10-30
Illite	20-55	80-120	100-175
Smectite	600-700	80	700-800
Vermiculite	700	40-70	760
Chlorite	-	100-175	100-175

I.1.5.3 Cation exchange capacity

One of the crucial characteristics of clay minerals is their cationic exchange capacity (CEC). This gauges the clay mineral's capacity to swap out the solution's cations. The CEC fluctuates with pH and is evaluated at pH 7 because surface loading depends on pH [11]. The values of the cation exchange capacity of several clays are given in Table I.2.

Table I.2: Cation Echange Capacities (meq/100g) of clay Minerals [1].

Cation Echange Capacities (meq/100g) of clay Minerals	
Smectite	80-150
Vermiculite	120-200
Illite	10-40
Kaolinite	1_10
chlorite	<10

I.1.5.4 Water adsorption capacity (swelling)

The ability of various clay families to adsorb water varies. Some clay minerals can incorporate water molecules into their structure Figure I.11. This water makes the layer swell, which alters its size. They are known as swelling clays. The basic structure of the expanding minerals is 10 Å. A layer of water with a thickness of 2.5 or 5.2 Å develops depending on hydration. A 95% increase in volume results from this hydration.

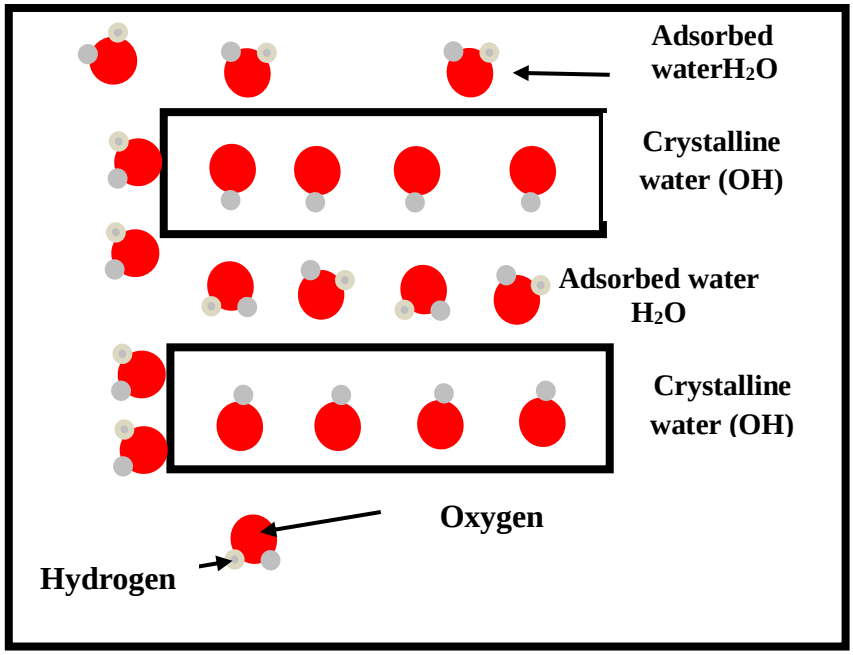

Figure I.11: Location of water in clay particles.

I.1.6 The use of clay

Clay minerals are widely employed in numerous fields (industry, environment, etc.) as a result of its physico-chemical characteristics.

Table I.3: Different fields of clay use.

Fields of use	Application
Food industry	Discoloration of oils The clarification of beverages
Petroleum industry	used as drilling mud and catalyst in oil refining
Cosmetics industry	Preparation of toothpastes and shampoos, creams, soaps, masks...)etc.
Chemical industry	Production of paints, paper, porcelain, pottery, bricks, and other building materials
Environment	Treatment of discharge wastewater.

I.1.7 Activation of clay

The adsorption capacity of natural clay is low, but activated clay is a method that increases these qualities by several techniques. The common modification techniques proposed mainly include thermal activation, chemical activation, and surfactant modification.

I.1.7.1 Thermal activation

Thermal treatment, also known as calcination, entails heating the clay material to a specified temperature in order to cause the octahedral layer to undergo dehydroxylation. All atoms in the octahedral sheet have less bonding coordination as a result of the dehydroxylation process, making them more reactive. Many variables, such as heating rate, holding temperature and time, atmosphere (oxidizing or reducing), and cooling rate, affect the precise nature of the structural alteration [29].

I.1.7.2 Chemical activation

In order to increase the SSA and porosity of clay, the naturally existing cations in the interlayers are frequently removed by proton exchange through activation with an acid solution (HCl, H_2SO_4, HNO_3, and H_3PO_4).

Additionally, the opening of the platelet edges caused by the cations' escape from the octahedra and tetrahedra during pickling increases the SSA of clays.

Although inorganic acids have received the majority of attention when using acid reagents, research has revealed that organic acids like acetic acid and oxalic acid are also useful.

The main variables influencing the characteristics of acid-washed clays are the acid dosage and treatment time [30].

I.1.7.3 Surfactant modification

Interlayer cations play a significant part in surfactant modification due to their capacity to exchange with organic cations and their ability to create pathways for surfactants to enter the interlayer. Additionally, certain surfactants may stick to the clay's surface, serving as the pollutants' adsorption sites. Since clays are always negatively charged, cationic surfactants attract more attention than anionic and nonionic ones [30].

I.2 ADSORPTION PHENOMENON

I.2.1 Definition

Adsorption is the process in which molecules contained in a fluid (gas or liquid) and called (adsorbate) attach to the surface of a solid called (adsorbent). Sites where adsorbate molecules bind are called active sites [31].

The transference of the adsorbate from the liquid phase to the solid phase continues until the equilibrium is reached between the amount of adsorbate linked to the adsorbent and the amount of adsorbate remaining in the solution. The affinity degree between the adsorbent and adsorbate determines this distribution in liquid and solid phases [32].

I.2.2 Types of adsorption

Depending on the value and nature of the adsorbent/adsorbate bonding energy, there are two types of adsorption processes: physical adsorption or (physisorption) and chemical adsorption or (chemisorption).

I.2.2.1 Physical adsorption

In physisorption, the cohesion forces between the adsorbent/adsorbent pair are relatively low, and of an electrostatic nature (Van der Waals, dipole). The interaction energy is about 5 to 40 kJ mol^{-1}. The phenomenon is rapid and reversible [33].

I.2.2.2 Chemical adsorption

In chemisorption, there is electron exchange and thus the formation of a chemical bond between the adsorbent and the adsorbent surface.

The interaction energy involved varies from 200 to 400 kJ mol^{-1}. The process is slow, irreversible, and excludes any possibility of multimolecular (multilayer) layer formation [33].

I.2.2.3 Differences between physical and chemical adsorption

Table I.4 shows the differences between the two types of adsorption.

Table I.4: Differences between physical and chemical adsorption.

Parameter	physical adsorption	chemical adsorption
Type of binding	Van der Waals	Chemical
Specificity	Non-specific process	Specific process
Process temperature	Less than the boiling temperature of the adsorbate	Elevated
Kinetic	Quick	Slow
Desorption	Easy	Difficult
Adsorption energy	<50 kJ/mol	>100 kJ/mol
Reversibility	Reversible	Irreversible
Layer formation	Monolayer or multilayer formation	Monolayer formation

I.2.3 The main adsorbents

The main adsorbents used in the industry are:

- Activated carbon
- Zeolite
- Activated clay
- Silica gel
- Activated alumina

I.2.4 Factors influencing adsorption

The adsorption equilibrium between adsorbent and adsorbate depends on many factors, the main ones being:

I.2.4.1 Influence of pH

pH is a predominant parameter in the adsorption process. It directly affects the load state of the adsorbent and adsorbate. Its effect on contaminant retention is often studied. In most cases, the low pH promotes the adsorption of anions while the alkaline medium promotes that of cations [34].

I.2.4.2 Specific surface area

One of the main factors affecting the absorption capacity is the surface area because the amount absorbed is directly proportional to the surface area, the increase in specific surface area provides more active sites to increase the amount absorbed [35].

I.2.4.3 Influence of temperature

Adsorption is generally an exothermic process; thus, increasing the temperature can decrease adsorption capacity, as higher temperatures may reduce the interaction between adsorbate and adsorbent. However, in chemisorption, there might be an initial increase in adsorption with temperature due to activation energy requirements, followed by a decrease at

higher temperatures. Thus, the increase in temperature promotes the processes of chemisorption while its lowering promotes physical adsorption [36].

I.2.4.4 Nature of adsorbate

The physical and chemical properties of the adsorbate, such as molecular size, polarity, and ability to be liquefied, influence adsorption. For there to be good adsorption there must first be an affinity between the solid and the solute. In general, polar solids preferentially adsorb polar bodies. In contrast, non-polar solids preferentially adsorb non-polar substances and the affinity for the substrate increases with the molecular weight of the adsorbate [34].

I.2.4.5 Nature of adsorbent

The structure and nature of adsorbents play an important role in trapping the various organic and inorganic compounds present in the waters. Particle size, specific surface area, and porosity are the main properties that affect the affinity of an adsorbent for the solute.

The adsorption of a substance increases proportionally to the decrease in the size of the particles of the adsorbent, which promotes the penetration of the compounds of the solution into the capillaries of the substance, therefore the subdivision of the particle of the solid directly influences the pores of the latter as well as its specific surface which will be developed [37].

I.2.5 Adsorption isotherms

Adsorption isotherm models can provide mechanism information on the adsorption process, the maximum adsorption capacity, as well as the properties of adsorbents. Where it describes the interaction of adsorbate with adsorbent. An isotherm is a plot of the amount of solute adsorbed per unit of adsorbent (Q_{ads}) as a function of the equilibrium concentration of the solute in the bulk solution (Ce) at constant pH and temperature [38].

The amount adsorbed per unit mass can be calculated according to the following equation [39].

$$Q_{ads} = \frac{(C_i - C_e)V}{m} \quad \text{(Eq. I.1)}$$

Where:

Q_{ads}: Adsorbed amount expressed as mg solute per gram adsorbent ($mg.g^{-1}$).

C_i: Initial concentration of solute ($mg.l^{-1}$).

C_e: Equilibrium solute concentration in ($mg.l^{-1}$).

V: volume of solute in liters (L).

m: mass of adsorbent in grams (g).

I.2.5.1 Classification of adsorption isotherms

Giles et al., [40] classified adsorption isotherms in the case of liquids for solutions of low concentrations in four main classes generally observed. These classes are shown in Figure I.12.

S Curves

The S-type isotherm exhibits a gradual incline, followed by a vertical orientation. At the outset, as the concentration of the adsorbate rises, there is an opportunity for the adsorbate to locate an available site to which it can attach itself, due to competition between solute molecules. Consequently, the adsorption capacity is constrained and reaches a plateau. However, this behavior in type S isotherms is contrary, resulting in an increase in the curve's slope. This is due to a vertical orientation tendency of the solute molecules at a higher concentration, which results in an increased availability of sites for adsorption [31].

L Curves

The Langmuir isotherms are most commonly observed in the context of solute adsorption in aqueous solutions. The initial shape of the equilibrium curve is consistent with the fundamental premise that the higher the solute concentration, the greater the adsorption capacity. However, this capacity is ultimately limited by the number of available adsorption sites, which can be occupied by competing solute molecules. In most cases, this indicates that the molecules are adsorbed flat on the surface or, on occasion, vertically oriented with adsorbed ions exhibiting particularly strong intermolecular attraction.

This isotherm type indicates that the adsorption occurs due to relatively weak forces, such as van der Waals forces [31].

H Curves

The fundamental distinction between the standard isotherms, designated as L-type, and the high-affinity isotherm can be observed at the initial point of the equilibrium curve. The L-type isotherm commences at the origin, whereas the H-type isotherm exhibits an initial portion with a vertical orientation and qe values exceeding zero, even when the concentration of solute approaches zero.. The adsorbed species are often large units, such as, ionic micelles or polymeric molecules However, sometimes, they can be simple ions, that exchange with others of much lower affinity with adsorbent surface. An example of this is the sulfonate dye. This isotherm type indicates chemisorption and adsorption by electrostatic forces. Other classifications commonly used for H type isotherms include irreversible isotherm, as when an adsorption occurs at a high concentration, a concentration reduction does not change the adsorption capacity [31].

C Curves

The isotherms with partition constant are characterized by a linear behavior of the equilibrium data at low concentrations of solute. This behavior follows Henry's law for ideal gas equilibrium phases, which when translated to adsorption processes, suggests that the adsorption capacity is proportional to the solute concentration, up until the maximum possible adsorption, where an abrupt change to a horizontal plateau occurs. This is the type of curve that is obtained

for the partition of a solute between two practically immiscible solvents. In such cases, the affinity of the solute for the solid is greater than its affinity for the solvent. Alternatively, when the adsorption sites are available in quantities sufficient for the adsorption of all the solute, but the bonding forces between the solute and the solvent are weak and depend on the liquid phase concentration [31].

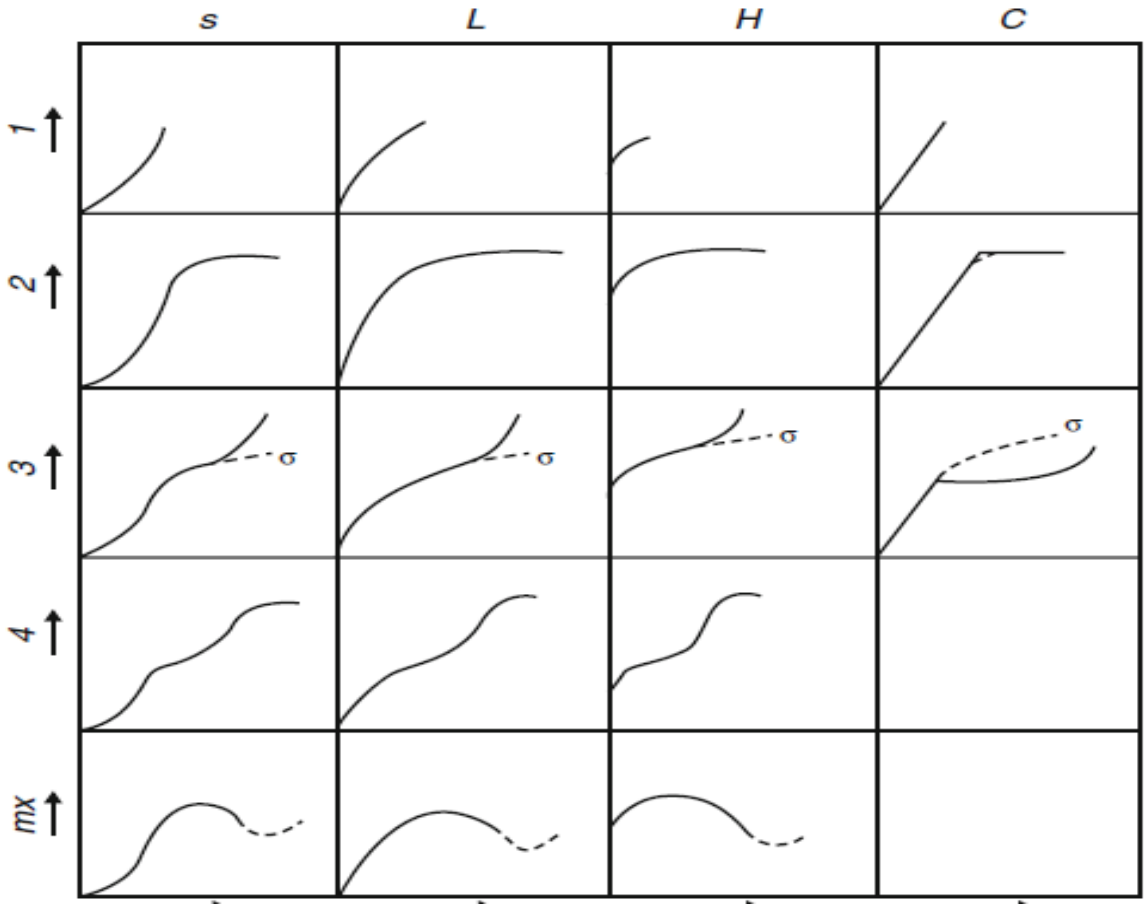

Figure I.12: Classification of adsorption isotherms.

I.2.5.2 Modeling of adsorption isotherms

Isotherm modelling is used to represent experimental data and describe the performance of the adsorbent/adsorbate system in a wide range of concentrations.

There are several isotherm models available to analyze experimental data and to describe adsorption equilibrium. These are the isotherms of Langmuir, Freundlich, Sips, Temkin, etc…. used in the solid-liquid system to describe adsorption isotherms.

The adsorption models used in our study for the adjustment of experimental data are:

I.2.5.2.1 Freundlich isotherm

The Freundlich model is the first empirical model and is based on the relationship between the adsorbed amount (Q_{ads}) and the concentration in the aqueous solution of the solute (Ce). It is considered to be applicable in many cases, particularly in the case of multilayer adsorption with possible interactions between adsorbed molecules [41].

The non-linear form of this model is expressed by the following equation:

$$\mathbf{Q_{ads} = K_F C_e^{\frac{1}{n}}} \quad \text{(Eq. I.2)}$$

Where:

Q_{ad}: Amount of adsorption in ($mg.g^{-1}$).

K_F: Freundlich constant.

C_e: Equilibrium concentration of solute ($mg.L^{-1}$).

1/n: Freundlich constant that reflects adsorption intensity.

The K_F and 1/n constants can be determined from the following linear form:

$$\mathbf{\ln Q_{ads} = \ln K_F + \frac{1}{n} \ln C_e} \quad \text{(Eq. I.3)}$$

I.2.5.2.2 Langmuir isotherm

The Langmuir isotherm was proposed in 1918 and is based on the following assumptions: [42].

- Adsorption is limited to single layer
- Only one molecule is adsorbed per site
- All adsorption sites are energy equivalent
- There are no interactions between adsorbed molecules

The non-linear form of this model is expressed by the following equation:

$$\mathbf{Q_{ads}} = \frac{\mathbf{Q_m K_L C_e}}{\mathbf{1+K_L C_e}} \quad \text{(Eq. I.4)}$$

Where:

Q_{ads}: Amount of adsorption ($mg.g^{-1}$).

Q_m: The maximum adsorption capacity ($mg.g^{-1}$).

C_e: Equilibrium concentration of solute in ($mg.L^{-1}$).

K_L: Langmuir Constant.

The K_L and Q_m constants can be determined from the following linear form:

The maximum adsorption capacity (Q_m) and constant K_L are determined from the linear form of the Langmuir equation.

$$\frac{\mathbf{C_e}}{\mathbf{Q_{ads}}} = \frac{\mathbf{C_e}}{\mathbf{Q_m}} + \frac{\mathbf{1}}{\mathbf{K_L Q_m}} \quad \text{(Eq.I.5)}$$

Langmuir parameters can be used to show the affinity between adsorbate and adsorbent using the dimensionless separation factor R_L [43].

$$\mathbf{R_L} = \frac{\mathbf{1}}{\mathbf{1+K_L C_i}} \quad \text{(Eq. I.6)}$$

Where:

C_i: This is the initial concentration of solute in the liquid phase ($mg.L^{-1}$).

R_L values are classified essentially into four groups and indicate the shape of the isotherm as shown in the following Table I.5.

Table I.5: The types of Langmuir isotherm.

R_L	**Type of isotherm**
$R_L > 1$	Unfavorable
$R_L = 1$	Linear
$0 < R_L < 1$	Favorable
$R_L = 0$	Irreversible

I.2.5.2.3 Sips isotherm

The Sips isotherm, which combines the Langmuir and Freundlich isotherms, can be used to predict adsorption on heterogeneous surfaces. It predicts the Freundlich model at low adsorbate concentrations and the Langmuir model at high adsorbate concentrations [44].

The non-linear form of this model is expressed by the following equation:

$$\mathbf{Q_{ads}} = \frac{\mathbf{Q_s K_s C_e^{n_s}}}{\mathbf{1 + K_s C_e^{n_s}}} \text{.....(Eq. I.7)}$$

Where:

Q_s: The highest possible adsorption level ($mg.g^{-1}$).

C_e: The equilibrium concentration of the adsorbate ($mg.L^{-1}$).

K_S: The equilibrium binding constant ($L.mg^{-1}$).

n_s: The constant related to the heterogeneity of adsorbent without unit.

The highest possible adsorption level (Q_s) and constants (K_s, n_s) are determined from the linear form of the Sips equation:

$$\ln\left(\frac{Q_{ads}}{C_e}\right) = \ln(Q_s K_s) + n_s \ln(C_e) \quad \text{(Eq. I.8)}$$

I.2.5.2.4 Temkin isotherm

Temkin and Pyzhev examined the effects of certain adsorbate /adsorbent interactions on adsorption isotherms and suggested that, because of these interactions, the heat of adsorption of all molecules in the layer would decrease linearly [45].

A common form of the Temkin isotherm as used in environmental adsorption research can be written as

$$Q_{ads} = \frac{RT}{b_T} \ln(K_T C) \quad \text{(Eq.I.9)}$$

Where:

Q_{ads}: Amount of adsorption in ($mg.g^{-1}$).

R: The universal constant of perfect gas.

T: Is the temperature in (K).

b_T: Is related to the heat of the adsorption ($J.mol^{-1}$).

K_T: Is the equilibrium binding constant ($L.mg^{-1}$).

C: Is the concentration of the equilibrium solute ($mg.L^{-1}$).

The Temkin isotherm, as defined by Eq. I.9, is called the Tempkin isotherm in several sources. Is typically rewritten as Eq. I.10 in order to fit it to a type I isotherm using a linear regression technique. Plotting q against ln(c) should result in a straight line if this equation is followed [46].

$$\mathbf{Q_{ads} = \frac{RT}{b_T} ln(K_T) + \frac{RT}{b_T} lnC} \text{..... (Eq. I.10)}$$

I.2.6 Adsorption kinetics

Adsorption kinetics determines the time required to balance the solute and adsorbent. It also gives an idea of the adsorption mechanism and the transfer mode between the liquid and solid phases. Several kinetic models have been developed to describe adsorption kinetics and to specify the nature of interactions at the solid-liquid interface [47].

Among these adsorption kinetics models, there are those:

I.2.6.1 First order pseudo kinetic model

This kinetic model was proposed by Lagergren and supposes that the adsorption rate at a time (t) is proportional to the difference between the adsorbed amount at equilibrium (Q_e) and that at time (Q_t) [48].

$$\mathbf{\frac{dQ}{dt} = K_1(Q_e - Q_t)} \text{ .....(Eq. I.11)}$$

Where:

Q_t: Amount adsorbed at time t in ($mg.g^{-1}$).

Q_e: Equilibrium adsorbed amount in ($mg.g^{-1}$).

K_1: First order speed constant (min^{-1}).

After integration, linearization of the previous equation:

$$\mathbf{ln(Q_e - Q_t) = lnQ_e - K_1 t}\text{.....} \quad \text{(Eq. I.12)}$$

Plot of ln (Q_e-Q_t) = f(t), gives a line of slope K and of ordered to the origin ln Q_e

I.2.6.2 Second order pseudo kinetic model

The equation of adsorption of the pseudo-second-order allows us to characterize the adsorption kinetics taking into account both the rapid fixation of the solutes on the most reactive sites and the slow fixation on the sites of low energy; it depends on the amount adsorbed on the surface of the adsorbent and the amount adsorbed in equilibrium [49].

The equation of pseudo-second-order kinetics obeys the following relation:

$$\frac{\mathbf{dQ}}{\mathbf{dt}} = \mathbf{K_2(Q_e - Q_t)^2}\text{.....} \quad \text{(Eq. I.13)}$$

Where:

Q_t: Amount adsorbed at time t in (mg.g^{-1}).

Q_e: Equilibrium adsorbed amount in (mg.g^{-1}).

K_2:constante de vitesse du pseudo-second ordre (g. mg^{-1}. min^{-1}).

After integration, linearization of the previous equation.

$$\frac{\mathbf{t}}{\mathbf{Q_t}} = \frac{\mathbf{1}}{\mathbf{K_2 Q_e^2}} + \frac{\mathbf{1}}{\mathbf{Q_e}}\mathbf{t}\text{.....} \quad \text{(Eq. I.14)}$$

The adsorbed quantity qe and the velocity constant K_2 can be determined from the slope and the ordinate at the origin of the t/Q_t curve as a function of t.

I.2.6.3 Intra particle diffusion

The intra-particle diffusion model is proposed by [50]. It is represented by the following equation.

$$\mathbf{Q_t = K_{ID}\sqrt{t} + C} \quad \text{(Eq. I.15)}$$

Where:

Q_t: The adsorption capacity at time t ($mg.g^{-1}$).

K_{ID}: The intraparticle diffusion constant ($mg.g^{-1}. min^{1/2}$).

t: The time (min).

C: Constant.

The values of k_{ID} and constant C can be determined from the slope and the ordinate at the origin of the Q_t curve as a function of $\sqrt{t}$.

I.2.7 Thermodynamic study

Thermodynamic parameters offer further details about energetic changes in the adsorption process (exothermic or endothermic, spontaneity or no spontaneity)

The variation of a system is accompanied by a variation of the Gibbs free enthalpy ($\Delta G°$), this variation depends on the initial state and the final state of the free enthalpy

The Gibbs energy [51] is calculated using the following equation Eq.I.16

$$\mathbf{\Delta G° = \Delta H° - T\Delta S°} \quad \text{(Eq.I.16)}$$

Therefore the Van't Hoff equation becomes as following [52].

$$\ln K_d = \frac{\Delta S^\circ}{R} - \frac{\Delta H^\circ}{RT} \quad \text{(Eq.I.17)}$$

The ΔS° and ΔH° values are calculated only after studying the influence of temperature on adsorption, so an equation is determined from the graph designed by ln K_d as a function1/T, with T the temperature studied during the adsorption reaction.

Where:

ΔH°: enthalpic which expresses the interaction energies between the molecules and the surface of the adsorbent.

ΔS°: entropic which expresses the modification and arrangement of the molecules in the liquid phase on the surface.

K_d: Equilibrium constants of the adsorption reaction.

T: Temperature studied (K).

R: Perfect gas constant (J/mol K).

If

ΔG°< 0 the adsorption process is spontaneous.

ΔG°> 0 the adsorption process is no spontaneous.

If

ΔH°< 0 the adsorption process is exothermic.

ΔH°> 0 the adsorption process is endothermic.

I.3 HEAVY METALS

I.3.1 Definition

Heavy metals are defined as natural metal elements with a density greater than 5g.cm^{-3}. They occur naturally in our environment (water, air, and soil). Generally emitted as very fine particles, they are carried by the wind and spread in soils and aquatic environments, contaminating flora and fauna and ending up in the food chain [53].

I.3.2 Emission source

Heavy metals are present in rocks (safe nature reserves). However, the exploitation of deposits, erosion and volcanic eruptions spread traces of these elements in the environment. They can then become toxic if they are found in sufficient quantities in living organisms. In addition to these natural phenomena, human activity, (vehicle exhaust, mining, agriculture, waste incineration, domestic and industrial effluents, liquid and solid discharges, etc.). Even if it does not create, heavy metals participate in their diffusion into the environment.

I.3.3 Many Heavy Metals

I.3.3.1 Copper

Copper is a semi-noble, ductile and malleable metal with high electrical and thermal conductivity and good resistance to corrosion and fatigue. Copper is a chemical element bearing the symbol Cu and atomic number 29, belonging to group 11 of the periodic classification, and is in the same column as silver and gold. Its electronic configuration is: [Ar] 4s^1 3d^{10}[54].

There are three different types of copper: metal (Cu^0), cupric ion (Cu^{2+}), and cuprous ions (Cu^+). Cupric ions are more poisonous and are abundant in the environment [55].

Figure I.13: Copper [56].

a) Utilization of copper

One of the heavy metals that is frequently used in many different applications is copper (Cu). It is typically used in

- Electrical and electronic equipment: (electrical magnets, batteries, mobile phones, keys).
- Architecture: roofs, lightning rods.
- Chemical compounds: dietary supplements and fungicides for agriculture, fertilizer industry, catalysts.
- Drugs: Manufacture of antimicrobial compounds.
- Pulp and Paper Industry.
- Kitchen equipment and metal processing products.

b) **Toxicity of copper**

Cu is essential for proper growth. In any event, People who are deficient in copper may experience anemia, bone and cardiovascular problems, weakening of the nervous and sensory systems, hair loss, a drop in synapses, dopamine, and nor ephedrine levels, and faulty myelination in the brain stem and spinal cord [57]. Due to its toxicity and broad use in industrial applications, copper is of particular concern. Copper contamination of drinking water can result

in dermatitis, keratinization of the hands and feet's soles, and itching. In numerous occasions, symptoms such as nausea, vomiting, diarrhea, and other acute symptoms have been described as being caused by local irritation brought on by ingested copper (II) ions. Based on health considerations, 2.0 mg/l of copper is the maximum permissible concentration in drinking water [35].

To comply with environmental regulations for different bodies of water, the concentration of copper in drinking water must be decreased.

I.3.3.2 Lead

Lead is a chemical element bearing the symbol Pb and atomic number 82, belonging to group 14 of the periodic classification, and is in the same column as Tin and carbon. Its electronic configuration is: [Xe] $6s^2$ $4f^1$ $5d^1$ $6p^2$.

Hazardous metal lead is easily accumulated in the human body. In the form of cerussite ($PbCl_2$), galena, and sulfide, it is a heavy and soft metal [58].

In nature, lead has four isotopes and is found under degrees of oxidation (+II) and (+IV). Inorganic species are most often in the (+II) state, while the degree of oxidation (+IV) occurs in lead organic compounds. Lead is resistant to sulphuric acid. However, it is rapidly dissolved by nitric acid and solubilized by organic acids (acetic acid, acidic foods) as well as by water, especially if it contains nitrates or ammonium salts. On the other hand, the presence in water of calcareous salts can prevent its solubilization [59].

Figure I.14: Lead [60].

a) Utilization of Lead

The usage of lead, a hazardous, non-biodegradable heavy metal, is widespread in a variety of industries, including.

- transportation (vehicle manufacturing, brake pads, tires and lubricating additives)
- agriculture (insecticide as lead arsenate)
- Alloys, mainly tin-lead alloys (solder), mainly in industry
- electronics Glass and ceramic products
- paints and batteries
- Cable sheaths

b) Toxicity of Lead

Lead contamination of soil and water has been acknowledged as a severe concern to human health. Pb(II) is known to harm the brain, liver, kidney, reproductive system, and basic biological activities [61]. Exposure to lead can cause serious adverse health effects and even be fatal at high doses. Lead can accumulate in the body and its exposure, even at very low doses, can be dangerous. Lead is particularly harmful to infants, young children, and pregnant women, and can permanently impair child development, intellectual and behavioral development [62].

The World Health Organization (WHO) has set a0.01 mg/L maximum allowable level for Pb(II) in drinking water [63].

I.3.3.3 Chromium

Chromium (Cr) is a silver-colored hard metal naturally occurring in rocky soils, and volcanic dust [64]. Chromium is a chemical element bearing the symbol Cr and atomic number 24, It is the first element in group 6 of the periodic classification, is in the same column as molybdenum (Mo)and tungsten (W), also called wolfram. Its electronic configuration [Ar] $3d^5 4s^1$).Although it can exist in a variety of oxidation states, the most prevalent and stable forms are "trivalent" Cr (III) and "hexavalent" Cr (VI). According to reports, Cr (VI) is more hazardous than Cr (III) [65].

Figure I.15: Chromium [66].

a) Utilization of chromium

Chromium is utilized in a wide range of industrial processes, including those that create stainless steel that can withstand high temperatures, refractory materials like brick and mortar, and pigment synthesis. In the chemical industry, it is used as an oxidant and in the production of other chromium compounds, as well as for treating metal surfaces, tanning leather, and preserving wood [67].

b) Toxicity of chromium

Chromium (Cr) is a group 1 carcinogen classified by the International Agency for Research on Cancer (IARC) and is pervasive throughout the environment.

I.3.3.4 Nickel

Nickel is a hard, ductile, silvery-white transition metal [68]. It is resistant to very high temperatures, corrosion and oxidation. Nickel is a chemical element bearing the symbol Ni and atomic number 28, belonging to group 10 of the periodic classification, is in the same column as palladium and platinum. Its electronic configuration [Ar] $3d^8 4s^2$).

Nickel is a crucial commercial element in industrialized cultures and is mostly found in nature as the sulfide, oxide, and silicate minerals [68]. Although it can exist in a number of oxidative states (ranging from 1 to +4), the +2 oxidationstate (Ni^{2+}) is the most prevalent in the environment and biological systems [69].

Figure I.16: Nickel [70].

a) Utilization of Nickel

Nickel is one of the transition metals that is currently employed most frequently in a variety of sectors. Because of its unique (catalytic) qualities as a conductor of electricity and heat. It is applied in: [71].

- alloys for the production of jewelry and coins
- used in stainless steel fabrication
- metal mining and painting
- dye manufacturing
- battery manufacturing industries
- resistance wires and machinery parts
- burning of fossil fuels

b) Toxicity of Nickel

At low quantities, Ni (II) is an essential macronutrient for life, but at excessive concentrations, it can have harmful consequences on health, including cancer, cardiovascular disease, and kidney disease [71].

Nickel is heavily used, which causes a number of environmental issues. Nickel can cause a dry cough, chest pain, breathing difficulties, nausea, diarrhea, skin eruptions, pulmonary fibrosis, gastrointestinal pain, renal edema, and other adverse consequences [55].

The permissible nickel concentration in drinking water is 0.01 $mg.L^{-1}$, and in wastewater is 2.0 $mg.L^{-1}$ [72]. However, the maximum contaminant level (MCL) for Nickel in drinking water, as defined by Environmental Protection Agency (EPA), is 0.02 $mg.L^{-1}$ [73].

I.3.3.5 Mercury

Mercury, represented by the symbol Hg and atomic number 80, is a heavy, silvery-white metallic element that is liquid at room temperature [74], belonging to group 12 of the periodic table, in the same column as Zinc and Cadmium is classified as a d-block. Its electronic configuration [Xe] $4f^{14}5d^{10}6s^{2}$) known as quicksilver. It is unique among metals for remaining in a liquid state at standard conditions, with a melting point of −38.83°C and a boiling point of 356.73°C. In nature Mercury is found in three chemical forms such as inorganic mercury, elemental mercury, and organic forms like methyl mercury [75].

Figure I.17: Mercury [76].

a) Utilization of Mercury

Mercury (Hg) has various applications:

- Thermometers and Barometers: Its thermal expansion properties make it ideal for measuring temperature and pressure.
- Electrical Switches: Mercury's conductivity allows it to be used in electrical components.
- Dental Amalgams: It forms amalgams with metals like silver and tin for dental fillings.
- Fluorescent Lamps: Mercury vapor produces ultraviolet light, which excites phosphors to emit visible light.

- Chemical Industry: Used as a catalyst in various chemical processes.
  However, due to its toxicity, many uses are being phased out.

b) Toxicity of Mercury

Mercury (II) has attracted particular attention as an important pollutant because of its toxicity and bio accumulative properties, when mercury is detected above the maximum level in the human body, it can cause serious health risks such as cancer, hypertension, headache, gastrointestinal damage, liver damage, and kidney failure [77, 78]. Therefore, the World Health Organization (WHO) has set the maximum permissible dose of 10 $\mu g/L^{-1}$ for mercury in wastewater and the highest allowable limit in drinking water to 1 µg/L due to its extreme toxicity [79, 80].

I.4 CONCLUSION

This chapter of the literature review examined three fundamental issues: clays, the adsorption process and the problem of heavy metals. Firstly, clays were presented not only as geological entities, but also as materials with multiple industrial and environmental applications. Their varied structures, from kaolinite to expandable smectites, offer a complex balance between chemistry and functionality. Various activation processes, whether thermal, chemical or surfactant-based, optimize their properties, making them adaptable to contemporary challenges.

Secondly, adsorption has been thoroughly studied as an essential process, playing a central role in many scientific and industrial applications. Its ability to effectively eliminate contaminants and its flexibility depending on the type of adsorbent and experimental conditions make it an essential technique, particularly in the fields of pollution control and water treatment.

Finally, the issue of heavy metals was addressed, highlighting their ubiquitous presence in the environment and the risks they pose. While some of these elements are essential to biology, their toxicity at high concentrations necessitates rigorous management, and anthropogenic pollution exacerbates this threat, underlining the urgent need to develop effective mitigation strategies.

I.5 REFERENCES

[1] Caillere, S., Henin, S., & Rautureau, M. (1982). Minéralogie des Argiles, I. Structure et Propriétés Physico-Chimiques, 2nd Edition, Masson.

[2] Grekov, D., Pré, P., & Grambow, B. (2019). On the use of manometry method for measurement of gas adsorption equilibria and characterization of clay texture with Derivative Isotherm Summation. Applied Clay Science, 184, 105372. https://doi.org/10.1016/j.clay.2019.105372.

[3] Cherian, C., Kollannur, N. J., Bandipally, S., & Arnepalli, D. N. (2018). Calcium adsorption on clays: Effects of mineralogy, pore fluid chemistry and temperature. Applied Clay Science, 160, 282–289. https://doi.org/10.1016/j.clay.2018.02.034.

[4] Djellabi, R., Ghorab, M., Cerrato, G., Morandi, S., Gatto, S., Oldani, V., Di Michele, A., & Bianchi, C. (2014). Photoactive TiO2–montmorillonite composite for degradation of organic dyes in water. Journal of Photochemistry and Photobiology a Chemistry, 295, 57–63. https://doi.org/10.1016/j.jphotochem.2014.08.017.

[5] Djellabi, R., Ghorab, M. F., Smara, A., Bianchi, C. L., Cerrato, G., Zhao, X., & Yang, B. (2019). Titania–Montmorillonite for the Photocatalytic Removal of Contaminants from Water: Adsorb & Shuttle Process. In Environmental chemistry for a sustainable world (pp. 291–319). https://doi.org/10.1007/978-3-030-17724-9_13.

[6] Schöny, G. (2015). Post Combustion CO2 Capture based on Temperature Swing Adsorption – from Process Evaluation to Continuous Bench Scale Operation. PhD Thesis, Vienna University of Technology.

[7] Uddin, M. K. (2016). A review on the adsorption of heavy metals by clay minerals, with special focus on the past decade. Chemical Engineering Journal, 308, 438–462. https://doi.org/10.1016/j.cej.2016.09.029.

[8] Velde, B. (1995). Composition and mineralogy of clay minerals. In Springer eBooks (pp. 8–42). https://doi.org/10.1007/978-3-662-12648-6_2.

[9] Caillere, S., & Henin, S. (1957). Proposition pour normaliser la nomenclature des minéraux Argileux, Bulletin du Groupe français des Argiles, 9-4, 77-83.

[10] Murray, H.H. (2006). Book. Applied clay mineralogy: occurrences, processing and applications of kaolins, bentonites, palygorskite-sepiolite, and common clays. Elsevier.

[11] Eslinger, E., & Pevear, D. (1988). Clay minerals for petroleum geologists and engineers (SEPM Short Course Notes No. 22, 405 pp.). Society of Economic Paleontologists and Mineralogists.

[12] Liu, H., Chang, L., Liu, W., Xiong, Z., Zhao, Y., & Zhang, J. (2019). Advances in mercury removal from coal-fired flue gas by mineral adsorbents. Chemical Engineering Journal, 379, 122263. https://doi.org/10.1016/j.cej.2019.122263.

[13] Rautureau, M., De Sousa Figueiredo Gomes, C., Liewig, N., & Katouzian-Safadi, M. (2017). Clay and Clay Mineral Definition. In Springer eBooks (pp. 5–31). https://doi.org/10.1007/978-3-319-42884-0_2.

[14] Prasad, Reid, K., & Murray, H. (1991). Kaolin: processing, properties and applications. Applied Clay Science, 6(2), 87–119. https://doi.org/10.1016/0169-1317(91)90001-p.

[15] Weaver, C. E. (1989). Clay, muds, and shales (Developments in Sedimentology, Vol. 44). Elsevier.

[16] Grim, R. E., Bray, R. H., & Bradley, W. F. (1937). The mica in argillaceous sediments. American Mineralogist, 22, 813–829.

[17] Mukherjee, S. (2013). Clays: Industrial Applications and their Determinants. In Springer eBooks (pp. 113–122). https://doi.org/10.1007/978-94-007-6683-9_7.

[18] Ismadji, S., Soetaredjo, F. E., & Ayucitra, A. (2015). Clay materials for environmental remediation (Springer Briefs in Molecular Science). Springer.

[19] Grim, R.E. (1962). Applied Clay Mineralogy. McGraw Hill Book, New York.

[20] Valasková, M., & Martynková, G. S. (2012). Clay minerals in nature: Their characterization, modification and application. In InTechOpen (pp. 209–238). https://doi.org/10.5772/b.bookID.

[21] Addison, J. (1995). Vermiculite: A review of the mineralogy and health effects of vermiculite exploitation. Regulatory Toxicology and Pharmacology, 21(3), 397–405. https://doi.org/10.1006/rtph.1995.1054.

[22] Borchardt, G. (2013). Smectites. In Soil Science Society of America book series (pp. 675–727). https://doi.org/10.2136/sssabookser1.2ed.c14.

[23] Ross, C. S., & Hendricks, S. B. (1945). Minerals of the montmorillonite group: Their origin and relation to soils and clays (79 pp.). U.S. Government Printing Office.

[24] Li, C., Shen, P., Zhao, Y., Li, P., Zhang, L., & Pan, H. (2022). Mineral chemistry of chlorite in different geologic environments and its implications for porphyry Cu ± Au ± Mo deposits. Ore Geology Reviews, 149, 105112. https://doi.org/10.1016/j.oregeorev.2022.105112.

[25] Gomes, C. S. F., & Rautureau, M. (2021). General data on clay science, crystallochemistry and systematics of clay minerals, clay typologies, and clay properties and applications. In Springer eBooks (pp. 195–269). https://doi.org/10.1007/978-3-030-65706-2_6.

[26] Theng, B. (2012). The Clay Minerals. In Developments in clay science (pp. 3–45). https://doi.org/10.1016/b978-0-444-53354-8.00001-3.

[27] Tournassat, C., Bourg, I. C., Steefel, C. I., & Bergaya, F. (2015). Surface properties of clay minerals. In Developments in clay science (pp. 5–31). https://doi.org/10.1016/b978-0-08-100027-4.00001-2.

[28] Morel, R. (1996). Les sols cultivés (373 p.). Lavoisier.

[29] Heller-Kallai, L. (2006). Chapter 7.2 Thermally Modified clay Minerals. In Developments in clay science (pp. 289–308). https://doi.org/10.1016/s1572-4352(05)01009-3.

[30] Zhang, T., Wang, W., Zhao, Y., Bai, H., Wen, T., Kang, S., Song, G., Song, S., & Komarneni, S. (2020). Removal of heavy metals and dyes by clay-based adsorbents: From natural clays to 1D and 2D nano-composites. Chemical Engineering Journal, 420, 127574. https://doi.org/10.1016/j.cej.2020.127574.

[31] Bonilla-Petriciolet, A., Mendoza-Castillo, D. I., & Reynel-Ávila, H. E. (2017). Adsorption processes for water treatment and purification. In Springer eBooks. https://doi.org/10.1007/978-3-319-58136-1.

[32] Rouquerol, F., Rouquerol, J., Sing, K. S. W., Llewellyn, P., & Maurin, G. (2013). Adsorption by powders and porous solids: Principles, methodology and applications (2nd ed., 626 p.). Elsevier.

[33] Salih, A.M. (2018). The purification of industrial wastewater to remove heavy metals and investigation into the use of zeolite as a remediation tool. PhD Thesis, University of Wolverhampton. http://hdl.handle.net/2436/621859.

[34] Emene, A.U. (2018). Biosorption of selected heavy metal ions and methylene blue from aqueous solution using chemically treated Luffa cylindrical. PhD Thesis. University of Sheffield, Sheffield, UK.

[35] Uwamariya, V. (2013). Adsorptive Removal of Heavy Metals from Groundwater by Iron Oxide based Adsorbents. PhD Thesis. University of the Witwatersrand, Johannesburg, South Africa.

[36] Belhaj, A. F., Elraies, K. A., Mahmood, S. M., Zulkifli, N. N., Akbari, S., & Hussien, O. S. (2019). The effect of surfactant concentration, salinity, temperature, and pH on surfactant adsorption for chemical enhanced oil recovery: a review. Journal of Petroleum Exploration and Production Technology, 10(1), 125–137. https://doi.org/10.1007/s13202-019-0685-y.

[37] Yousef, R., Qiblawey, H., & El-Naas, M. H. (2020). Adsorption as a process for produced water treatment: a review. Processes, 8(12), 1657. https://doi.org/10.3390/pr8121657.

[38] Wang, J., & Guo, X. (2020). Adsorption isotherm models: Classification, physical meaning, application and solving method. Chemosphere, 258, 127279. https://doi.org/10.1016/j.chemosphere.2020.127279.

[39] Bentahar, Y. (2016). Caractérisation physico-chimique des argiles marocaines : application à l'adsorption de l'arsenic et des colorants cationiques en solution aqueuse. PhD Thesis, Abdelmalek EssaâdiUniversity (Tetouan, Morocco).

[40] Giles, C. H., MacEwan, T. H., Nakhwa, S. N., & Smith, D. (1960). 786. Studies in adsorption. Part XI. A system of classification of solution adsorption isotherms, and its use in diagnosis of adsorption mechanisms and in measurement of specific surface areas of solids. Journal of the Chemical Society (Resumed), 3973. https://doi.org/10.1039/jr9600003973.

[41] Freundlich, H. (1932). Of the adsorption of gases. Section II. Kinetics and energetics of gas adsorption. Introductory paper to section II. Transactions of the Faraday Society, 28, 195. https://doi.org/10.1039/tf9322800195.

[42] Langmuir, I. (1918). The adsorption of gases on plane surfaces of glass, mica and platinum. Journal of the American Chemical Society, 40, 1361–1403.

[43] Nibou, D., Mekatel, H., Amokrane, S., Barkat, M., & Trari, M. (2009). Adsorption of Zn2+ ions onto NaA and NaX zeolites: Kinetic, equilibrium and thermodynamic studies. Journal of Hazardous Materials, 173(1–3), 637–646. https://doi.org/10.1016/j.jhazmat.2009.08.132.

[44] Sips, R. (1948). On the Structure of a Catalyst Surface. The Journal of Chemical Physics, 16(5), 490–495. https://doi.org/10.1063/1.1746922.

[45] Temkin, M. J., & Pyzhev, V. (1940). Recent modifications to Langmuir isotherms. Acta Physicochimica URSS, 12, 217–222.

[46] Chu, K. H. (2021). Revisiting the Temkin isotherm: dimensional inconsistency and approximate forms. Industrial & Engineering Chemistry Research, 60(35), 13140–13147. https://doi.org/10.1021/acs.iecr.1c01788.

[47] Wang, J., & Guo, X. (2020). Adsorption kinetic models: Physical meanings, applications, and solving methods. Journal of Hazardous Materials, 390, 122156. https://doi.org/10.1016/j.jhazmat.2020.122156.

[48] Lagergren, S. (1898). Zur Theorie der sogenannten Adsorption gelöster Stoffe. Kungliga Svenska Vetenskapsakademiens Handlingar, 24, 1–39.

[49] Ho, Y., & McKay, G. (1999). Pseudo-second order model for sorption processes. Process Biochemistry, 34(5), 451–465. https://doi.org/10.1016/s0032-9592(98)00112-5.

[50] Weber, W. J., & Morris, J. C. (1963). Kinetics of Adsorption on Carbon from Solution. Journal of the Sanitary Engineering Division, 89(2), 31–59. https://doi.org/10.1061/jsedai.0000430.

[51] Gibbs, J. W. (1873). A method of geometrical representation of the thermodynamic properties of substances by means of surfaces. Transactions of the Connecticut Academy of Arts and Sciences, 2, 382–404.

[52] Hoff, J. H. V. (1887). Die Rolle des osmotischen Druckes in der Analogie zwischen Lösungen und Gasen. Zeitschrift Für Physikalische Chemie, 1U(1), 481–508. https://doi.org/10.1515/zpch-1887-0151.

[53] Magna, E.K. (2020). Ecological and human health implications of contaminants linked with cage aquaculture in the volta basin of Ghana. PhD Thesis. University of Ghana.

[54] Halka, M., & Nordstrom, B. (2019). Transition metals (2nd ed., 146 p.). Chelsea House.

[55] Carolin, C. F., Kumar, P. S., Saravanan, A., Joshiba, G. J., & Naushad, M. (2017). Efficient techniques for the removal of toxic heavy metals from aquatic environment: A review. Journal of Environmental Chemical Engineering, 5(3), 2782–2799. https://doi.org/10.1016/j.jece.2017.05.029.

[56] https://fr.wikipedia.org/wiki/Cuivre.

[57] Vardhan, K. H., Kumar, P. S., & Panda, R. C. (2019). A review on heavy metal pollution, toxicity and remedial measures: Current trends and future perspectives. Journal of Molecular Liquids, 290, 111197. https://doi.org/10.1016/j.molliq.2019.111197.

[58] Acharya, J., Sahu, J., Mohanty, C., & Meikap, B. (2008). Removal of lead(II) from wastewater by activated carbon developed from Tamarind wood by zinc chloride activation. Chemical Engineering Journal, 149(1–3), 249–262. https://doi.org/10.1016/j.cej.2008.10.029.

[59] Atallah, B.M. (2021). Etude comparative de l'analyse de la regressionlineaire et non lineaire de l'echange d'ions metalliques sur des materiaux poreux, PhD Thesis, Houari Boumediene University of Science and Technology.

[60] https://fr.wikipedia.org/wiki/Plomb.

[61] Pandey, P. K., Sharma, S., & Sambi, S. (2015). Removal of lead(II) from waste water on zeolite-NaX. Journal of Environmental Chemical Engineering, 3(4), 2604–2610. https://doi.org/10.1016/j.jece.2015.09.008.

[62] Dórea, J. G. (2019). Environmental exposure to low-level lead (Pb) co-occurring with other neurotoxicants in early life and neurodevelopment of children. Environmental Research, 177, 108641. https://doi.org/10.1016/j.envres.2019.108641.

[63] Ravulapalli, S., & Kunta, R. (2018). Removal of lead (II) from wastewater using active carbon of Caryota urens seeds and its embedded calcium alginate beads as adsorbents. Journal of Environmental Chemical Engineering, 6(4), 4298–4309. https://doi.org/10.1016/j.jece.2018.06.033.

[64] Sharma, A., Kapoor, D., Wang, J., Shahzad, B., Kumar, V., Bali, A. S., Jasrotia, S., Zheng, B., Yuan, H., & Yan, D. (2020). Chromium bioaccumulation and its impacts on plants: An overview. Plants, 9(1), 100. https://doi.org/10.3390/plants9010100.

[65] DesMarias, T. L., & Costa, M. (2019). Mechanisms of chromium-induced toxicity. Current Opinion in Toxicology, 14, 1–7. https://doi.org/10.1016/j.cotox.2019.05.003.

[66] https://stock.adobe.com/dz/search?k=chromium.

[67] Hezil, N., Fellah, M., Assala, O., Touhami, M. Z., & Guerfi, K. (2018). Elimination of Chromium (VI) by Adsorption onto Natural and/or Modified Kaolinite. Diffusion Foundations, 18, 106–112. https://doi.org/10.4028/www.scientific.net/df.18.106.

[68] Genchi, G., Carocci, A., Lauria, G., Sinicropi, M. S., & Catalano, A. (2020). Nickel: Human Health and Environmental Toxicology. International Journal of Environmental Research and Public Health, 17(3), 679. https://doi.org/10.3390/ijerph17030679.

[69] Buxton, S., Garman, E., Heim, K. E., Lyons-Darden, T., Schlekat, C. E., Taylor, M. D., & Oller, A. R. (2019). Concise review of nickel Human Health toxicology and ecotoxicology. Inorganics, 7(7), 89. https://doi.org/10.3390/inorganics7070089.

[70] https://en.wikipedia.org/wiki/Nickel.

[71] Parades-Aguilar, J., Reyes-Martínez, V., Bustamante, G., Almendáriz-Tapia, F. J., Martínez-Meza, G., Vílchez-Vargas, R., Link, A., Certucha-Barragán, M. T., & Calderón, K. (2020). Removal of nickel(II) from wastewater using a zeolite-packed anaerobic bioreactor: Bacterial diversity and community structure shifts. Journal of Environmental Management, 279, 111558. https://doi.org/10.1016/j.jenvman.2020.111558.

[72] Ahmed, A. M. M., Ali, A. E., & Ghazy, A. H. (2019). Adsorption separation of nickel from wastewater by using olive stones. Advanced Journal of Chemistry – Section A, 2, 79–93.

[73] Ifegwu, C., & Anyakora, C. (2012). Screen for eight heavy metals from groundwater samples from a highly industrialized area in Lagos, Nigeria. African Journal of Pharmaceutical Sciences and Pharmacy, 3.

[74] Gassim, F. a. G. (2023). Mercury pollution: Dangers and treatment. In IntechOpen eBooks. https://doi.org/10.5772/intechopen.108390.

[75] Bjørklund, G., Crisponi, G., Nurchi, V. M., Cappai, R., Djordjevic, A. B., & Aaseth, J. (2019). A review on coordination properties of Thiol-Containing chelating agents towards

mercury, cadmium, and lead. Molecules, 24(18), 3247. https://doi.org/10.3390/molecules24183247.

[76] https://www.linkedin.com/pulse/mercury-liquid-metal-asha-t-h.

[77] Balali-Mood, M., Naseri, K., Tahergorabi, Z., Khazdair, M. R., & Sadeghi, M. (2021). Toxic mechanisms of five heavy metals: mercury, lead, chromium, cadmium, and arsenic. Frontiers in Pharmacology, 12. https://doi.org/10.3389/fphar.2021.643972.

[78] Genchi, G., Sinicropi, M., Carocci, A., Lauria, G., & Catalano, A. (2017). Mercury exposure and heart diseases. International Journal of Environmental Research and Public Health, 14(1), 74. https://doi.org/10.3390/ijerph14010074.

[79] Albatrni, H., Qiblawey, H., & El-Naas, M. H. (2020). Comparative study between adsorption and membrane technologies for the removal of mercury. Separation and Purification Technology, 257, 117833. https://doi.org/10.1016/j.seppur.2020.117833.

[80] World Health Organization. (2018). Assessment of prenatal exposure to mercury: Human biomonitoring survey – The first survey protocol (No. 15, pp. 1–59).

CHAPTER II

MATERIALS & METHODS

INTRODUCTION

This chapter comprehensively overviews the methodologies utilized to characterize natural and modified kaolin samples. It highlights various analytical techniques, including thermal analysis, morphological, and structural characterization methods, to examine the properties and behavior of materials.

These techniques are indispensable for understanding the samples' physical, chemical, and thermal attributes. By detailing each technique's principles, apparatus, and procedures, this chapter ensures a robust understanding of the experimental process and its applications to material science.

II.1 Characterization Methods

II.1.1 Morphological Characterization

Several Morphological Characterization techniques were used to analyze the samples obtained including them: scanning electron microscopy (SEM) coupled with energy dispersive spectroscopy (EDS) and Brunauer-Emmett-Teller (BET) analysis.

II.1.1.1 Scanning Electron microscopy

The scanning electron microscope is a powerful imaging technique used to identify the morphology and structure of samples and is equipped with an energy dispersive spectroscopy (EDS) device to examine chemical elements.

a. Principle

Scanning electron microscopy is based on the interaction between an electron beam and the surface of the sample to be analyzed. The impact of this beam, secondary electrons, backscattered electrons, and X-ray photons are emitted by the target. The electrons are selectively collected by detectors that transmit the signal to a cathode screen whose scanning is synchronized with the scanning of the beam on the sample and reconstructs a three-dimensional

image of the sample surface, where the secondary electrons provide topographic information while the backscattered electrons highlight the chemical contrast of the sample [1]

Figure II.1 displays the SEM principle schematic diagram.

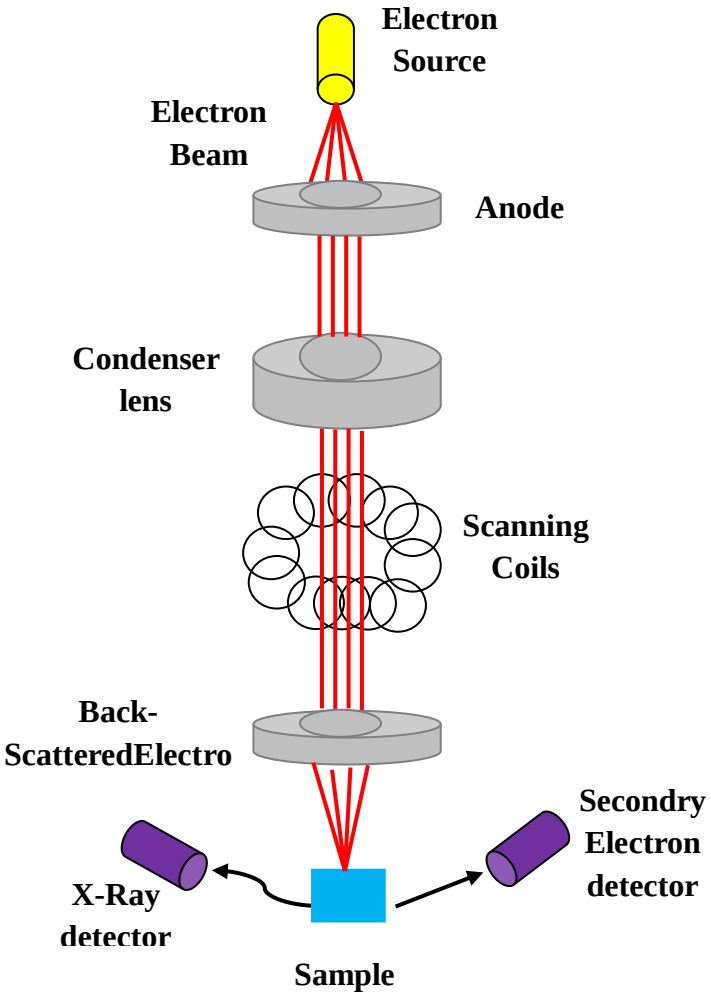

Figure II.1: Schematic representation of the principle of SEM.

b. Apparatus

The technique of scanning electron microscopy (SEM, TESCAN MIRA Germany) was employed to identify the morphology and structure of specimens (clays).

Figure II.2: SEM type TESCAN MIRA, Germany.

II.1.1.2 Surface Area Analysis

The determination of the specific surface area represents an essential parameter to obtain information on the structure and morphology of samples, especially for porous materials such as clays, and it has been estimated by the so-called BET method (Brunauer, Emmett and Teller, which is based on the adsorption of gas (nitrogen) on the surface of the material, the amount of gas adsorbed, at a given pressure, makes it possible to determine the specific surface area, the volume and the distribution of the pores as well as the energies of the adsorption and desorption reactions.

The BET model is based on the following assumptions:

- The surface of the adsorbent is considered homogeneous, without significant irregularities.
- All adsorption sites are equivalent in energy (Identical adsorption sites).
- Formation of multilayers.
- The interactions between the adsorbed molecules are negligible due to weak Van Der Waals type bonds.

The specific surface area can be determined from the following equation **(**Eq. II.1**).**

$$S_{BET} = \frac{v_m * s * N}{V * m} \quad \text{..... (Eq. II.1)}$$

Where:

S_{BET} : specific BET surface ($m^2.g^{-1}$).

v_m: monolayer volume (cm^3).

s : Surface area occupied by an adsorbate molecule (cm^2).

N : Avogadro number ($molecule.mol^{-1}$).

V : the molar volume of the adsorbate gas ($L.mol^{-1}$).

m : masse of the sample (g).

The monolayer volume is determined by the following BET equation **(**Eq. II.2**).**

$$\frac{P}{V(P_0 - P)} = \frac{1}{V_m C} + \frac{C-1}{V_m C}\frac{P}{P_0} \quad \text{..... (Eq. II.2)}$$

Where:

P: Equilibrium pressure.

P_0 : Saturation pressure at the adsorption temperature.

V: Volume of the adsorbed gas.

V_m: monolayer volume.

C: BET constant.

This equation is valid only in the range for which the relative pressure is between 0.05 and 0.3.

a. Apparatus

The surface area, pore size, and volume of Nat-kaolin and DPA-kaolin were characterized by using (BET, NOVA 4000e) N_2 sorption-desorption at 77 K.

Figure II.3: BET, NOVA 4000e.

II.1.2 Structural Characterization

Structural Characterization techniques are essential for analyzing a material's properties and behaviors include: X-ray diffraction (XRD), Fourier Transform Infrared Spectroscopy (FTIR), and Thermogravimetric Analysis (TGA).

II.1.2.1 X-ray diffraction

X-ray diffraction is a fundamental technique for the characterization of materials. It consists of diffracting X-rays on a flat solid sample or a powder, and it is used to identify the nature and structure of crystallized products. Indeed, this method only applies to crystalline media (rocks, crystals, minerals, pigments, clays, etc.) presenting the characteristics of the crystalline state.

a. Principle of X-ray diffraction

This technique relies on projecting an X-ray beam onto the crystalline sample. This phenomenon results from an interaction between the X-ray beam and the crystalline sample [2]. The crystalline property of the latter requires preferred directions for the incident X-ray beam. This phenomenon was discovered by Max Von Laue [3] (Figure II.4).

Bragg [3] suggested a different measurement method and a straightforward explanation for monochromatic X-ray diffraction. Bragg's analysis assumes that the crystals or atomic planes (lattice planes—hkl) are in layers, and we can determine the interplanar distance dhkl from the following formula (Eq. II.3).

$$2.d_{hkl}.\sin\theta = n.\lambda \quad \text{(Eq. II.3)}$$

Where:

d_{hkl} is the interplanar distance (Å).

θ is the diffraction angle (°).

n is the order of reflection.

λ Wavelength of radiation used (nm).

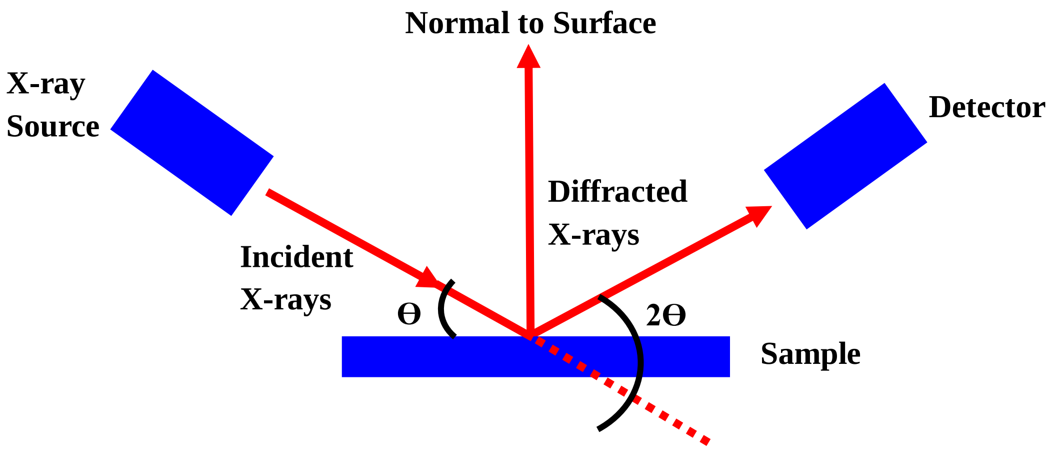

Figure II.4: Schematic representation of the principle of XRD.

b. Apparatus

Powder XRD was utilized to record the X-ray diffractogram using Cu-kα copper radiation of (λ = 1.5406 Å works in the 2θ range between (2-80) with a step of 0.02° and a scan time of 1 s/step at 40 KV and 20 mA.

II.1.2.2 FTIR Analysis

Fourier transform infrared spectroscopy (FTIR) is an analytical technique used to identify functional groups in organic and inorganic compounds by measuring their absorption of infrared radiation across a range of wavelengths.

a. Principle of FTIR Analysis

To obtain an infrared spectrum (a fingerprint) of the sample, the absorption of electromagnetic radiation by chemical species in the infrared region of the electromagnetic spectrum from 4000 to 400 cm^{-1} will excite the vibrational movements of chemical bonds. These vibrations can be classified into two types: elongation vibrations (symmetric and asymmetric), called valence vibrations. They occur when two atoms periodically move closer or further apart along their common axis, and the second type, angular deformation vibrations, correspond to a modification of the bond angle. There are four possible vibrations (rocking, scissoring, wagging and twisting) [4].

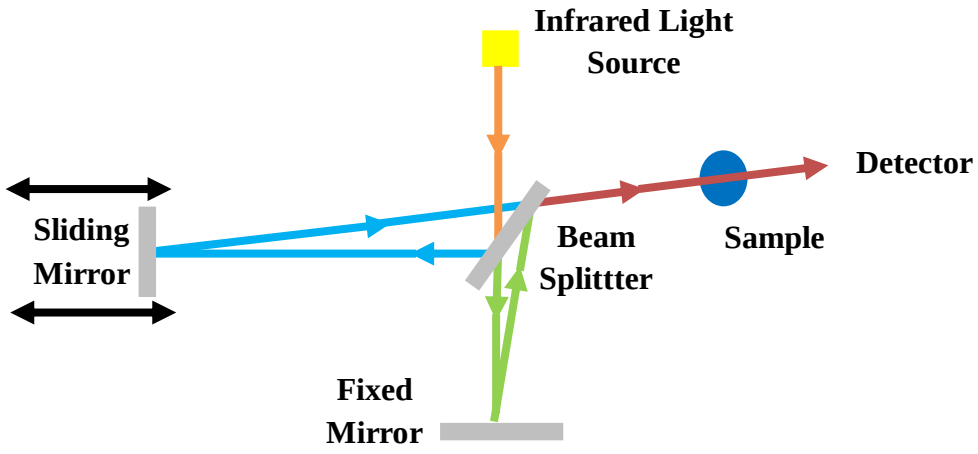

Figure II.5: Schematic representation of the principle of FTIR.

b. Apparatus

Infrared spectroscopy (PerkinElmer) (Figure II.6) was utilized to recognize the chemical substances found in our samples. Approximately 1 mg of the sample was mixed with 250 mg of KBr powder to obtain pellets. The pellets were obtained after applying a pressure of 10 bars for one minute using a Uniaxial press machine (Figure II.7). The measurements were carried out in the range 4000-400 cm^{-1} in transmission mode, with a resolution of 4 cm^{-1}.

Figure II.6: Infrared spectroscopy (PerkinElmer).

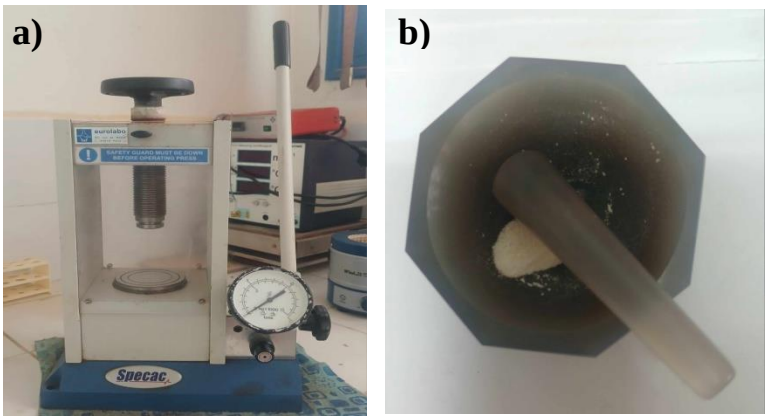

Figure II.7: a) Uniaxial press machine b) a mortar.

II.1.3 Thermal Analysis

a. Thermogravimetric and differential thermal analyzes

Gravitational thermal analysis (TGA) coupled with differential thermal analysis (DTA) allows for monitoring of the physicochemical properties of materials during heating: TGA consists of monitoring the mass loss of a material as a function of the treatment temperature, which allows monitoring the phenomena of dehydration, dehydroxylation, and combustion. On the other hand, DTA consists of monitoring the evolution of the heat flow of a material within its environment, which allows for monitoring the thermal reactions (endothermic, exothermic) and the oxidation phenomena of organic matter that occur when a compound is heated.

b. Apparatus

Thermogravimetric analysis (TGA) and differential thermal analysis (DTA) of the materials were performed on a TGA instrument (TGA/ DSC 3+ 1600°, METTLER TOLEDO) under an argon atmosphere. The instrument was heated from room temperature to a maximum temperature of 1000 °C at a rate of 10 °C per minute.

Figure II.8: TGA instrument (TGA/ DSC 3+ 1600°, METTLER TOLEDO).

II.2 Materials and methods of study

II.2.1 Material

Diphenylamine DPA (Figure II.9) ($C_{12}H_{11}N$; MW = 169.23 g/mol) was purchased from Fluka (purity > 99 %), and their properties and chemical compositions are shown in Table II.1. BIOCHEM Chemopharma (France) supplied lead nitrate [$Pb(NO_3)_2$], copper nitrate [$Cu(NO_3)_2$], Sodium hydroxide (NaOH), and hydrochloric acid (HCl) were acquired from Merck in Germany. Sodium lauryl sulfate (SLS) (Figure II.10) ($C_{12}H_{25}SO_4Na$; 288,38 g/mol) and Sodium dodecylbenzenesulfonate (SDBS) (Figure II.11) ($C_{18}H_{29}NaO_3S$; 348,48 g/mol), these products were purchased from Fluka (purity > 99 %), and their properties and chemical compositions are shown in Table II.2. Mercuric sulfate ($HgSO_4$) was acquired from Merck in Germany. The solutions of these products were prepared in double-distilled water.

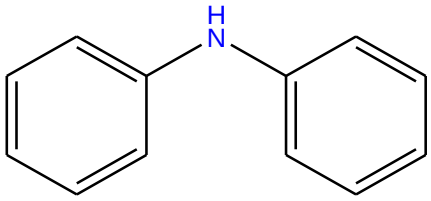

Figure II.9: Chemical formula of DPA.

Table II.1: Properties and chemical compositions of DPA.

Properties	DPA
Chemical formula	$C_{12}H_{11}N$
Purity	>98%
Solubility	0.05 g/l
Melting point	53 °C
Density	1.2 g/cm^3

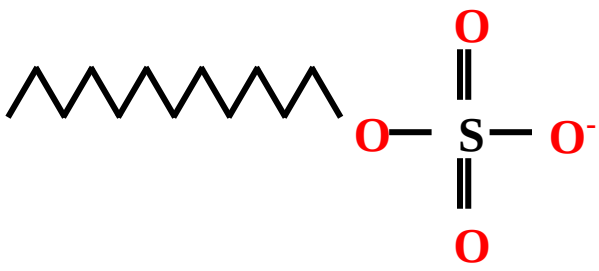

Figure II.10: Chemical formula of SLS

.

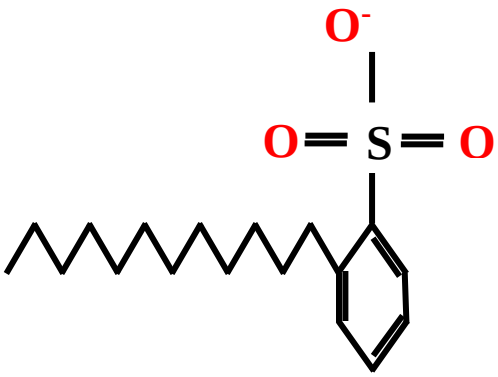

Figure II.11: Chemical formula of SDBS.

Table II.2: Properties and chemical compositions of SLS, and SDBS.

Properties	SLS	SDBS
Chemical formula	$NaC_{12}H_{25}SO_4$	$C_{12}H_{25}C_6H_4SO_3Na$
Purity	>99%	>99%
Solubility	100 $g.L^{-1}$	100 $g.L^{-1}$
Melting point	204 to 207 °C	287.63 °C
Density	1.01 $g.cm^{-3}$	1.02 $g.cm^{-3}$

II.2.2 Sampling of kaolin studied

The kaolin utilized in this paper was acquired from the Guelma region in northeastern Algeria. Its chemical composition examined using X-ray fluorescence is as follows. 45.12 % SiO_2, 11.20% Al_2O_3, 24.03% Fe_2O_3, 0.24% MnO, 0.53% MgO, 0.15% CaO, and 18.73% H_2O.

II.2.3 The modification of kaolin

The kaolin powder was subjected to a triple cleaning cycle with deionized water, followed by a drying process at 105°C for a duration of six hours in an oven, with the objective of achieving complete elimination of contaminants.

II.2.3.1 The modification of kaolin by DPA

Kaolin powder was cleaned three times with deionized water and dried for twenty-four hours at 105 °C in an oven to eliminate contaminants. At first, the solid (kaolin) is treated with HCl solution, concentration 1 M, after filtration and washing with deionized water several times to remove chloride ions, then the kaolin is modified by adding DPA (0.5M) solution, and the organic cations tend to occupy each exchangeable site on the surface as they exchange with the mineral cations. After the reaction is complete, the altered clay is rinsed with deionized water, dried, and ground again.

II.2.3.2 The modification of kaolin by SDBS, and SLS

In order to prepare kaolin modified with sodium dodecyl benzene sulfonate (K-SDBS) and sodium lauryl sulfate (K-SLS), it is necessary to first disperse 25 g of kaolin powder into 500 ml of deionized water. Subsequently, 0.015 mol of SDBS solution and 0.017 mol of SLS solution are introduced into the kaolin emulsion in a stepwise manner, with continuous stirring, at a temperature (approximately 25 °C) higher than the critical micelle concentration (CMC) of SDBS and SLS. The resulting modified kaolin is then subjected to filtration, washing, and drying at 105 °C for 6 h and then ground using a mortar passing through a 200 μm sieve.

II.2.3.3 The modification of kaolin by mixture of (SLS+SDBS)

The preparation of K-M involves the gradual addition of a solution consisting of a mixture of sodium dodecyl benzene sulfonate (SDBS) 0.015 mol and sodium lauryl sulfate (SLS) 0.017 mol in equal proportions to the kaolin emulsion, while stirring continuously. Subsequent to this, the kaolin is washed, filtered, and dried.

Figure II.12 represents an overview of the preparation of natural and modified Kaolin, as well as the characterization techniques employed.

II.2.4 Preparation of metal solutions

Stock solutions of Pb(II) (1g/L), Cu(II) (1g/L), and Hg(II) (1 g/L) were prepared by dissolving a known quantity of metal salts of $Pb(NO_3)_2$, $Cu(NO_3)_2$, and $HgSO_4$, respectively, in deionized water. The desired concentrations were obtained by diluting the stock solution to defined concentrations, ranging from 10 to 100 mg/L. Calibration curves were established to determine the equilibrium concentrations.

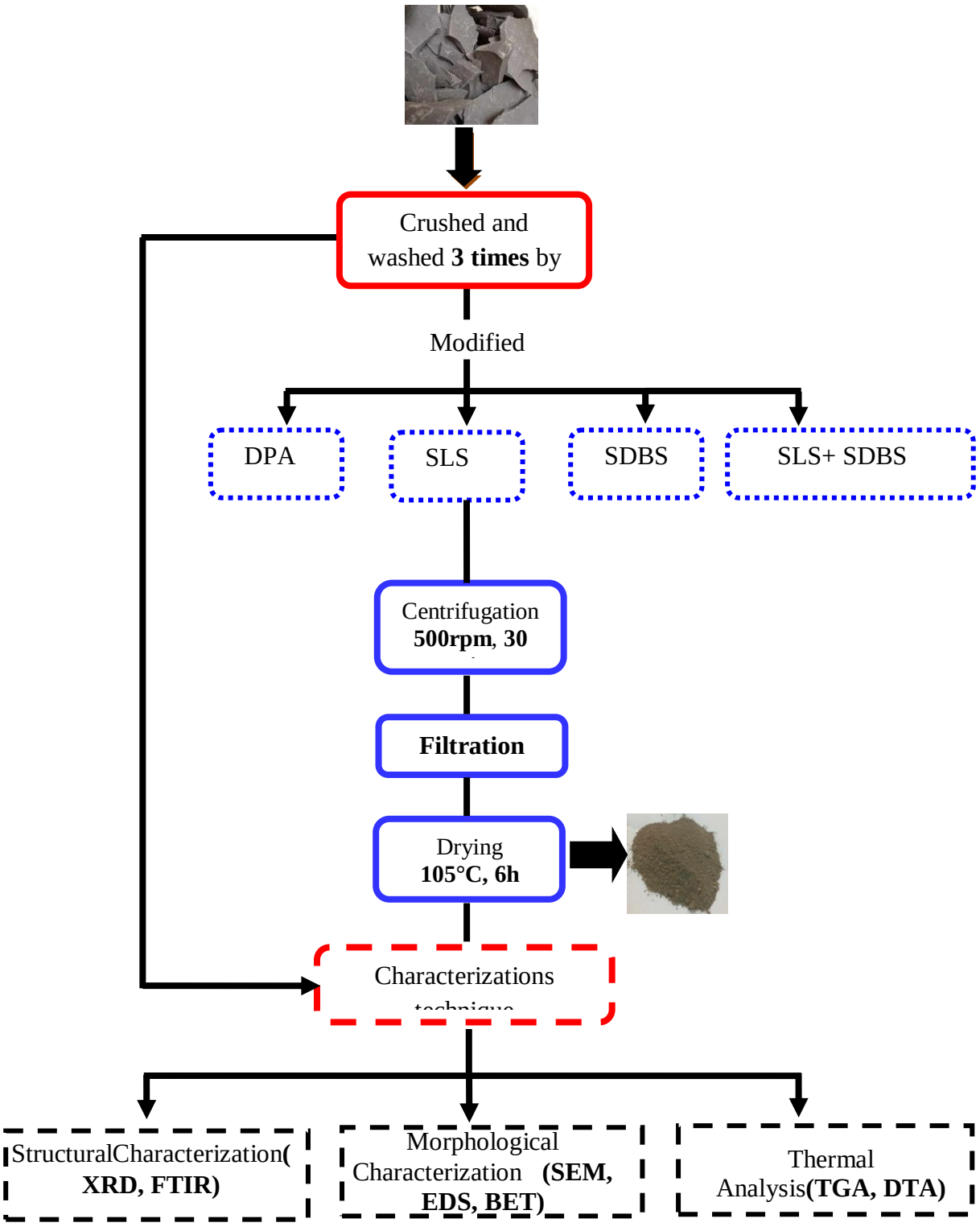

Figure II.12: Sample preparation process and characterization methods of both natural kaolin and modified kaolin.

II.3 CONCLUSION

This chapter underscores the significance of experimental techniques in characterizing and understanding material properties. The integration of thermal, morphological, and structural analyses provides a holistic approach to investigating the complex nature of kaolin samples. The detailed descriptions of methodologies and their applications pave the way for reproducibility and further advancements in material characterization studies. In addition to the characterization techniques, this chapter also presents the materials and methods used for the modification of kaolin and for adsorption experiments. The methodological details presented in this chapter ensure a comprehensive understanding of the experimental approach and contribute to the reliability and reproducibility of the study.

II.4 REFERENCES

[1] Akhtar, K., Khan, S. A., Khan, S. B., & Asiri, A. M. (2018). Scanning Electron Microscopy: Principle and applications in Nanomaterials characterization. In Springer eBooks (pp. 113–145). https://doi.org/10.1007/978-3-319-92955-2_4.

[2] Ali, A., Chiang, Y. W., & Santos, R. M. (2022). X-ray Diffraction Techniques for Mineral Characterization: A review for engineers of the fundamentals, applications, and research directions. Minerals, 12(2), 205. https://doi.org/10.3390/min12020205.

[3] Surdu, V., & Győrgy, R. (2023). X-ray Diffraction Data Analysis by Machine Learning Methods—A review. Applied Sciences, 13(17), 9992. https://doi.org/10.3390/app13179992.

[4] Patrizi, B., De Cumis, M. S., Viciani, S., & D'Amato, F. (2019). Dioxin and related compound detection: Perspectives for Optical Monitoring. International Journal of Molecular Sciences, 20(11), 2671. https://doi.org/10.3390/ijms20112671.

CHAPTER III

KAOLIN CHARACTERIZATION

INTRODUCTION

This chapter focuses on the detailed characterization of natural kaolin (K) and its modifications using diphenylamine and two anionic surfactants, sodium lauryl sulfate (SLS) and sodium Dodecylbenzene sulfonate (SDBS), as well as their mixture (K-M). Various analytical techniques have been employed to evaluate these kaolin samples' structural, thermal, and textural properties. The objective is to understand how surfactant modification influences kaolin's physical and chemical behavior, particularly its thermal stability, morphology, and surface properties. The chapter explores these aspects through thermal analyses (TG/DTA), infrared spectroscopy (FT-IR), microscopy (SEM), elemental analysis (EDX), X-ray diffraction (XRD), and nitrogen sorption-desorption isotherms.

III.1 DPA modified-kaolin characterization

III.1.1 Particle size distribution of Nat-kaolin

The determination of the particle size distribution of kaolin involves analyzing the range and proportion of particle sizes present in the sample. This process is essential for understanding and optimizing kaolin's properties.

The particle size distribution of Nat-kaolin and DPA-kaolin is shown in Figure III.1 The results of this analysis indicate that half of the particles were smaller than 30 µm, as shown by Nat-kaolin in Figure III.1 These results are consistent with earlier studies [1,2] which found that the majority of kaolin particle sizes were in the 25–35 µm range. There is not much of a change in the profile of the DPA-kaolin particle size curve displayed in Figure III.1 Thus, it may be said that the particle size is unaffected by the alteration.

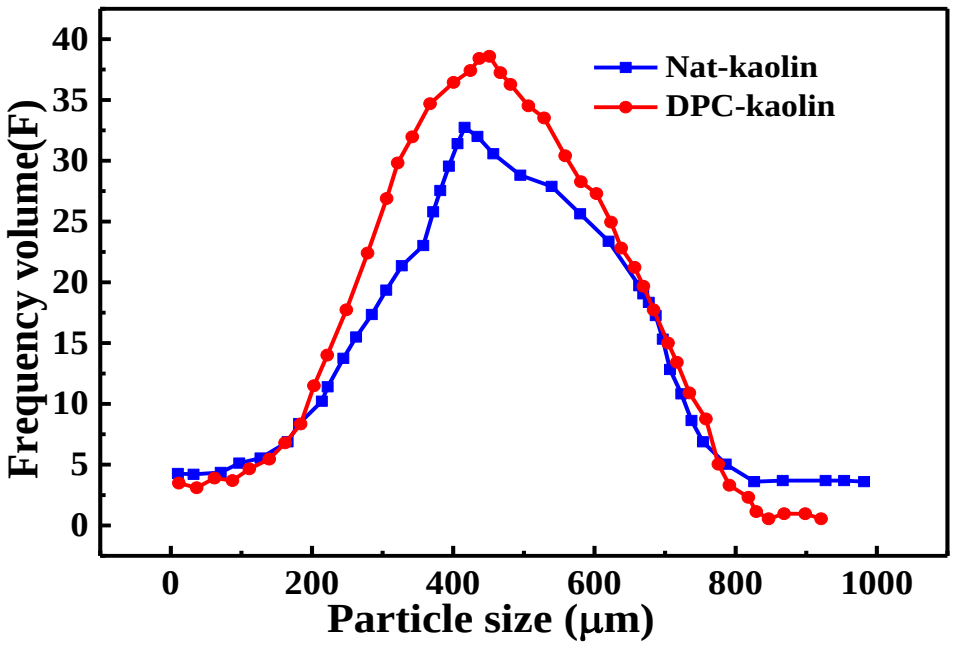

Figure III.1: Particle size distribution on Nat-kaolin and DPA-kaolin.

III.1.2 Microscopy analysis

Scanning electron microscope (SEM) observation was used for the sole purpose of examining the morphology of the different adsorbents prepared.

The SEM pictures of the Nat-kaolin and DPA-kaolin are shown in Figure III.2 Regarding the Nat-kaolin clay, Figure III.2a demonstrates that the sample is made up of platelet-shaped, fine, flat, hexagonal particles [3,4] The crystalline structure of the minerals that make up kaolin, primarily kaolinite, is responsible for this shape [5,6], in addition to sizable white clusters of undesirable particles. A similar result was found by *Hezil et al*., [7] when the cationic surfactant DTAC modified kaolin. Figure III.2b shows that the altered sample retained some structural resemblance to Nat-kaolin [8-10].

Nevertheless, it was found that the DPA-kaolin's morphology had a slight distortion in the particles due to impurities, which make up nearly all of Nat-kaolin's surface, being treated with HCl [11-13], after the removal of big white clusters.. Additionally, the successful alteration of kaolin by acid and then DPA was validated by the findings of the morphological change (SEM) of Nat-kaolin and the characteristics XRD and FTIR of DPA-kaolin.

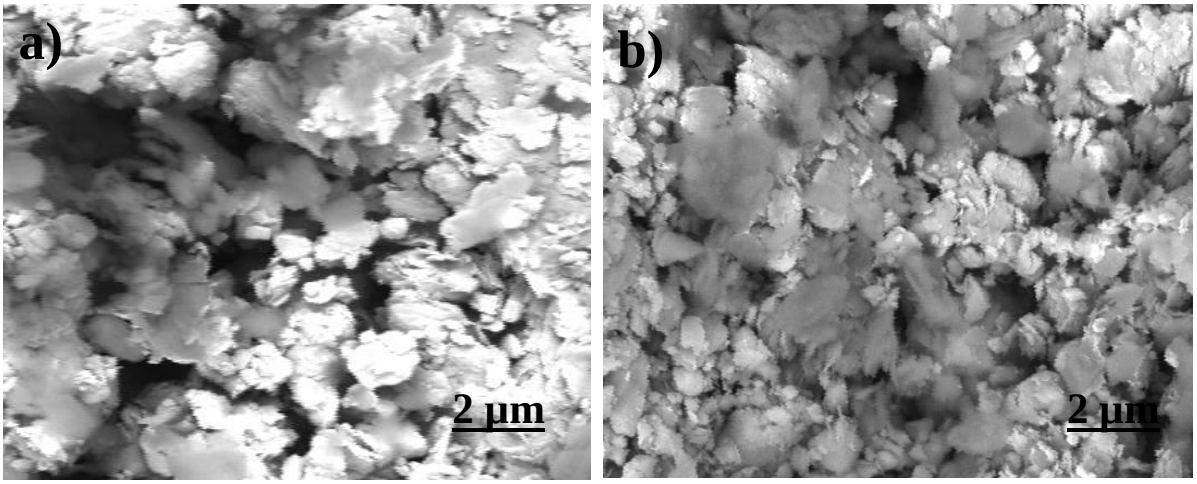

Figure III.2: Scanning electron microscopy of the Kaolin, a) natural Kaolin, b) modified Kaolin.

III.1.3 Energy dispersion X-ray (EDX)

Energy dispersion X-ray (EDX) is primarily used to identify and quantify the elemental composition of materials. it is a technique often integrated with scanning electron microscopy to provide compositional information at the micro or nanoscale.

The energy dispersive X-ray values of Nat and DPA kaolin are shown in Table III.1 The measured concentrations of Si, Al, and O are significantly higher, coming in at 29.52, 32.00, and 38.48 percent, respectively, as shown in Table III.1 They are caused by the layered aluminosilicates structures seen in Nat-kaolin. (Al_2O_3 and SiO_2 layer) [14].

When kaolin is treated with inorganic acid (HCl), the kaolin particles disintegrate and impurities are removed, changing the kaolin's chemical compositions and structures and resulting in a decrease of approximately 10.76% in Al and 10.38% in Si in the DPA-kaolin [15]. This result aligns with the conclusions reached by *Yahaya et al.*, [16]. The presence of DPA in the DPA-kaolin sample was verified by the arrival of trace amounts of C and N, roughly 5.13 and 3.16 percent, respectively. According to *Zhang et al.*, [17], this result is in line with their study, which found that the kaolin was modified by 3-(aminopropyl) triethoxysilane ($C_9H_{23}NO_3Si$) and that nitrogen was present on its surface at a weight percentage of 1.98 and carbon at a weight percentage of 7.35.

Table III.1: EDX analysis of Nat-kaolin and DPA-kaolin.

	O		Al		Si		C		N	
	wt.%	**Error %**	**wt. %**	**Error %**	**wt. %**	**Error %**	**wt. %**	**Error %**	**wt. %**	**Error %**
Nat-kaolin	38.48	1.29	32	1.13	29.52	1.32	/	/	/	/
DPA-kaolin	51,32	1.41	21,24	1.25	19,14	1.17	5.13	0.845	3.16	0.787

III.1.4 X-ray Diffraction Analysis

The XRD diffraction pattern of both Nat-kaolin and DPA-kaolin is shown in Figure III.3 Large, asymmetric peaks from the mineral kaolinite (K) are visible on the diffractogram, along with small-intensity peaks from impurities including mica (M) and quartz (Q)**.** The International Centre for Diffraction Data (ICDD) card numbers 14–164 state that kaolinite, which has the chemical formula $Si_2Al_2O_5(OH)_4$, is a component of Nat-kaolin, while ICDD card numbers 33–1161 show quartz, which has the chemical formula SiO_2. [18,19] Using ICDD 00–029–1490 [20], ICDD 001–0527 [21], ICDD 00–014–016 [22], and ICDD 00–029–1488 [23], as reference codes, the crystalline planes of (001), (-110), (002), (-202), and (-133) are identified as belonging to the diffraction patterns of 12.3, 20.7, 23.8, 38.4, and 55.12◦, respectively, and are suggestive of kaolinite. Furthermore, additional patterns that corresponded to the codes ICDD 070–3755 showed the presence of quartz [21, 24], and ICDD 00–046–1045 [23]. Similar outcomes were mentioned by *Shaban et al*., [25], *Khabbouchi et al*., [26], and *Aimdate et al*., [27]. The presence of quartz was demonstrated by the discovery of additional peaks at two theta angles of roughly 26.88° [26, 27]. The presence of DPA chains between the kaolin sheets is demonstrated by the d-spacing value of kaolin increasing from 7.15 Å to 7.25 Å and the recognizable diffraction peak of kaolin moving from 12.3◦ to 12.5◦ following the alteration of kaolin by DPA. Similar outcomes were noted by *Maged et al*., [28] for a functionalized biochar-clay composite containing a particular chemical. The kaolinite interlayer spacing in the composite increased from 7.26 Å to 10.17 Å. *Belachew and Hinsene* [29] also reported the similar performance during the CTAB surfactant modification of kaolin.

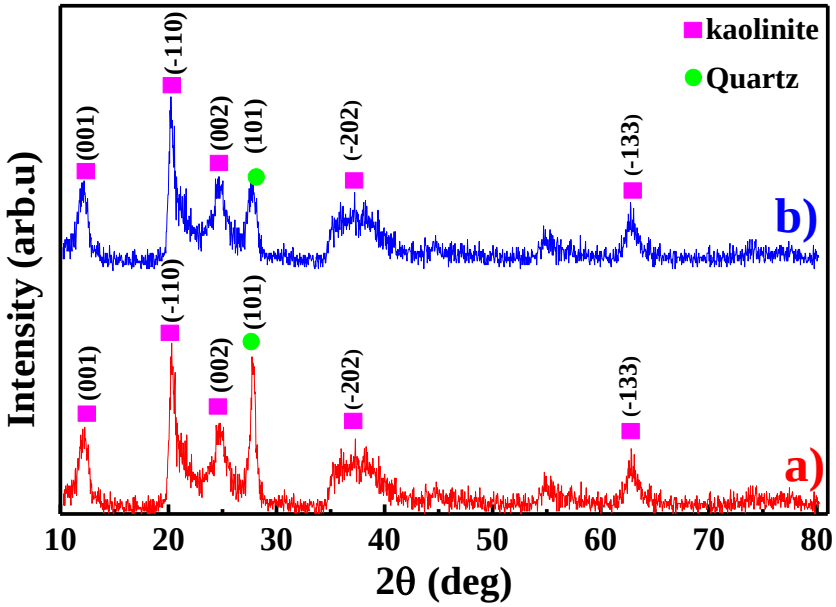

Figure III.3: The XRD pattern of Kaolin, a) Nat-kaolin and b) DPA-kaolin.

III.1.5 Thermogravimetric and differential thermal analyses of kaolin

The results of the thermogravimetric and differential thermal analyses performed on kaolin are shown in Figure III.4 There was a two-step weight decrease on the TG curve, as seen in Figure III.4 At 60°C, the evaporation of adsorbed water and the production of kaolin caused the first weight loss (1.5%), whereas at 500°C, the dehydroxylation of kaolin caused the second weight loss (9%), which corresponded to the endothermic peak at 500°C. [14, 30-32]. As the DTA curve (Figure III.4) illustrates. According to *Torres-Luna and Carriazo* [33], commercial natural kaolin (Caomin C08) caused weight loss of roughly 4.5% and 13.5% at 45 and 500 ◦C, respectively. Additionally, these findings are consistent with those reported by *Saukani et al*., [34]. Kaolin was pre-dehydroxylated between 20 and 50 °C, and during the dehydroxylation process, which took place between 430 and 650 °C, 9.3% of its mass was lost.

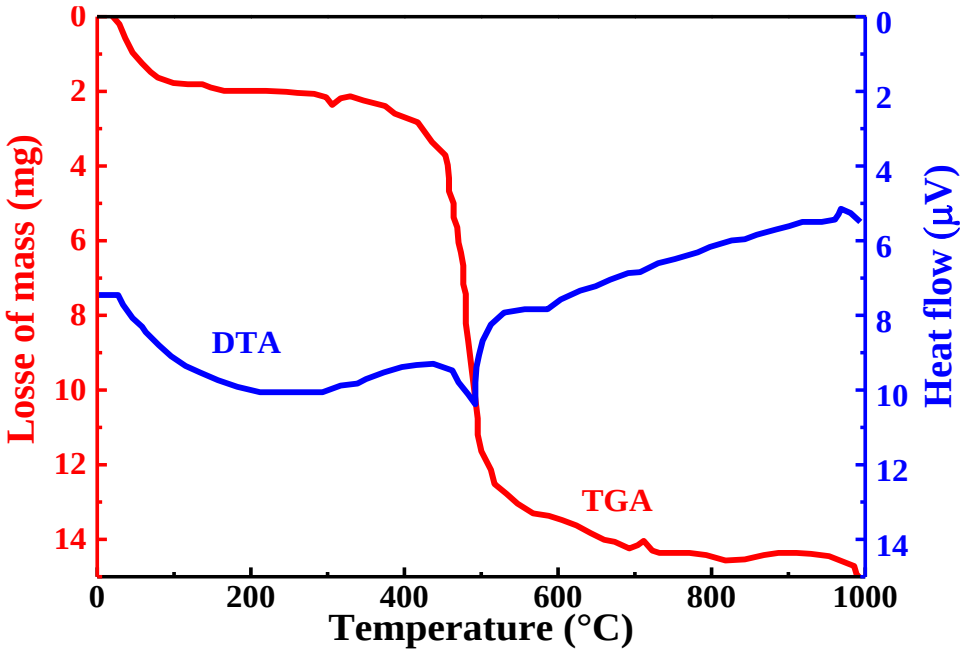

Figure III.4: DTA/TG curves of Nat-kaolin at a rate of 10° C/min.

III.1.6 Fourier-transform infrared spectroscopy

The bands at 3698.61 cm^{-1} and 3467.41 cm^{-1} in Figure III.5 relate to the OH stretching vibration of inner-surface hydroxyl groups in the Nat-kaolin clay. Furthermore, it was determined that the OH inner-hydroxyl group was responsible for the band at 3623.28 cm^{-1} [35, 36] In the meantime at 1091.04, 1035.32, and 470.82 cm^{-1}, respectively, the bands emerged, corresponding to the Si-O bending vibration. [37, 38]. The band at 911.67 cm^{-1} represented the Al–OH bending vibration [39, 40]. The bands that appeared at 752.42 cm^{-1} and 690.74 cm^{-1} were due to the Al-OH deformation [36]. Finally, the band at 535.22 cm^{-1} corresponded to the Si-O-Al stretching vibration [38]. The occurrence of absorption bands at 528 cm^{-1} and 460 cm^{-1}, which correspond to the bonding of Si-O, was proof of Si-O-Al bonding in previous research [28].

The DPA-kaolin shown in Figure III.5 exhibits the typical absorption bends of Nat-kaolin with the appearance of new vibration bands at 1248 cm^{-1}, corresponding to the C-N of DPA [41]. According to a different study the C-N mode appears at about 1235 cm^{-1}. The aromatic C-H stretching vibration band is located at 3032 cm^{-1} [42].

On the other hand, the phenyl ring C—C vibration was represented by the bands at 1528 cm^{-1}, 1597 cm^{-1}, and 1662 cm^{-1}, whereas the N-H bonds (amine group) of DPA were responsible for the band at 3360 cm^{-1}. An Ag/ESM sample showed N-H stretching at about 3275 cm^{-1} in research by *Maged et al.*, [28]. The results showed that the kaolin modification was effective.

By adding arginine salt (Arg salt) to montmorillonite [43], achieved the same outcomes. The C-N stretching vibration was found to be an absorption peak at 1348 cm^{-1} in their investigation. Additionally, the carboxyl vibration was identified as the band that emerged at 1502 cm^{-1}, whereas the N-H vibration was identified as the band at 3377 cm^{-1}. Additionally, when they synthesized a cobalt-diphenylamine complex to explore the removal of heavy metals from wastewater, another study [44, 24], discovered infrared spectroscopy results comparable to ours.

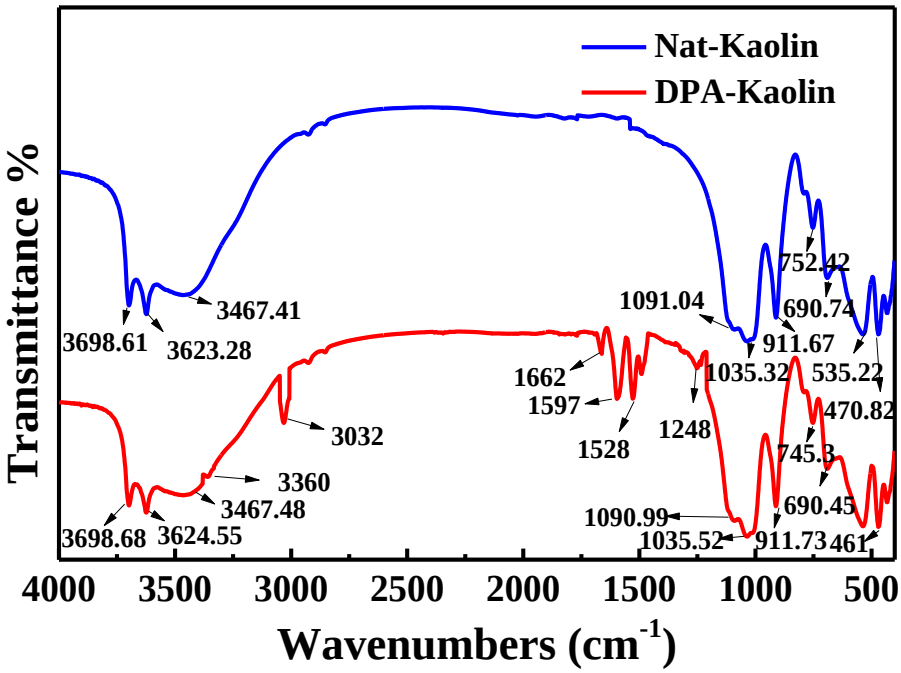

Figure III.5: The FT-IR spectral of Nat-kaolin and DPA-kaolin from 4000 to 400 cm^{-1}.

III.1.7 Nitrogen adsorption-desorption isotherms and specific surface area of both Nat-kaolin and DPA-kaolin

The N_2 adsorption-desorption isotherms of Nat-kaolin and organic DPA-kaolin at 77 K, as shown in Figure III.6a**,** show that both kaolin's isotherms closely resemble the category IV isotherm according to the International Union of Pure and Applied Chemistry's (IUPAC) isotherm categorization [45]. Since the amount of N_2 adsorbed by both kaolin increased gradually, each sample also contained H3 hysteresis loops made up of irregularly sized agglomerated particles [46]. However, because the modification altered the pore size of the Kaolin, the amount of N_2 adsorbed by organically altered kaolin was greater than that of Nat-kaolin. It is possible to calculate the BET plot, which is shown in Figure III.6b. The measurement values in the relative pressure area between 0.05 and 0.35 are applied to determine the Brunauer-Emmett-Teller (BET) surface area in accordance with IUPAC guidelines [47]. The obtained surface area increased by 25% after the modification (from 66.69 $m^2.g^{-1}$ to 71.35 $m^2.g^{-1}$) *Chai et al*., [48] reported similar outcomes, finding that after acid treatment, the specific pore volume and BET surface area of raw kaolin from Malaysia Sdn increased by 3.57% and 84.58%, respectively, with the BET surface area of modified kaolin being 1.85 times greater than that of unprocessed kaolin.

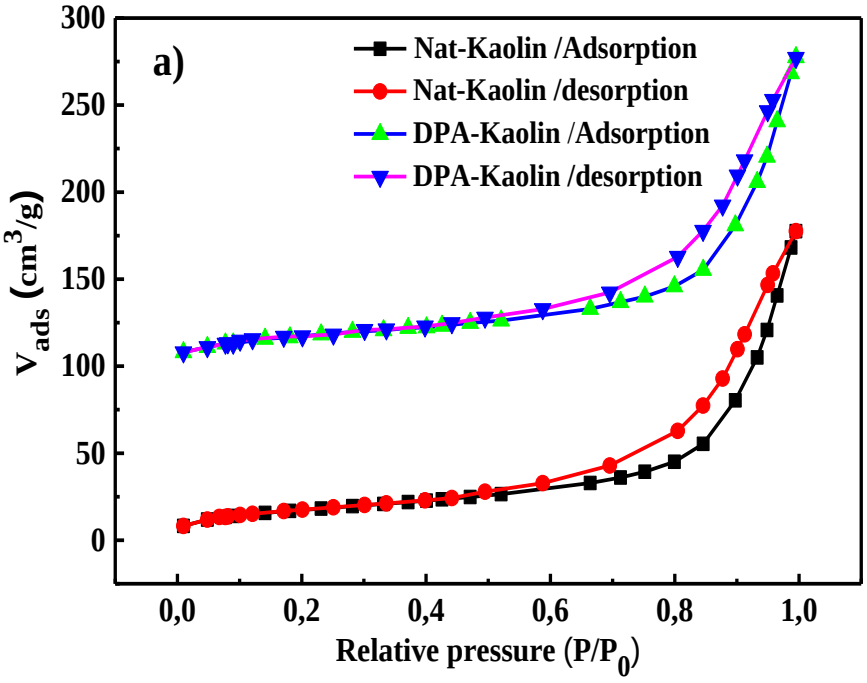

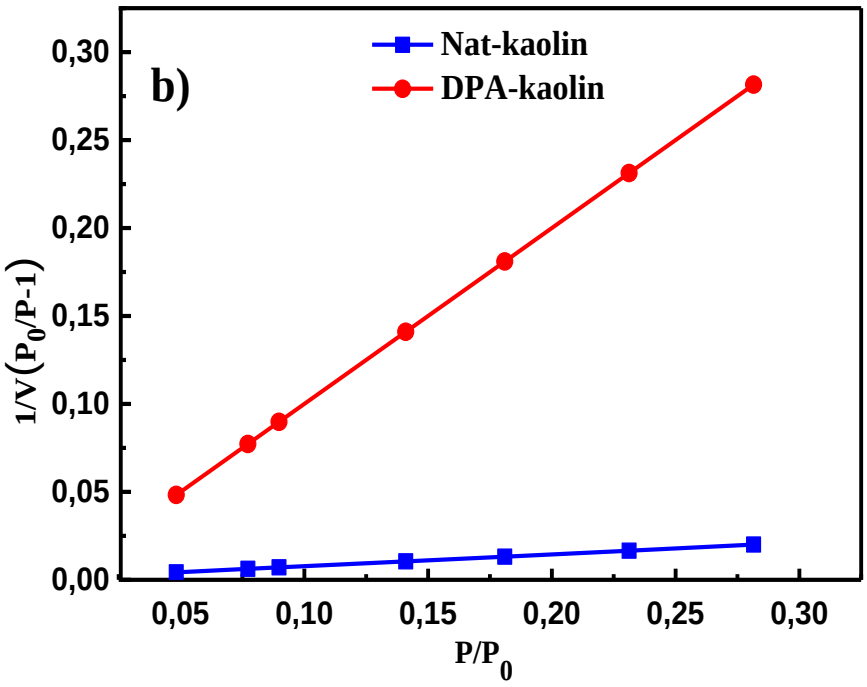

Figure III.6: a) Adsorption / desorption isotherms of nitrogen and b) the BET surface area plot on Nat-kaolin and DPA-kaolin.

III.2 Surfactants modified-kaolin characterization

III.2.1 Thermal analyses

In order to perform thermogravimetric and differential thermal analyses (TG/DTA), the mass change and the heat flow of each specimen were plotted against temperature. The differential thermal analysis and thermogravimetric curves for the four kaolin types (K(a), K-SLS(b), K-SDBS(c), and K-M(d)) are shown in Figure III.7.

Within the temperature range of 100 °C to 200 °C, the TG curves of K (Figure III.7a) show a 1.5% mass loss, indicative of the loss of interlayer and adsorbed water. A mass loss of 3.27% was found between 400 °C and 600 °C. This is attributed to the process of dehydroxylation of kaolinite, which results in the formation of metakaolin through the removal of hydroxyl groups from the kaolin structure.

The DTG curves (Figure III.7a) exhibited two endothermic peaks that corresponded to the weight loss phases. These peaks, indicative of thermal processes such as dehydration and dehydroxylation, occurred at approximately 400 °C and 600 °C, respectively. At 995 °C, an

exothermic signal was detected, indicating the transformation of metakaolin into amorphous silica SiO_2 and mullite [49, 50]. These results are consistent with those of [30], where two endothermic peaks and one exothermic peak were discovered on Algerian Tamazarte kaolinite at 133 °C, 580 °C, and 995 °C, respectively, along with a 1.5% weight loss at 114 °C and a 10% weight loss at 580 °C.

TG curves for modified kaolin K-SLS (Figure III.7b) demonstrate a weight loss of 1.18% at approximately 300 °C, attributable to the removal of adsorbed water, which corresponds to the endothermic peak between 100 and 300 °C. At approximately 600 °C, a more pronounced weight loss of 5.39% is observed. This observation indicates the occurrence of a significant dehydroxylation process, a phenomenon that may be amplified by the incorporation of chemicals (SLS) that serve to reduce the decomposition temperature. This reduction in temperature corresponds to the aforementioned endothermic peak, which is observed between 400 and 600 °C [51]. These findings are consistent with those reported by *Zuo et al.*, [52], who identified an endothermic peak accompanied by a mass loss of 2.2% between 400 and 600 °C. Furthermore, a notable endothermic peak with a mass loss of 12.5% between 60 and 200°C was identified on kaolinite treated with sodium dodecyl sulfate [52].

In addition, the TG/DTA curves of K-SDBS (Figures III.7c) demonstrate an initial weight loss of only 0.5%, the smallest among the samples, suggesting minimal moisture content or reduced water adsorption capability. The major thermal decomposition stage shows a weight loss of 2.35%, which is significantly lower than both K and K-SLS. This suggests that SDBS may inhibit the dehydroxylation process by increasing the structural stability of kaolin, and the numerous organic groups in SDBS may prevent hydroxyl from being released [53].

Finally, K-M (Figure III.7d) displays an initial weight loss of 0.59%, which is greater than K-SDBS, although this is still minimal. However, due to the presence of additives, the main weight loss event is more significant at 4.85%.

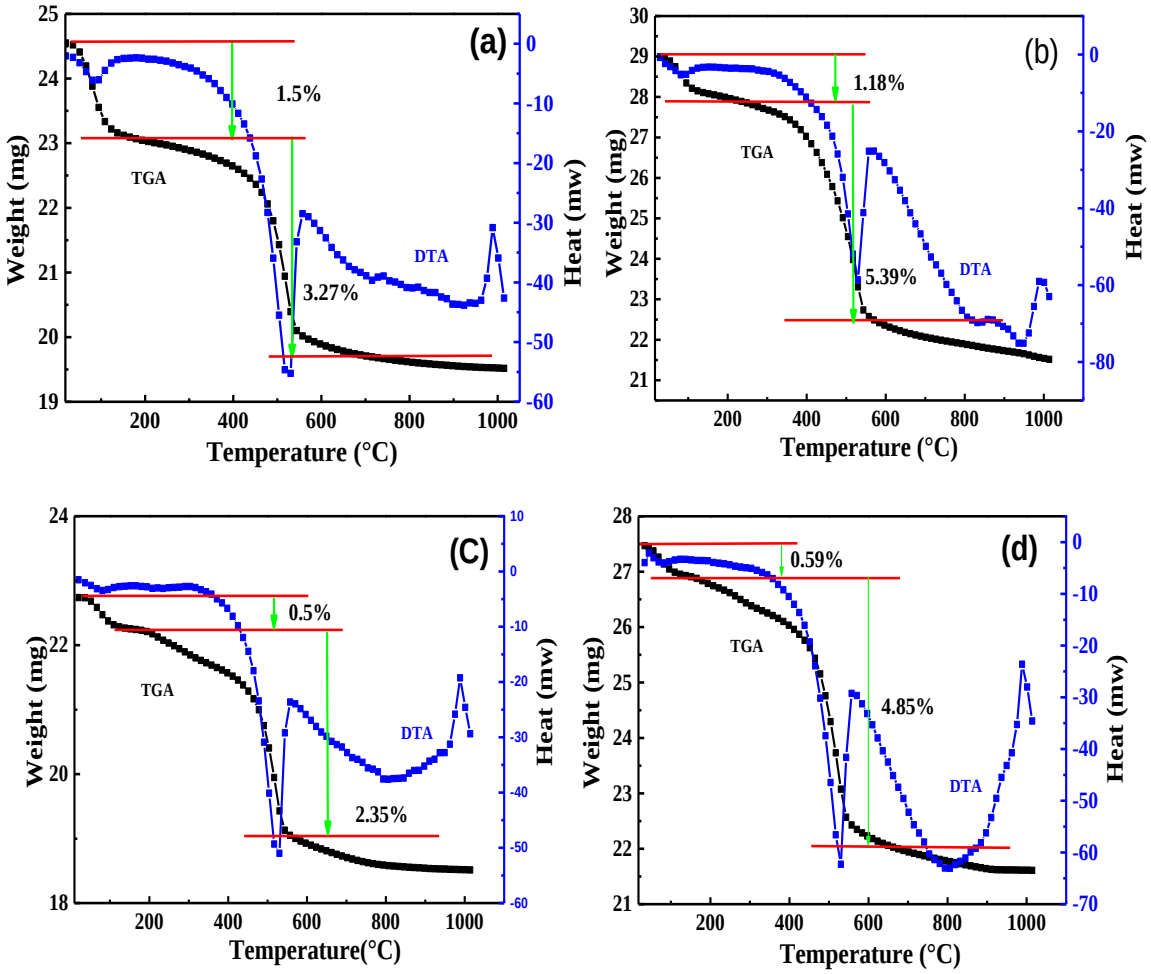

Figure III.7: The thermogravimetric and differential thermal analyses (TG/DTA) of: K(a), K-SLS(b), K-SDBS(c) and K-M(d).

III.2.2 Infrared spectroscopy analysis

The infrared spectrum of the four kaolin types, K(a), K-SLS(b), K-SDBS(c), and K-M(d), is displayed in Figure III.8. In the case of K (a) samples (Figure III.8), the bands situated at 3698 cm^{-1} and 3623 cm^{-1} were assigned to the stretching vibrations of hydroxyl groups (OH) [54]. The bands recorded at 3465 cm^{-1} and 1635 cm^{-1} correspond to the bending vibrations of water molecules [55]. Furthermore, the bands observed at 1090 cm^{-1}, 1036 cm^{-1}, and 471 cm^{-1} are attributed to Si-O the stretching vibrations [56]. Additionally, the sharp band at 912 cm^{-1} represents the Al–OH bending vibration [39]. The two bands located at 753 cm^{-1} and 691 cm^{-1} are attributed to Al-OH deformation [57]. The last band situated at 536$cm^{-1}$is attributed to the Si-O-Al stretching vibration [58]. As illustrated in Figure III.8, the typical absorption bends

observed in K(a) samples exhibit the emergence of new vibration bands located at 2927 cm^{-1} and 2855 cm^{-1}. These bands correspond to the C-C chain's symmetric and asymmetric stretching vibrations, respectively [52]. The bands situated at 1472 cm^{-1} and 1383 cm^{-1} are ascribed to C-O and S=O, respectively [59, 60], which suggests the existence of SLS. In addition to the analogous peaks observed in the K-SLS (b) samples, the K-SDBS (c) samples exhibit a novel band at 1600 cm^{-1}, which is corresponding to the C=C vibration of the benzene ring.

The K-M (d) samples (Figure III.8) exhibit comparable absorption bends to those observed in the K-SLS (b) and K-SDBS (c) samples, thereby confirming the successful alteration of kaolin by SLS, SDBS, and a combination of both. A previous investigation by *Merrikhpoura et al*., [61] has demonstrated that the formation of a bending vibration of the H–C–H groups between 1,625–1,750 cm^{-1} in the region from 1,400 to 1,500 cm^{-1}, after SDS modification of bentonite. In another investigation published by *Andrunikand Bajda*., [55] where they confirm the effectiveness of the modification of bentonite with TX100 by the presence of the following weak absorption bands, which represent methylene groups ($-CH_2$), 1541 cm^{-1}, 1354 cm^{-1}, and 1246 cm^{-1}, which represent CH stretching and bending as well as CO and OH bending vibrations of TX100 molecules, and a band at 1643 cm^{-1}, which represents C–C bonds of phenyl rings.

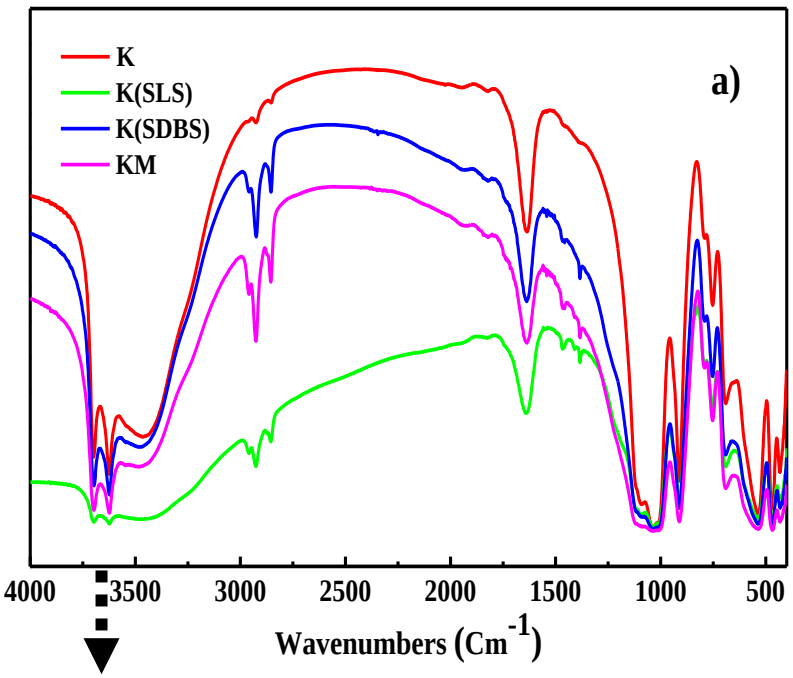

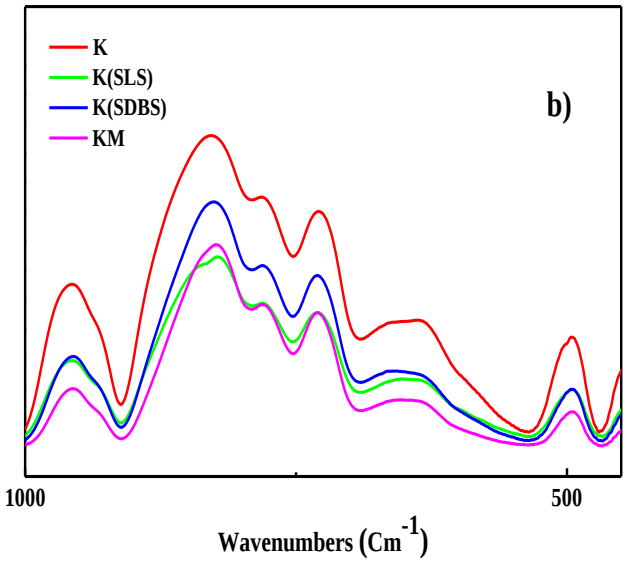

Figure III.8: a) The FT-IR spectral of K(a), K-SLS(b), K-SDBS(c) and K-M(d)from 4000 to 400 cm^{-1} and b) presentation of the peaks from 1000 to 500 cm^{-1}.

III.2.3 Microscopy analysis

The pictures from the scanning electron microscope of the four kaolin types K(a), K-SLS(b), K-SDBS(c), and K-M(d), are presented in Figure III.9. It was observed that the natural kaolin (K(a)) exhibits a relatively homogeneous and compact structure with irregularly shaped particles [62]. The particles appear relatively smooth with some larger aggregates visible [63].

Moreover, the SEM image of K-SLS (b) displays a less compact structure in comparison to the natural kaolin K(a), resulting in a surface that is rough with noticeable voids or pores [64]**.** This evidence corroborates the assertion that the surfactant has altered the particle arrangement [65].

Furthermore, the K-SDBS(c) structure shows greater clarity in porosity and a more disordered particle arrangement than that observed in previous samples. The particles are more irregularly shaped and dispersed [66]**.** The increased porosity and surface irregularity are indicative of effective surface modification [66].

Finally, the SEM of modified kaolin by the mixture of both surfactants K-M exhibits a structure that seems to combine characteristics of both K-SLS and K-SDBS. It shows a

moderately porous and less compact structure [55], with particles that are more uniformly dispersed compared to the natural kaolin.

The modification of the kaolin by surfactants has resulted in notable alterations to its morphology, characterized by a rougher surface, a less compact structure and a clear porosity. These findings are in accordance with the findings of a previous research [52, 55, 60].

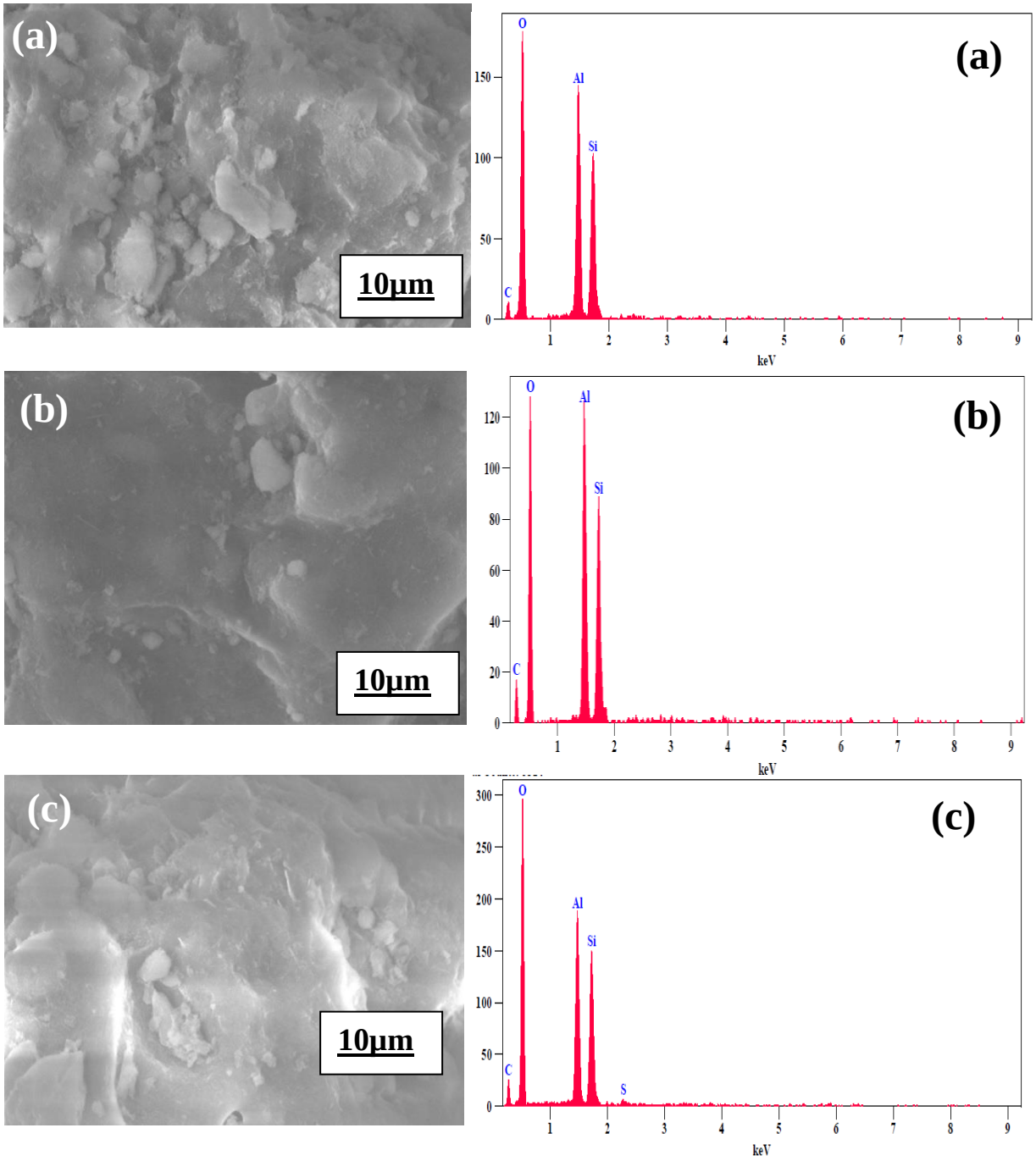

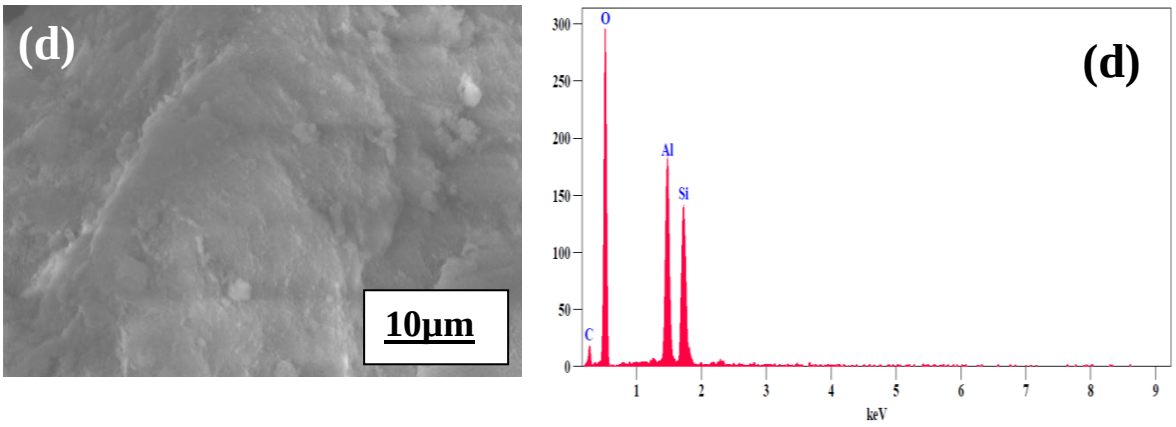

Figure III.9. The SEM and EDS images of: K(a), K-SLS(b), K-SDBS(c)and K-M(d).

III.2.4 Energy dispersion X-ray (EDX)

Figure III.9 illustrates the EDS images of the four kaolin types K(a), K-SLS(b), K-SDBS(c), and K-M(d), It is evident that the presence of Silicon (Si), aluminum (Al),and oxygen (O) in with a value of 18.03%, 19.11%, and 56.42%, respectively, on natural kaolin K(a) as munched in Table III.2 indicated that these elements constitute the main components of kaolin ($Al_2Si_2O_5(OH)_4$) [67], and the tiny carbon (C) peak around 6.44% could be due to surface contamination [68]. In contrast, the EDS spectrum of K-SLS (b) displays comparable peaks to those observed in natural kaolin K (a), albeit with diminished intensity, suggestive of surface alterations. The presence of carbon (C) by 23.97% is pronounced, potentially attributable to the hydrocarbon chains of the SLS surfactant [69]. Furthermore, in the case of K-SDBS(c), the existence of sulfur (S) peak at 0.76%, and the increase in the amount of carbon (C) at about 19.21% confirmed the addition and adsorption of SDBS surfactant onto kaolin samples surface, in addition to the presence of oxygen (O), aluminum (Al), Silicon (Si) with a value of 54.13%, 13.08%, and 12.83%, respectively [70].

Ultimately, the modified kaolin, K-M (d), exhibits analogous peaks to those observed in K-SDBS (c), thereby substantiating the intercalation of SDBS surfactant between the silicate layers. Conversely, the overall diminution in the intensity of the Al and Si peaks indicates that both surfactants were involved in the modification process [70].

Similar findings were also reported by *Monteiro et al.*, [71] demonstrating the existence of ionic and nonionic surfactant mixture functional groups in between the bentonite's silicate layers.

Table III.2: EDX analysis of four types of kaolin: K, K-SLS, K-SDBS, and K-M.

	O	Al	Si	C	S
	wt.%	wt. %	wt. %	wt. %	wt. %
k	56.42	19 .11	18.03	6.44	/
K-SLS	48.18	14.82	13.04	23.97	/
K-SDBS	54.13	13.08	12.83	19.21	0.76
K-M	56.79	14.13	14.28	14.80	/

III.2.5 X-ray Diffraction Analysis

The patterns of XRD diffraction of the four kaolin types K(a), K-SLS(b), K-SDBS(c), and K-M(d) are displayed on Figure III.10 Using the ICDD (International Centre for Diffraction Data) database cards to verifying and contrasting kaolin lines of diffraction.

From Figure III.10 the natural kaolin K(a) (black spectrum) shows intense peaks mainly located around 2theta= 12.03°, 20.09°, 24.50°,26.47°,29.97°, 36.51°,54.75°,62.66°,73.93°, and 77.15°. According to ICDD 00-029-1488 [72], ICDD 00-029-1490 [22], ICDD 00-014-016 [73], and ICDD 001-0527 [34], as reference codes. These peaks correspond to the crystal planes (001), (-110), (002), (012), (111), (003), (220), (222), (132), and (320) respectively, indicative of kaolinite. Other patterns revealed the presence of quartz in kaolin based on these codes JCPDS no. 46-1045 [39], and JCPDS no 085-0504 [74]. Whereas, the modified kaolin by SLS surfactant K-SLS (red spectrum),displayChanges in the intensity and two new peaks appearing at around 2theta=21.00° and 42.58° are observed, the diffraction peak shifted from 12.3° to 12.6°indicating successful intercalation of SLS molecules onto kaolin samples. This modification enhances the hydrophobic properties of the kaolin, as the surfactant replaces exchangeable cations and alters the surface characteristics. a modification compared to natural kaolin. *Bayram et al.*, [75] mentioned the same performance throughout the modification of montmorillonite using sodium dodecyl sulfate surfactant.

Furthermore the modified kaolin by SDBS surfactant K-SDBS (blue spectrum) shows similair peaks to those observed in the natural kaolin they are often less intense with a new peak

appeared at 2theta=8.85° this demonstrates the interaction of SDBS surfactant on kaolin layers was sucssessfly. A similar finding was reported *by Ni et al.,* [68] during the modification of montmorillonite by anionic surfactant sodium Dodecylbenzene sulfonate.

Finally in the case of modified kaolin by mixture of both surfactant K-M (magenta spectrum) display a similair peaks of the natural kaolin K (black spectrum) with no change was observed after kaolin modification by the mixture of both surfactant this might suggest that the adsorption of each surfactant onto the surface of kaolin did not affect its interlayers. The same remarks were mentioned in a previous literature [55].

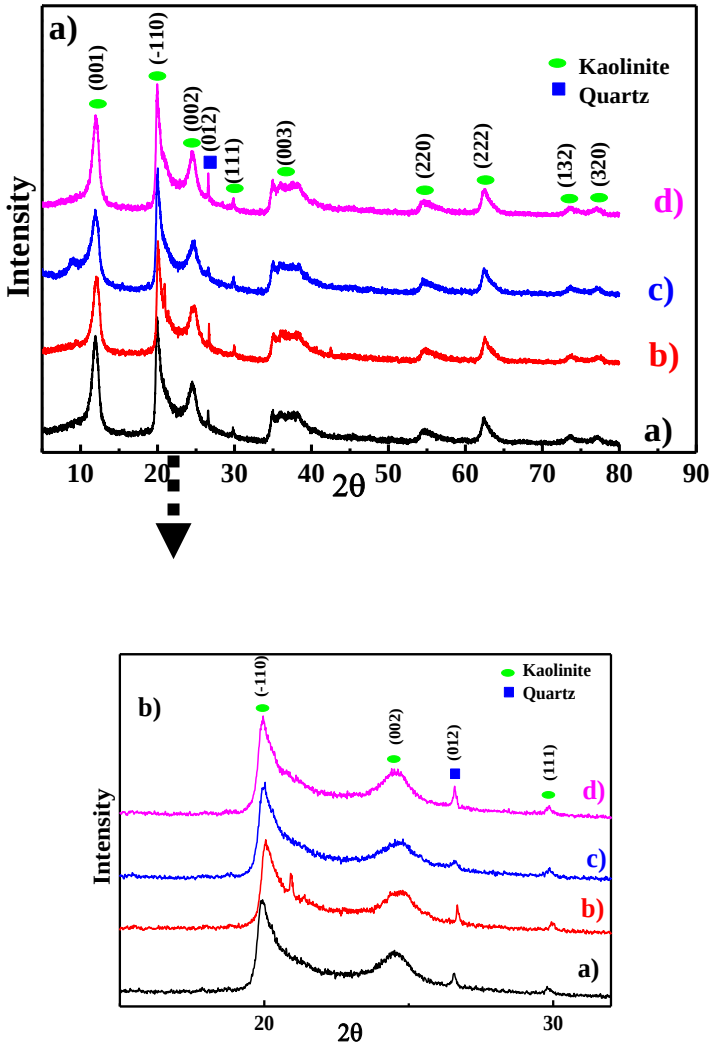

Figure III.10: a)The XRD pattern of: K(a), K-SLS(b), K-SDBS(c)and K-M(d) from 10° to 80° and b) presentation of the peaks from 15° to 30°.

III.2.6 Nitrogen sorption-desorption isotherms and specific surface area

Figure III.11a displays the N_2 adsorption-desorption isotherms of four types of kaolin (K, K-SDBS, K-M, and K-SLS) at 77 K, based on the International Union of Pure and Applied Chemistry (IUPAC), the isotherms of all types of kaolin approximate the category IV isotherm [76]. Indicating that the mesoporous structures all samples were consistent with monolayer-multilayer adsorption and included some macro- and micro porosity [76-78]. Every sample also contained H3 hysteresis loops, consisting of aggregated particles [78].

According to the isotherms, the amount of nitrogen gas adsorbed by four types of kaolin is raised gradually until all of the pores are saturated, whereas the amount of N_2 adsorbed by surfactant-modified kaolin K-SLS was higher than the other three types of kaolin due to enhanced mesoporosity by altering the arrangement of clay particles, creating more interparticle voids, improving the surface structure to allow more adsorption sites for nitrogen molecules.

The BET transformation in Figure III.11b was performed by representing $P/V(P_0-P)$ as a function of the relative adsorbed pressures P/P_0 from 0.05 to 0.35 to calculate the specific surface area BET of four types of kaolin, where the resulting surface area increased by 38.3%, 31.9% and 17.5% of K-SLS, K-SDBS and K-M respectively after modification, *Budash et al.*, [79] obtained similar outcomes after treating montmorillonite with acid, they discovered that the montmorillonite's specific BET surface area increased from 83.61 to 216.43 m^2/g.

Table III.3: Total Pore Volume, Average Pore Size, and BET surface area values of four types of kaolin: K, K-SLS, K-SDBS, and K-M.

Adsorbent	BET surface area($m^2.g^{-1}$)	Average Pore Size (A°)	Total Pore Volume ($cm^3.g^{-1}$)
K	44.6	93.2	0.082
K-SLS	82.9	93.2	0.139
K-SDBS	62.1	98.3	0.103
K-M	76.5	87.6	0.127

Table III.3 provides an overview of Total Pore Volume, Average Pore Size, and BET surface area of four types of kaolin. According to the Table III.3, the value of specific surface area of natural kaolin increased by 38.3% from44.6 $m^2.g^{-1}$ to 82.9 $m^2.g^{-1}$ after the modification of kaolin by sodium lauryl sulfate (SLS) anionic surfactant, and by 17.5% from 44.6 $m^2.g^{-1}$ to 62.1 $m^2.g^{-1}$after the modification of kaolin by sodium lauryl sulfate (SDBS) anionic surfactant, and by 31.9% from 44.6 $m^2.g^{-1}$ to 76.5 $m^2.g^{-1}$ after the modification of kaolin by the mixture of two anionic surfactant (SLS) and (SDBS). After these results, we can conclude that the ideal surfactant used to modify kaolin is sodium lauryl sulfate (SLS) anionic surfactant which had a higher BET surface.

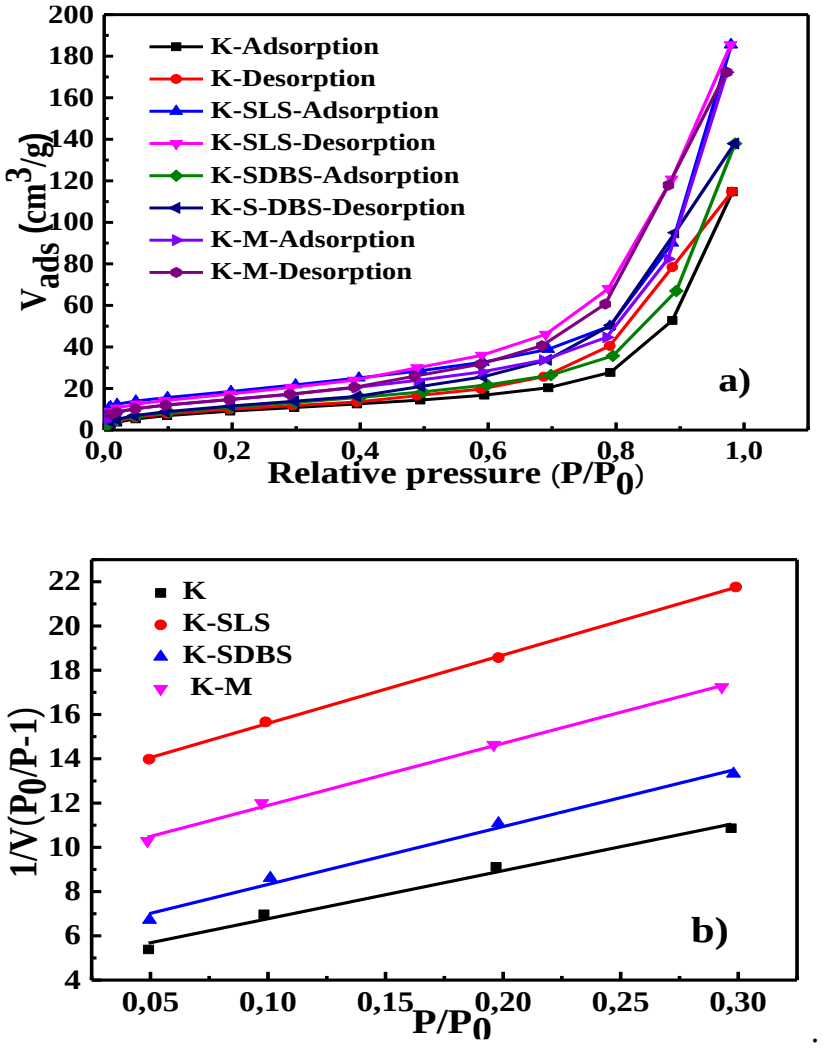

Figure III.11: a) Adsorption/desorption isotherms of nitrogen and b) The BET surface area plot of K, K-SLS, K-SDBS and K-M.

III.3 CONCLUSION

The characterization of diphenylamine-modified kaolin revealed significant structural and textural changes. FT-IR spectra confirmed the presence of diphenylamine functional groups, indicating successful modification. XRD analysis showed slight shifts in diffraction peaks, suggesting interactions between diphenylamine and the kaolin layers. SEM images displayed noticeable modifications in surface morphology, with an increase in porosity. BET surface area analysis demonstrated an enhancement in surface area and pore volume, contributing to improved adsorption performance. These results highlight the potential of diphenylamine-functionalized kaolin as an advanced adsorbent for heavy metal removal.

This chapter has also successfully demonstrated the impact of surfactant modification on kaolin's thermal, structural, and morphological characteristics. Thermogravimetric analysis revealed changes in weight loss patterns, highlighting the influence of surfactants on dehydroxylation processes. FT-IR spectroscopy confirmed the successful adsorption of SLS and SDBS through the appearance of new vibrational bands. Microscopy and EDX analyses showed alterations in kaolin's surface morphology and elemental composition, while XRD results confirmed the intercalation of surfactants into the kaolin structure. Furthermore, BET surface area analysis indicated a significant increase in surface area, particularly for SLS-modified kaolin. Sodium lauryl sulfate (SLS) is the most effective surfactant for enhancing kaolin's surface properties.

III.4 REFERENCES

[1] Maged, A., Al-Hagar, O. E., El-Magd, S. a. A., Kharbish, S., Bhatnagar, A., & Abol-Fotouh, D. (2024). Bacterial nanocellulose-clay film as an eco-friendly sorbent for superior pollutants removal from aqueous solutions. Environmental Research, 257, 119231. https://doi.org/10.1016/j.envres.2024.119231.

[2] Zhang, S., Tan, D., Zhu, H., Pei, H., & Shi, B. (2024). Rheological behaviors of Na-montmorillonite considering particle interactions: A molecular dynamics study. Journal of Rock Mechanics and Geotechnical Engineering. https://doi.org/10.1016/j.jrmge.2024.07.003.

[3] Fatima, H., Kadi, S., Lellou, S., Marouf, R., & Benhebal, H. (2022). Synthesis, characterization and application of intercalated and tubular kaolinite for the removal of basic yellow 28. Journal of the Iranian Chemical Society, 19(12), 4687–4697. https://doi.org/10.1007/s13738-022-02634-4.

[4] Zegeye, A., Yahaya, S., Fialips, C. I., White, M. L., Gray, N. D., & Manning, D. A. (2013). Refinement of industrial kaolin by microbial removal of iron-bearing impurities. Applied Clay Science, 86, 47–53. https://doi.org/10.1016/j.clay.2013.08.041.

[5] Murray, H. H. (2000). Traditional and new applications for kaolin, smectite, and palygorskite: a general overview. Applied Clay Science, 17(5–6), 207–221. https://doi.org/10.1016/s0169-1317(00)00016-8.

[6] Habeeb, M. A., Mahdi, S. M., & Mamoun, F. (2024). Boosting of structural, optical, and dielectric characteristics of PVA polymer using COO-SIO2 nanoparticles for advanced optoelectronic applications. Silicon, 16(9), 3917–3928. https://doi.org/10.1007/s12633-024-02970-5.

[7] Hezil, N., Fellah, M., Assala, O., Touhami, M. Z., & Guerfi, K. (2018). Elimination of Chromium (VI) by Adsorption onto Natural and/or Modified Kaolinite. Diffusion Foundations, 18, 106–112. https://doi.org/10.4028/www.scientific.net/df.18.106.

[8] Cherono, F., Mburu, N., & Kakoi, B. (2021). Adsorption of lead, copper and zinc in a multi-metal aqueous solution by waste rubber tires for the design of single batch adsorber. Heliyon, 7(11), e08254. https://doi.org/10.1016/j.heliyon.2021.e08254.

[9] Edama, N. A., Sulaiman, A., Hamid, K. H. K., Rodhi, M. N. M., Mohibah, M., & Rahim, S. N. A. (2013). The effect of hydrochloric acid on the surface area, morphology and Physico-Chemical Properties of Sayong kaolinite clay. Key Engineering Materials, 594–595, 49–56. https://doi.org/10.4028/www.scientific.net/kem.594-595.49.

[10] Mañosa, J., La Rosa, J. C., Silvello, A., Maldonado-Alameda, A., & Chimenos, J. M. (2023). Kaolinite structural modifications induced by mechanical activation. Applied Clay Science, 238, 106918. https://doi.org/10.1016/j.clay.2023.106918.

[11] Al Rabadi, S. J., Al-Mahasneh, M., & Awwad, A. M. (2023). Amelioration of nano-kaolinite deportation for heavy Pb(II), Cd(II), and Cu(II) ions from aquatic environments. Jordan Journal of Earth and Environmental Sciences, 14, 308–317.

[12] Amari, A., Alzahrani, F. M., Katubi, K. M., Alsaiari, N. S., Tahoon, M. A., & Rebah, F. B. (2021). Clay-Polymer nanocomposites: Preparations and utilization for pollutants removal. Materials, 14(6), 1365. https://doi.org/10.3390/ma14061365.

[13] Bouchareb, N., Hezil, N., Hamadi, F., & Fellah, M. (2024). Effect of milling time on structural, mechanical and tribological behavior of a newly developed Ti-Ni alloy for biomedical applications. Materials Today Communications, 38, 108201. https://doi.org/10.1016/j.mtcomm.2024.108201.

[14] Fellah, M., Hezil, N., Guerfi, K., Djellabi, R., Montagne, A., Iost, A., Borodin, K., & Obrosov, A. (2020). Mechanistic pathways of cationic and anionic surfactants sorption by kaolinite in water. Environmental Science and Pollution Research, 28(6), 7307–7321. https://doi.org/10.1007/s11356-020-11083-6.

[15] Shuma, H. E., Mkayula, L. L., & Makame, Y. M. (2019). Assessment of the effect of acid activation of kaolin from Malangali on water defluoridation. Tanzania Journal of Science, 45, 279–296.

[16] Yahaya, S., Jikan, S. S., Badarulzaman, N. A., & Adamu, A. D. (2017). Effects of acid treatment on the SEM-EDX characteristics of kaolin clay. Path of Science, 3(9), 4001–4005. https://doi.org/10.22178/pos.26-6.

[17] Zhang, Q., Yan, Z., Ouyang, J., Zhang, Y., Yang, H., & Chen, D. (2018). Chemically modified kaolinite nanolayers for the removal of organic pollutants. Applied Clay Science, 157, 283–290. https://doi.org/10.1016/j.clay.2018.03.009.

[18] Hilal, R. H., & Nassif, R. A. (2023). Study on adsorption of some metals from waste solution by (unsaturated polyester-kaolin) composite. Kuwait Journal of Science, 50(3), 257–261. https://doi.org/10.1016/j.kjs.2023.01.010.

[19] Merabtene, M., Kacimi, L., & Clastres, P. (2019). Elaboration of geopolymer binders from poor kaolin and dam sludge waste. Heliyon, 5(6), e01938. https://doi.org/10.1016/j.heliyon.2019.e01938.

[20] Fellah, M., Hezil, N., Touhami, M. Z., AbdulSamad, M., Obrosov, A., Bokov, D. O., Marchenko, E., Montagne, A., Alain, I., & Alhussein, A. (2020). Structural, tribological and antibacterial properties of (α + β) based ti-alloys for biomedical applications. Journal of Materials Research and Technology, 9(6), 14061–14074. https://doi.org/10.1016/j.jmrt.2020.09.118.

[21] Fellah, M., Hezil, N., Touhami, M. Z., Obrosov, A., Weiß, S., Kashkarov, E. B., Lider, A. M., Montagne, A., & Iost, A. (2019). Enhanced structural and tribological performance of nanostructured Ti–15Nb alloy for biomedical applications. Results in Physics, 15, 102767. https://doi.org/10.1016/j.rinp.2019.102767.

[22] Salgado-Campos, V. M. J., De Souza Carvalho, I., Bertolino, L. C., Duarte, T. A., Araújo, B. C., & Borghi, L. (2021). Clay mineralogy and lithogeochemistry of lutites from the Lower Cretaceous Crato Member, Araripe Basin, NE Brazil: Implications for paleoenvironmental, paleoclimatic and provenance reconstructions. Journal of South American Earth Sciences, 110, 103329. https://doi.org/10.1016/j.jsames.2021.103329.

[23] Fellah, M., Hezil, N., Hussein, M. A., Samad, M. A., Touhami, M. Z., Montagne, A., Iost, A., Obrosov, A., & Weiss, S. (2019). Preliminary investigation on the bio-tribocorrosion behavior of porous nanostructured β-type titanium based biomedical alloys. Materials Letters, 257, 126755. https://doi.org/10.1016/j.matlet.2019.126755.

[24] Tian, L., Fu, K., Chen, S., Yao, J., & Bian, L. (2022). Comparison of microscopic adsorption characteristics of Zn(II), Pb(II), and Cu(II) on kaolinite. Scientific Reports, 12(1). https://doi.org/10.1038/s41598-022-20238-z.

[25] Shaban, M., Sayed, M. I., Shahien, M. G., Abukhadra, M. R., & Ahmed, Z. M. (2018). Adsorption behavior of inorganic- and organic-modified kaolinite for Congo red dye from water, kinetic modeling, and equilibrium studies. Journal of Sol-Gel Science and Technology, 87(2), 427–441. https://doi.org/10.1007/s10971-018-4719-6.

[26] Khabbouchi, M., Hosni, K., & Srasra, E. (2018). Physico-Chemical characterization of modified Tunisian kaolin by phosphoric acid. Surface Engineering and Applied Electrochemistry, 54(2), 219–226. https://doi.org/10.3103/s1068375518020072.

[27] Aimdate, K., Srifa, A., Koo-Amornpattana, W., Sakdaronnarong, C., Klysubun, W., Kiatphuengporn, S., Assabumrungrat, S., Wongsakulphasatch, S., Kaveevivitchai, W., Sudoh, M., Watanabe, R., Fukuhara, C., & Ratchahat, S. (2021). Natural Kaolin-Based NI Catalysts for CO2 methanation: on the effect of CE enhancement and Microwave-Assisted Hydrothermal Synthesis. ACS Omega, 6(21), 13779–13794. https://doi.org/10.1021/acsomega.1c01231.

[28] Maged, A., Elgarahy, A. M., Hlawitschka, M. W., Haneklaus, N. H., Gupta, A. K., & Bhatnagar, A. (2023). Synergistic mechanisms for the superior sorptive removal of aquatic pollutants via functionalized biochar-clay composite. Bioresource Technology, 387, 129593. https://doi.org/10.1016/j.biortech.2023.129593.

[29] Belachew, N., & Hinsene, H. (2019). Preparation of cationic surfactant-modified kaolin for enhanced adsorption of hexavalent chromium from aqueous solution. Applied Water Science, 10(1). https://doi.org/10.1007/s13201-019-1121-7.

[30] Redaoui, D., Sahnoune, F., Heraiz, M., Belhouchet, H., & Fatmi, M. (2017). Thermal decomposition kinetics of Algerian Tamazarte kaolinite by thermogravimetric analysis. Transactions of Nonferrous Metals Society of China, 27(8), 1849–1855. https://doi.org/10.1016/s1003-6326(17)60208-5.

[31] Zhang, A., Kang, L., Zhang, Y., Ding, D., & Zhang, Y. (2020). Thermal behaviors and kinetic analysis of two natural kaolinite samples selected from Qingshuihe region in Inner Mongolia in China. Journal of Thermal Analysis and Calorimetry, 145(6), 3281–3291. https://doi.org/10.1007/s10973-020-09869-4.

[32] Janković, B. Ž., Janković, M. M., Marinović-Cincović, M. M., Todorović, D. J., & Šarap, N. B. (2018). Thermal analysis testing and natural radioactivity characterization of kaolin as building material. Journal of Thermal Analysis and Calorimetry, 133, 481–487. https://doi.org/10.1007/s10973-018-7159-1.

[33] Torres-Luna, J., & Carriazo, J. (2018). Porous aluminosilicic solids obtained by thermal-acid modification of a commercial kaolinite-type natural clay. Solid State Sciences, 88, 29–35. https://doi.org/10.1016/j.solidstatesciences.2018.12.006.

[34] Saukani, M., Arief, S., Syahrillah, G. R. F., & Hidayat, N. (2019). The low concentration of sodium hydroxide influence on the compressive strength of Fly Ash/Natural Kaolin-Based geopolymer. IOP Conference Series Materials Science and Engineering, 515, 012063. https://doi.org/10.1088/1757-899x/515/1/012063.

[35] Cheng, H., Xu, P., Wang, D., & Frost, R. L. (2016). Thermal decomposition behavior and de-intercalation kinetics of kaolinite/quaternary ammonium salt complexes. Journal of Thermal Analysis and Calorimetry, 126(2), 421–433. https://doi.org/10.1007/s10973-016-5572-x.

[36] Wang, H., Feng, Q., & Liu, K. (2016). The dissolution behavior and mechanism of kaolinite in alkali-acid leaching process. Applied Clay Science, 132–133, 273–280. https://doi.org/10.1016/j.clay.2016.06.013.

[37] Segura, J. C. F., Cruz, V. E. R., De Jesús Pérez Bueno, J., Ascencio, E. M. L., & García, F. L. (2017). Characterization and electrochemical treatment of a kaolin. Applied Clay Science, 146, 264–269. https://doi.org/10.1016/j.clay.2017.06.004.

[38] Zhong, Z., Li, J., Ma, Y., & Yang, Y. (2021). The adsorption mechanism of heavy metals from coal combustion by modified kaolin: Experimental and theoretical studies. Journal of Hazardous Materials, 418, 126256. https://doi.org/10.1016/j.jhazmat.2021.126256.

[39] Gan, C., Hu, H., Meng, Z., Zhu, X., Gu, R., Wu, Z., Wang, H., Wang, D., Gan, H., Wang, J., & Dou, G. (2019). Characterization and Hemostatic Potential of Two Kaolins from Southern China. Molecules, 24(17), 3160. https://doi.org/10.3390/molecules24173160.

[40] Mudzielwana, R., Gitari, M. W., & Ndungu, P. (2019). Performance evaluation of surfactant modified kaolin clay in As(III) and As(V) adsorption from groundwater: adsorption kinetics, isotherms and thermodynamics. Heliyon, 5(11), e02756. https://doi.org/10.1016/j.heliyon.2019.e02756.

[41] Assi, N., Azar, P. A., Tehrani, M. S., Husain, S. W., Darwish, M., & Pourmand, S. (2018). Selective solid-phase extraction using 1,5-diphenylcarbazide-modified magnetic nanoparticles for speciation of Cr(VI) and Cr(III) in aqueous solutions. International Journal of Environmental Science and Technology, 16(8), 4739–4748. https://doi.org/10.1007/s13762-018-1868-7.

[42] Ahmed, A., Mohamed, F., Elzanaty, A. M., & Abdel-Gawad, O. F. (2020). Synthesis and characterization of diphenylamine grafted onto sodium alginate for metal removal. International Journal of Biological Macromolecules, 167, 766–776. https://doi.org/10.1016/j.ijbiomac.2020.11.159.

[43] Chu, Y., Khan, M. A., Wang, F., Xia, M., Lei, W., & Zhu, S. (2019). Kinetics and equilibrium isotherms of adsorption of Pb(II) and Cu(II) onto raw and arginine-modified montmorillonite. Advanced Powder Technology, 30(5), 1067–1078. https://doi.org/10.1016/j.apt.2019.03.002.

[44] Yimer, M., Ansari, S. N., Berehe, B. A., Gudimella, K. K., Gedda, G., Girma, W. M., Hasan, N., & Tasneem, S. (2024). Adsorptive removal of heavy metals from wastewater using Cobalt-diphenylamine (Co-DPA) complex. BMC Chemistry, 18(1). https://doi.org/10.1186/s13065-024-01128-z.

[45] Maged, A., Kharbish, S., Ismael, I. S., & Bhatnagar, A. (2020). Characterization of activated bentonite clay mineral and the mechanisms underlying its sorption for ciprofloxacin from aqueous solution. Environmental Science and Pollution Research, 27(26), 32980–32997. https://doi.org/10.1007/s11356-020-09267-1.

[46] Dinh, V., Nguyen, P., Tran, M., Luu, A., Hung, N. Q., Luu, T., Kiet, H. T., Mai, X., Luong, T., Nguyen, T., Ho, H. T., Nguyen, D., Pham, D., Hoang, A., Le, V., & Nguyen, T. (2021). HTDMA-modified bentonite clay for effective removal of Pb(II) from aqueous solution. Chemosphere, 286, 131766. https://doi.org/10.1016/j.chemosphere.2021.131766.

[47] Hua, J. (2017). Adsorption of low-concentration arsenic from water by co-modified bentonite with manganese oxides and poly(dimethyldiallylammonium chloride). Journal of Environmental Chemical Engineering, 6(1), 156–168. https://doi.org/10.1016/j.jece.2017.11.062.

[48] Chai, J., Au, P., Mubarak, N. M., Khalid, M., Ng, W. P., Jagadish, P., Walvekar, R., & Abdullah, E. C. (2020). Adsorption of heavy metal from industrial wastewater onto low-cost Malaysian kaolin clay–based adsorbent. Environmental Science and Pollution Research, 27(12), 13949–13962. https://doi.org/10.1007/s11356-020-07755-y.

[49] Mbey, J.A., Sabouang, C.J.N., Makon, T.B., Coulibaly, S.L., & Kong, S. (2021). The thermal dehydroxylation of kaolinite using thermogravimetric analysis and Controlled rate thermal analysis. Journal of The Cameroon Academy of Sciences. 16, 3. https://doi.org/10.4314/jcas.v16i4.

[50] Kgabi, D. P., & Ambushe, A. A. (2023). Characterization of South African bentonite and kaolin clays. Sustainability, 15(17), 12679. https://doi.org/10.3390/su151712679.

[51] Aghdam, S. K., Kazemi, A., & Ahmadi, M. (2023). Performance evaluation of different types of surfactants to inhibit clay swelling during chemical enhanced oil recovery. The Canadian Journal of Chemical Engineering, 102(1), 481–494. https://doi.org/10.1002/cjce.25028.

[52] Zuo, X., Wang, D., Zhang, S., Liu, Q., & Yang, H. (2018). Intercalation and Exfoliation of Kaolinite with Sodium Dodecyl Sulfate. Minerals, 8(3), 112. https://doi.org/10.3390/min8030112.

[53] Ma, X., Wu, Y., Li, L., & Wang, Y. (2021). Effect of SDBS on crystallization behavior of pseudoboehmite. The Journal of Physical Chemistry C, 125(47), 26039–26048. https://doi.org/10.1021/acs.jpcc.1c08074.

[54] Taleb, K., Pillin, I., Grohens, Y., & Saidi-Besbes, S. (2018). Gemini surfactant modified clays: Effect of surfactant loading and spacer length. Applied Clay Science, 161, 48–56. https://doi.org/10.1016/j.clay.2018.03.015.

[55] Andrunik, M., & Bajda, T. (2019). Modification of Bentonite with Cationic and Nonionic Surfactants: Structural and Textural Features. Materials, 12(22), 3772. https://doi.org/10.3390/ma12223772.

[56] Ghafar, H. H. A., Radwan, E. K., & El-Wakeel, S. T. (2020). Removal of Hazardous Contaminants from Water by Natural and Zwitterionic Surfactant-modified Clay. ACS Omega, 5(12), 6834–6845. https://doi.org/10.1021/acsomega.0c00166.

[57] Meroufel, B., Benali, O., Benyahia, M., Benmoussa, Y., & Zenasni, M. (2013). Adsorptive removal of anionic dye from aqueous solutions by Algerian kaolin: Characteristics, isotherm, kinetic and thermodynamic studies. Journal of Materials and Environmental Science. 4, 482−491.

[58] Deng, L., Zeng, H., Shi, Z., Zhang, W., & Luo, J. (2018). Sodium dodecyl sulfate intercalated and acrylamide anchored layered double hydroxides: A multifunctional adsorbent for highly efficient removal of Congo red. Journal of Colloid and Interface Science, 521, 172–182. https://doi.org/10.1016/j.jcis.2018.03.040.

[59] Anas, A. K., Pratama, S. Y., Izzah, A., & Kurniawan, M. A. (2021). Sodium dodecylbenzene Sulfonate-Modified Biochar as an adsorbent for the removal of methylene blue. BULLETIN OF CHEMICAL REACTION ENGINEERING AND CATALYSIS, 16(1), 188–195. https://doi.org/10.9767/bcrec.16.1.10323.188-195.

[60] Mbaye, A., Diop, C. a. K., Miehe-Brendle, J., Senocq, F., & Maury, F. (2014). Characterization of natural and chemically modified kaolinite from Mako (Senegal) to remove lead from aqueous solutions. Clay Minerals, 49(4), 527–539. https://doi.org/10.1180/claymin.2014.049.4.03.

[61] Merrikhpour, H., Mobarakpour, S., & Azimi, S. B. (2022). Adsorption of Cd2+, Cu2+, and Ni2+ onto surfactant modified bentonite. Desalination and Water Treatment, 271, 157–165. https://doi.org/10.5004/dwt.2022.28768.

[62] Golubeva, O. Y., Alikina, Y. A., & Kalashnikova, T. A. (2020). Influence of hydrothermal synthesis conditions on the morphology and sorption properties of porous aluminosilicates with kaolinite and halloysite structures. Applied Clay Science, 199, 105879. https://doi.org/10.1016/j.clay.2020.105879.

[63] Yu, M., Luo, D., Kuang, J., & Yuan, W. (2022). Synthesis and luminescence properties of Eu3+ doped sodalite phosphors using kaolin. Results in Physics, 41, 105887. https://doi.org/10.1016/j.rinp.2022.105887.

[64] Ghasemzadeh, H., Mehrpajouh, A., & Pishvaei, M. (2020). Laboratory analyses of Kaolinite stabilized by vinyl polymers with different monomer types. Engineering Geology, 280, 105938. https://doi.org/10.1016/j.enggeo.2020.105938.

[65] Spasojević, M., Daković, A., Rottinghaus, G. E., Obradović, M., Krajišnik, D., Marković, M., & Krstić, J. (2021). Influence of surface coverage of kaolin with surfactant ions on adsorption of ochratoxin A and zearalenone. Applied Clay Science, 205, 106040. https://doi.org/10.1016/j.clay.2021.106040.

[66] Ni, X., Zhao, Z., Li, Z., & Li, Q. (2021). The adsorptive behaviour of kaolinite to sodium dodecyl benzene sulphonate and the structural variation of kaolinite. Scientific Reports, 11(1). https://doi.org/10.1038/s41598-021-81283-8.

[67] González, J.A., Carreras, A.C., & Ruiz. M.C. (2007). Phase transformations in clays and kaolins produced by thermal treatment in chlorine and air atmospheres. Latin American applied research.

[68] Ni, X., Li, Z., & Wang, Y. (2018). Adsorption characteristics of anionic surfactant sodium dodecylbenzene sulfonate on the surface of montmorillonite minerals. Frontiers in Chemistry, 6. https://doi.org/10.3389/fchem.2018.00390.

[69] Flilissa, A., Venkataraman, S., Laouameur, K., Beroual, A., Flilissa, O., Omine, K., Chaabane, T., & Darchen, A. (2020). Surface modification of aluminum phosphate by sodium dodecylbenzenesulfonate (SDBS): A new nano-structured adsorbent for an improved removal of Ponceau S". Journal of Environmental Chemical Engineering, 8(3), 103625. https://doi.org/10.1016/j.jece.2019.103625.

[70] Rocha, D. R., Barber, X., Jordán-Vidal, M. M., Urbano, A., Melquiades, F. L., Thomaz, E. L., & Mataix-Solera, J. (2022). Multivariate Analysis with XRD Data as a Fingerprinting Technique to Study Burned Soils. Minerals, 12(11), 1402. https://doi.org/10.3390/min12111402.

[71] Monteiro, M. K. S., De Oliveira, V. R. L., Santos, F. K. G. D., De Barros Neto, E. L., De Lima Leite, R. H., Aroucha, E. M. M., & De Oliveira Silva, K. N. (2018). Influence of the ionic and nonionic surfactants mixture in the structure and properties of the modified bentonite clay. Journal of Molecular Liquids, 272, 990–998. https://doi.org/10.1016/j.molliq.2018.10.113.

[72] Olaremu, A. G. (2015). Physico-Chemical characterization of akoko mined kaolin clay. Journal of Minerals and Materials Characterization and Engineering, 03(05), 353–361. https://doi.org/10.4236/jmmce.2015.35038.

[73] Jamo,H.U., & Abdu. S.G. (2014). Structural Analysis and Surface Morphology of Kaolin. Science World Journal. 9, 33-37.

[74] Fosso-Kankeu, E., Waanders, F., Lemmer, N., & Steyn. R.H. (2017). Surfactant Impregnated Bentonite Clay for the Removal of Heavy Metals from Solution. 9th Int'l Conference on Advances in Science, Engineering, Technology and Waste Management. 27-28. https://doi.org/10.17758/EARES.EAP1117020.

[75] Bayram, T., Bucak, S., & Ozturk, D. (2020). BR13 dye removal using sodium dodecyl sulfate modified montmorillonite: Equilibrium, thermodynamic, kinetic and reusability studies. Chemical Engineering and Processing - Process Intensification. 158, 108186. https://doi.org/10.1016/j.cep.2020.108186.

[76] Elaheh, M., Ali, A.G., & Mohsen. J. (2017). Adsorptive separation of CO2 and CH4 by the broom sorghum based activated carbon functionalized by diethanolamine. Korean Journal of Chemical Engineering. 34, 413-424.https://doi.org/10.1007/s11814-016-0268-2.

[77] Julius, N.G., Dieudonné, T.N., Estella, B.N.T., Dodo, L.A., Julius, N.N., & Joseph, M.K. (2014). Adsorption of phenol from aqueous solutions onto natural and thermally modified kaolinitic materials. International Journal of Biological and Chemical Sciences. 8, 2325-2338.

[78] Hackley, V. A., & Stefaniak, A. B. (2013). "Real-world" precision, bias, and between-laboratory variation for surface area measurement of a titanium dioxide nanomaterial in powder form. Journal of Nanoparticle Research, 15(6). https://doi.org/10.1007/s11051-013-1742-y.

[79] Budash, Y., Plavan, V., Tarasenko, N., Ishchenko, O., & Koliada, M. (2023). Effect of acid modification on porous structure and adsorption properties of different type Ukrainian clays for water purification technologies. Journal of Ecological Engineering, 24(5), 210–221. https://doi.org/10.12911/22998993/161691.

CHAPTER IV
ADSORPTION TESTS

INTRODUCTION

This chapter discusses the adsorption capacities of natural (Nat-kaolin) and modified kaolin (diphenylamine-modified kaolin (DPA-kaolin), sodium lauryl sulfate-modified kaolin (K-SLS), sodium dodecyl benzene sulfonate- modified kaolin (K-SDBS), and SLS/SDBD modified kaolin (K-M) for the removal of lead (Pb(II)), copper (Cu(II)) and mercury (Hg(II)) Hg ions from aqueous solutions. Furthermore, the adsorption mechanisms, kinetics, thermodynamics, and isothermal absorption lines of Pb(II), Cu(II) and Hg(II)on all types of kaolin are analyzed in detail. Emphasis is placed on understanding the effect of the modification on the adsorption efficiency, as well as the influence of variables such as contact time, temperature, pH, and metal ion concentration. Equilibrium models, employing Langmuir, Freundlich, and Sips models are studied.

IV.1 Study of Lead and Copper adsorption capacity onto Nat-kaolin and DPA-kaolin

IV.1.1 Lead and Copper adsorption

Lead and copper adsorption onto Nat-kaolin and DPA-Kaolin was investigated as a function of time, temperature, and pH. At room temperature, the experiments were conducted in batch reactors that were closed.

IV.1.2 Effect of contact time on the adsorption of Pb, Cu on Nat-kaolin and DPA- Kaolin

The main objective of the study of the effect of contact time on adsorption is to determine the time required (ideal time) to reach the adsorption equilibrium. We therefore studied the effect of contact time on the adsorption of lead and copper on Nat-kaolin and DPA- Kaolin. Taking 50 ml of lead or copper solution with an initial concentration of C_0 = 0.1 g/L, it is put in contact with 0.2 g of NAT kaolin or DPA kaolin. The whole is put at a stirring speed of 4000 rpm for 9 hours at room temperature and pH equal to 7, aliquots of 2 ml of the solution are taken during different time intervals and are centrifuged for 5 min at 450 rpm. The supernatant is immediately dosed by an atomic absorption spectrometry (PinAAcle 900 T).

Contact time is a crucial parameter that can markedly influence the adsorption process. Understanding its impact can assist in optimizing the design of effective DPA-kaolin for the removal of Pb(II) and Cu(II) from aqueous solutions.

As illustrated in Figure IV.1, there is an initial rapid adsorption of both Pb(II) and Cu(II) on DPA-kaolin, followed by a slower equilibrium phase in which the adsorption rate gradually decreases. Indeed, after 120 minutes, the adsorption rates for Pb(II) and Cu(II) reached 77 % and 65 %, respectively. Similar results were observed by *Musumba et al.*,[1] in their investigation into the removal of Pb, Cu, and zinc from waste rubber tires. However, in a study of the adsorption of Pb(II) and Cu(II) on biochar [1], demonstrated that equilibrium was reached after 60 minutes. Another study carried out by *Hilal and Nassif* [2] on kaolin demonstrated that equilibrium was reached after 100 minutes. This is due to the fact that at the outset of the process, there are more adsorption sites available on the kaolin surface for the metal ions to bind to. As these sites become occupied, the rate of adsorption slows.

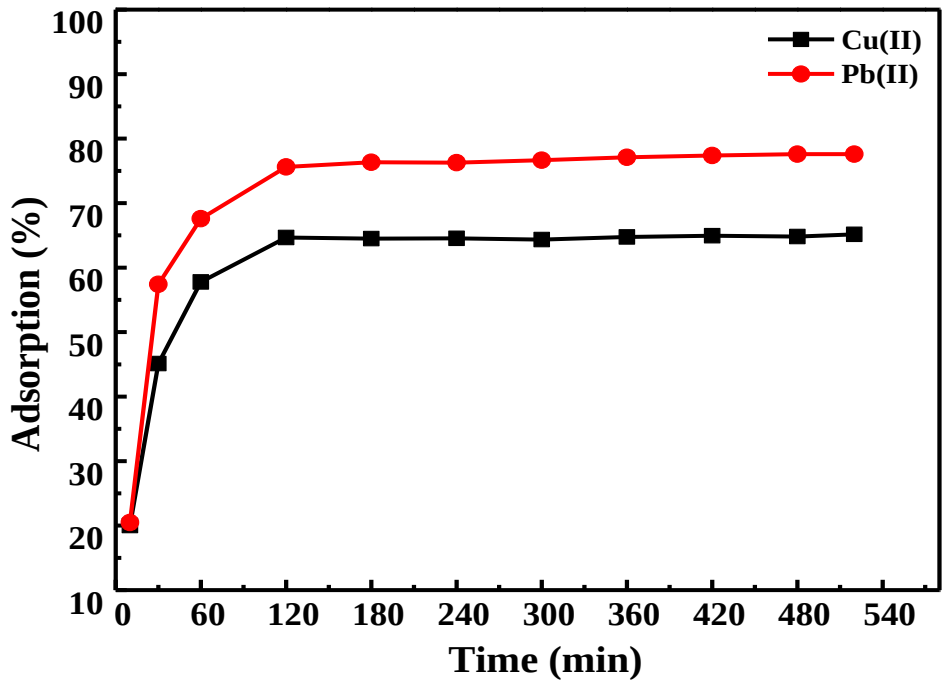

Figure IV.1: Effect of the contact time on the Adsorption of Pb(II) and Cu(II) by DPA-kaolin.

IV.1.3 Adsorption kinetic

The adsorption kinetics of heavy metals (Pb, Cu) on our clay adsorbents (natural and modified kaolin) was carried out using pseudo first order, pseudo second, and intraparticle diffusion models. The conformity between the experimental data and the model is based on the values of the correlation coefficients (R^2). The closer R^2 is to unity, the more adequate the model is to correctly describe the adsorption kinetics considered.

The experimental data obtained from Pb(II) and Cu(II) adsorption onto DPA-kaolin were analyzed using the pseudo-first-order (Figure IV.2), pseudo-second-order kinetic (Figure IV.3), and Weber-Morris intraparticle diffusion models (Figure IV.4).

Figure IV.3 illustrates the fitting of the pseudo-second-order kinetic models for Pb(II) and Cu(II) adsorption, with the parameters of the model listed in Table IV.1.

The curves in Figure IV.3 fit well with the pseudo-second-order model for both the Pb(II) and Cu(II) adsorption systems, with R^2 values of 0.999 and 0.996, respectively, which are higher than that of the pseudo-first-order (Figure IV.2). This indicates that chemisorption is the rate-controlling step in the adsorption process of Pb (II) ions and Cu (II) ions on natural kaolin [3, 4]. Congruent results were reported by *Trikkaliotis et al.*, [5] for the adsorption of Cu ions onto chitosan/poly (vinyl alcohol) beads.

The predicted Qe values are in accordance with experimental data for both Pb(II) and Cu(II). The rate constants for Pb(II) and Cu(II) adsorption were calculated as 0.002 ± 5.82E-05 $g.\mu mol^{-1}.h^{-1}$ and 0.006 ± 1.49E-04 $g.\mu mol^{-1}.h^{-1}$, respectively, based on the PSO kinetic data. For instance, the calculated qe of Pb(II) was 156 ± 0.025 $\mu mol.g^{-1}$, which is almost similar to the experimental Qe value of 151 $\mu mol.g^{-1}$. However, qe calculated by the pseudo-first-order model is considerably different from the experimental value of 134 $\mu mol.g^{-1}$. The same findings were observed for Cu(II).

Figure IV.4 illustrates the plot of Qt versus t 1/2. The fitted curves of the intraparticle diffusion model have R^2 greater than 0.9 for both Pb (II) and Cu(II) and did not pass through the origin, suggesting that mechanisms other than intraparticle diffusion may be at play [6]. The boundary layer also influences the adsorption process [7].

The higher K_{id} for Pb(II) compared with that of Cu(II) indicated a higher surface adsorption reaction of Pb(II) with the active sites of DPA-kaolin.

Table IV.1: Parameters of the PFO, PSO, and intraparticle diffusion kinetic models from the adsorption of Pb(II) and Cu(II) onto DPA-kaolin.

	PFO			**PSO**			**Intraparticle diffusion**	
	k_1 ($g.\mu mol^{-1}.h^{-1}$)	Q_e ($\mu mol.g^{-1}$)	R^2	k_2 ($g.\mu mol^{-1}.h^{-1}$)	Q_e ($\mu mol.g^{-1}$)	R^2	K_{id}	R^2
Pb(II)	0.704 ± 0,450	673 ± 0.072	0.912	0.002 ± 5.82E-05	156 ± 0.025	0.999	7.37 ± 0,622	0.938
Cu(II)	0.288 ± 0.214	259 ± 0.034	0.884	0.006 ± 1.49E-04	130 ± 0 .065	0.996	5.94 ± 0,480	0.933

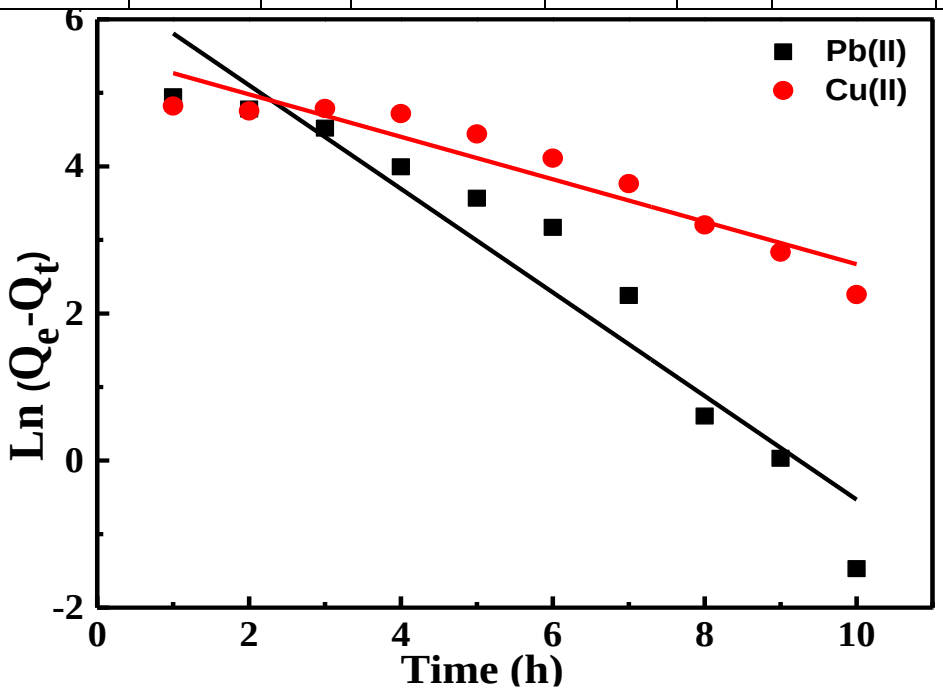

Figure IV.2: PFO Adsorption Kinetic of Pb(II) and Cu(II) ions adsorption by DPA-kaolin.

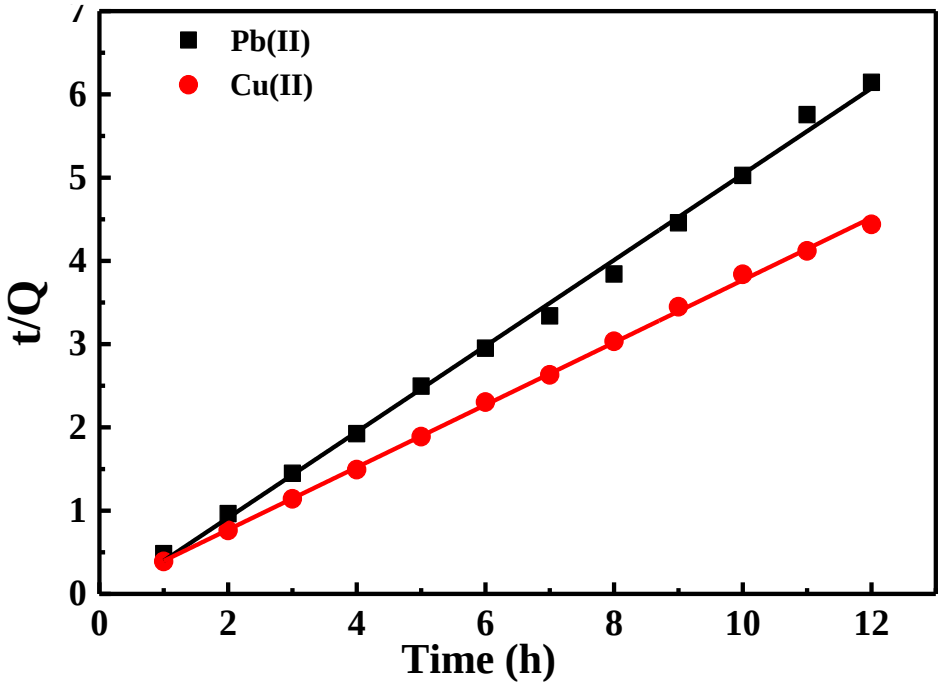

Figure IV.3: PSO Adsorption Kinetic of Pb(II) and Cu(II) ions adsorption by DPA-kaolin.

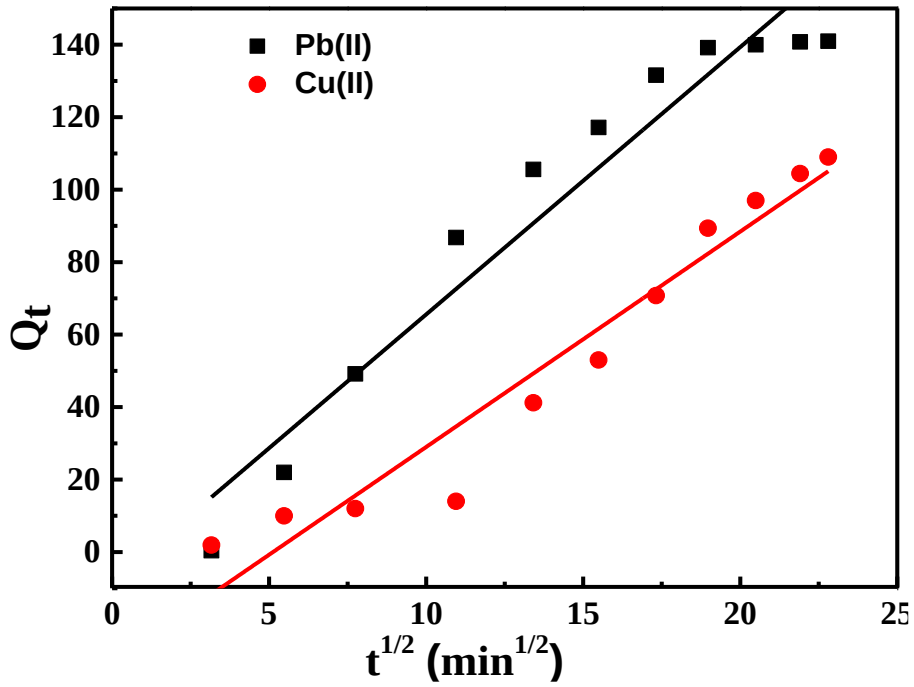

Figure IV.4: Weber-Morris intraparticle diffusion of Pb(II) and Cu(II) ions adsorption by DPA-kaolin.

IV.1.4 Effect of temperature on the adsorption of Pb, Cu by DPA-Kaolin and thermodynamic study

To understand the effect of temperature on the adsorption efficiency of lead and copper on Nat kaolin and DPA kaolin, 50 ml of artificial solutions of Pb, Cu with a concentration equal to 0.1 g/L were mixed in 0.2 g of solid (Nat kaolin or DPA kaolin) with stirring at 4000 rpm for one hour, and the temperature was varied in each operation for values of 25, 35, 45, 55 and 65 ° C, using a water bath to keep the temperature constant during the contact period. At the end, the samples were separated from the solid and kept until analysis by an atomic absorption spectrometry (PinAAcle 900 T).

The effect of temperature on adsorption is always accompanied by a thermal process because adsorption involves energy exchanges between the adsorbates (metal ions) and the adsorbent (kaolin) this process can be classified as exothermic or endothermic, depending on the interactions between the particles. Consequently, we have carried out the thermodynamic study on the adsorption of lead and copper on Nat-kaolin and DPA-Kaolin using the Gibbs free energy (ΔG) which is composed of two terms, an enthalpic term (ΔH) which expresses the interaction energies between the molecules and the surface of the adsorbent, and an entropic term (ΔS) which expresses the modification and arrangement of the molecules in the liquid phase on the surface**.**

Figure IV.5 illustrates the impact of temperature on the adsorption of Pb and Cu on DPA-kaolin. The temperature range tested was 25 ◦C to 65 ◦C with a 10 ◦C increment. The results demonstrate a decrease in the adsorption of both PTEs as temperature increases. Notably, the decrease is more significant for Pb than for Cu. The amount of Pb adsorbed decreases from 102.95 µmol.L^{-1} at 25 °C to 56.88 µmol.L^{-1} at 65 °C, while for Cu, the adsorbed quantity decreases from 76.88 µmol.L^{-1} at 25 °C to 59.14 µmol.L^{-1} at 65 °C. Cu adsorbs better than Pb, while at 65 °C, adsorption is better for Cu. This indicates that adsorption is exothermic. Several studies have found the same results concerning the effect of heavy metal adsorption [8-11].

The decrease in Pb(II) and Cu(II) adsorption onto DPA-kaolin at higher temperatures can be attributed to the acceleration of the desorption process due to the rise in temperature, causing previously adsorbed metal ions to detach from the surface of the DPA-kaolin particles.

This phenomenon occurs due to increased thermal energy, which promotes the movement and diffusion of metal ions away from the adsorption sites [12, 13]. Higher temperatures can also alter the structure of kaolin particles, leading to changes in surface properties such as surface area and surface charge, which can affect the adsorption capacity.

Additionally, increased temperature can enhance the solubility of metal ions in the solution phase, reducing their availability for adsorption onto the kaolin surface. These combined effects contribute to the observed decrease in Pb(II) and Cu(II) adsorption onto DPA-kaolin with increasing temperature.

In order to study the thermodynamics parameters, the obtained data was fitted by the formula in (Eq. IV.1), and (Eq. IV.2):

$$\Delta G = \Delta H - T\Delta S \quad \text{(Eq. IV.1)}$$

$$\ln\left(\frac{Q_{ads}}{C_e}\right) = \frac{\Delta S}{R} - \frac{\Delta H}{RT} \quad \text{(Eq. IV.2)}$$

Where:

Ce ($\mu mol.L^{-1}$) is the equilibrium ion concentration, Q_{ads} ($\mu mol.g^{-1}$) is the adsorption capacity, T (K) is thermodynamic temperature, and R is the universal gas constant.

The plot of Ln (Q_{ads}/C_e) as a function of 1/T (Figure IV.6) has enabled us to calculate the thermodynamic parameters: Gibbs free energy ΔG, entropy change ΔS, and enthalpy change ΔH shown in Table IV.2.

An examination of Table IV.2 reveals that the enthalpy values are negative, thereby confirming that the adsorption process for the two studied PTEs, Pb(II) and Cu(II), is exothermic. The negative values of Gibbs free energy (ΔG) for both heavy metals indicate that the process is thermodynamically favorable, meaning that it tends to occur spontaneously. As the absolute value of ΔG decreases with increasing temperature, it can be inferred that the adsorption process becomes increasingly unfavorable as the temperature rises. This could be attributed to a reduction in thermal energy, which impairs the mobility of adsorbate molecules and hinders their interaction with the adsorbent surface.

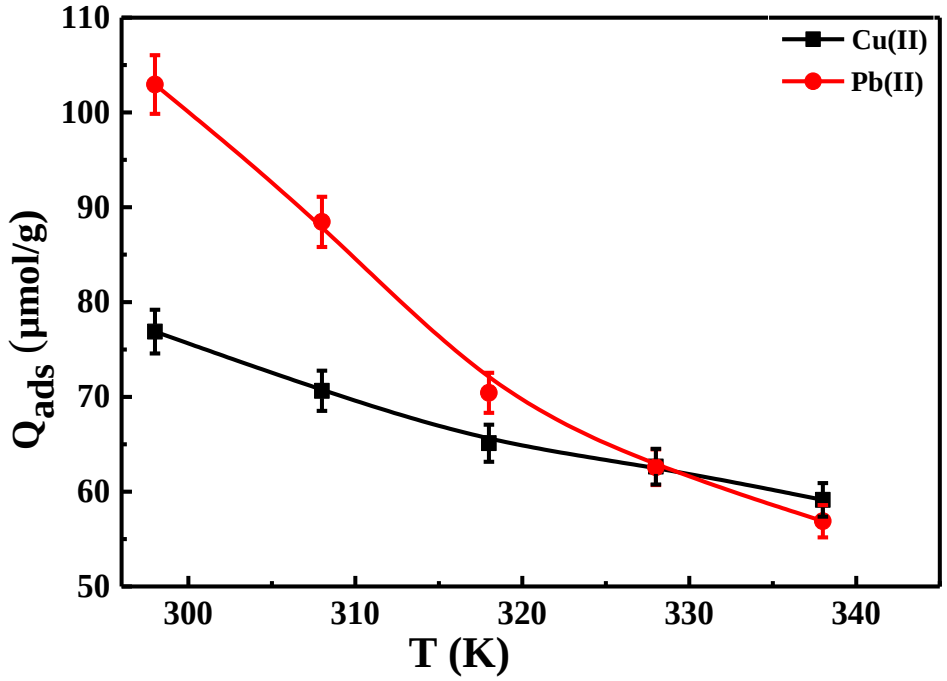

Figure IV.5: The effect of temperature on the adsorption of Pb(II) and Cu(II) ions by DPA-kaolin.

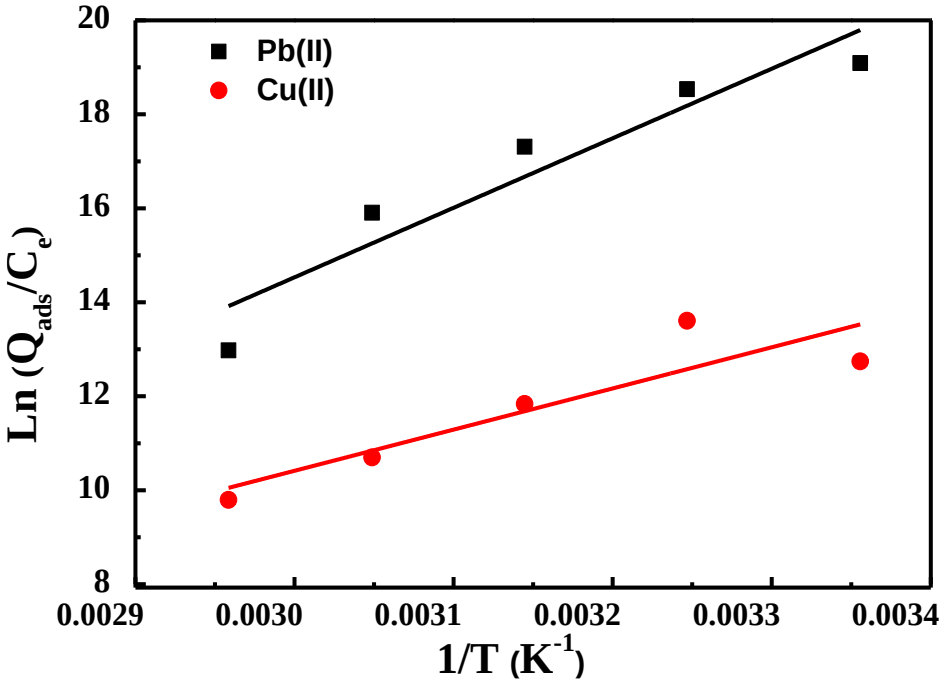

Figure IV.6: Thermodynamic study of Pb(II) and Cu(II) ions adsorption by DPA-kaolin.

Table IV.2: Thermodynamic parameters.

	ΔS (J.mol^{-1}.K^{-1})	ΔH (J.mol^{-1}.K^{-1})	ΔG (KJ.mol^{-1})				
			298.15 K	**308.15 K**	**318.15 K**	**328.15 K**	**338.15 K**
Pb(II)	-248	-123010	-49.11	-46.62	-44.13	-41.65	-39.17
Cu(II)	-132	-72839	-6898	-688	-686	-685	-684

IV.1.5 Effect of pH on the adsorption of Pb, Cu by DPA-Kaolin

The pH is an influential factor in all adsorption processes as it can affect the structure of the adsorbent and adsorbent as well as the adsorption mechanism. Therefore, we studied the effect of pH on the adsorption of lead and copper on natural kaolin by adding 50 ml of lead and copper ion solutions at the same concentrations with 0.2 g of natural kaolin or kaolin DPA and placing the mixture at a stirring speed of 4000 rpm for 9 hours at room temperature. The pH was changed in each process to values of 1, 2, 3, 4, 5, and 6 using a laboratory pH meter based on a microprocessor type "HANNA, HI 8521". The pH was adjusted by adding a few drops of sodium hydroxide (0.1M) and hydrochloric acid (0.1). Finally, the samples were separated from the solid material and stored until analysis by atomic absorption spectroscopy (PinAAcle 900 T).

The study investigated the effect of pH on the adsorption behavior of Pb(II) and Cu(II) on modified kaolin. The pH levels varied between 1 and 6 [14-17]. While the initial concentration of Pb(II) and Cu(II) in the solution was maintained at 25 mg.L^{-1} . The experimental procedure involved the preparation of solutions with varying pH levels, with the objective of examining the effect of pH on the adsorption of Pb(II) and Cu(II) onto the DPA-kaolin. This experimental approach enables a comprehensive understanding of the influence of pH on the adsorption of Pb(II) and Cu(II) on modified kaolin, which is essential for optimizing the removal of these heavy metal ions from aqueous systems.

The study of the influence of pH on the adsorption of Pb(II) and Cu(II) on DPA-kaolin revealed interesting results (Figure IV.7). At low pH values of around 1–3, the adsorption of Pb(II) and Cu(II) onto the DPA-kaolin is the lowest due to the protonation reaction that competes with heavy metal ions for adsorption sites on DPA-kaolin. As the pH rises to 4–5, the removal of

both metals improves significantly. This is due to the fact that as the pH increases, the surface of DPA-kaolin becomes more negatively charged, which increases the electrostatic attraction between the positive charge of heavy metal ions and the adsorbent [18, 19].

Thus, the adsorption of Pb(II) is significantly better at a pH of 5, with an adsorption rate of around 83 %. In contrast, Cu(II) adsorption at the same pH is less effective, at only 52 %. These results indicate that the adsorption of Pb(II) on DPA-kaolin is more favorable than that of Cu(II) at pH 5. The difference in adsorption rates can be attributed to the physico-chemical properties of Pb(II) and Cu(II) ions, as well as their interactions with DPA-kaolin. pH plays a pivotal role in the speciation of metals and influences their adsorption behavior. At pH 5, Pb can form more stable complexes with the active sites of the kaolin, thus favoring its adsorption [20, 21].

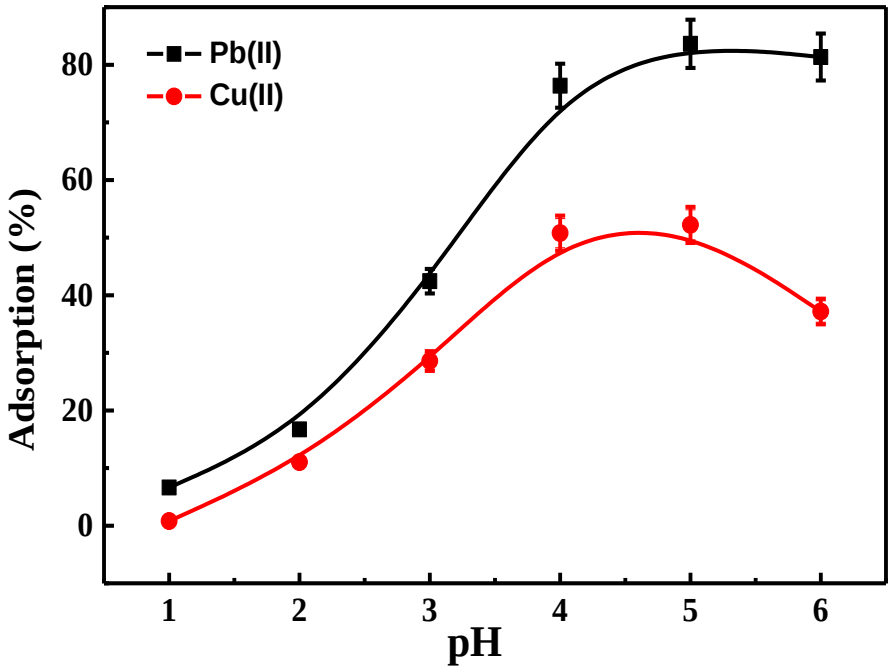

Figure IV.7: Effect of the pH on the Adsorption of Pb(II) and Cu(II) by DPA-kaolin.

IV.1.6 Lead, Copper adsorption isotherm

To study the adsorption isotherm of Pb and Cu onto Nat-Kaolin and DPA-Kaolin. A specific quantity of $Pb(NO_3)_2$ and $Cu(NO_3)_2$ were dissolved in deionized water (1000 ml) to prepare the metal ion solutions Concentrations of various metal ions ranging from 10 to 100 $mg.L^{-1}$ were created through dilution of the standard solutions. 0.5 g of Nat-kaolin or DPA-

Kaolin was mixed with an aqueous solution (100 ml) comprising Pb(II) and/or Cu(II) at varying concentrations. After that, the mixture was agitated for 24 hours at 25 ◦C until equilibrium was achieved then the supernatant was subsequently centrifuged at 4000 rpm for half an hour. The residual concentration of Pb(II) and Cu(II) was determined using an atomic absorption spectrometry (PinAAcle 900 T). The quantity of metal (Pb or Cu) adsorbed onto Nat-kaolin or DPA-Kaolin (the adsorption capacity) was estimated using (Eq. IV.3).

$$\mathbf{Q_{ads} = (C_0 - C_e).V / m} \quad \text{.....(Eq. IV.3)}$$

Where:

Q_{ads} (µmol.g^{-1}): The equilibrium adsorption capacity. C_0 (µmol.L^{-1}): The starting concentration of (Pb or Cu).Ce (µmol.L^{-1}): The equilibrium concentration of (Pb or Cu).V (mL): The volume of solution. m(g): The weight of the solid. The study examined the effect of contact time, pH, temperature, and thermodynamics on the adsorption of Pb(II) and Cu(II) ions.

The adsorption isotherm study examined Pb(II) and Cu(II) adsorption on Nat-kaolin and DPA-kaolin at 25 °C. Both materials demonstrated an increase in adsorption with elevated metal concentrations, resulting in the formation of L-type isotherms (monolayer adsorption). The adsorption of Pb(II) and Cu(II) (Figure IV.8) by Nat-kaolin was found to be 103 µmol.g^{-1} and 91 µmol.g^{-1}, respectively. In comparison, DPA-kaolin exhibited higher adsorption capacities of 151 µmol.g^{-1} for Pb(II) and 134 µmol.g^{-1} for Cu(II). This is attributed to the larger surface area of DPA-kaolin [15-17, 22]. In comparison, [23, 24] reported adsorption capacities of 30 mg·g^{-1} for Pb and 4.41 mg·g^{-1} for Cu on raw and heat-treated attapulgite clay. Additionally, *Kypritidou and Argyraki*, [25] *Dikra et al.*, [16] observed that the adsorption capacities on palygorskite clay, Fe-smectite clay, and a natural palygorskite-Fe-smectite mixed clay ranged from 27.6 to 52.1 mg·g^{-1} for Pb and 7.7–17.6 mg·g^{-1} for Cu. These results highlight the performance of DPA-kaolin in adsorbing both Pb and Cu as compared to other modified and natural clays.

The enhanced adsorption observed in DPA-kaolin was attributed to its chemical modification, which resulted in an expansion of the pore size [20, 26]. Pb(II) formed insoluble complexes with DPA, leading to precipitation, while Cu (II) showed a lower affinity for DPA.

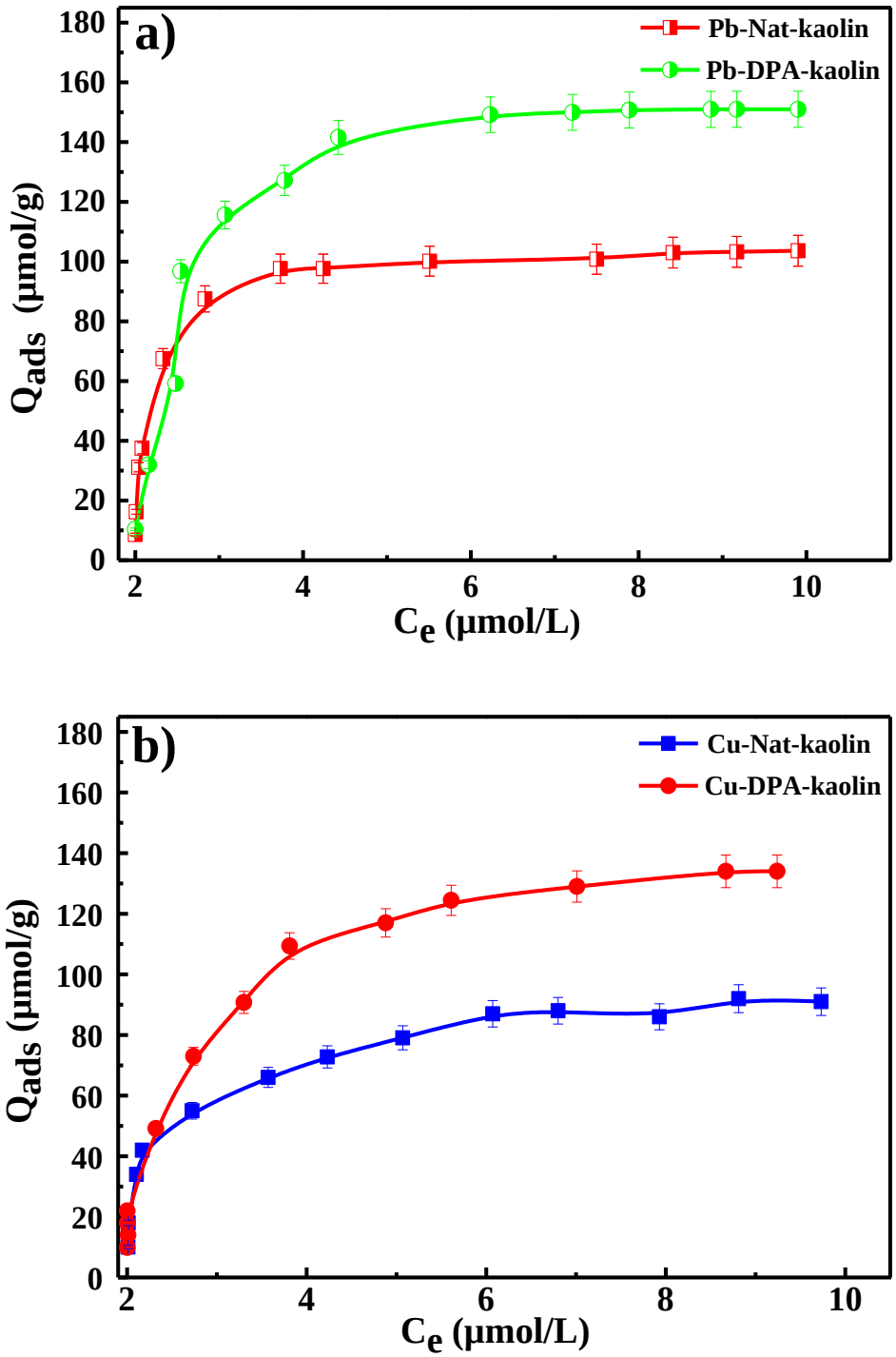

Figure IV.8: The adsorption isotherms of a) Pb(II) and b) Cu(II) onto 0.5 g of Nat-kaolin and DPA-kaolin at 25 °C, free pH.

IV.1.7 Lead, Copper isotherm models

To deepen the understanding of the mechanisms and physicochemical interactions between the adsorbates (Pb, Cu) and the adsorbent (kaolin), the adsorption isotherms for Pb(II) and Cu(II) were analyzed by fitting them to the linearized forms of the Freundlich and Langmuir adsorption models Using equations Eq. I.3 and Eq.I.5 (Chapter I), respectively.

The adsorption isotherms for Pb(II) and Cu(II) were analyzed by fitting them to the linearized forms of the Langmuir and Freundlich adsorption models (Figure IV.9 a and b).

Table IV.3 indicates that the R^2 values of the Langmuir model are 0.983 and 0.952, respectively, for the adsorption of Pb(II) and Cu(II) on DPA-kaolin. In comparison, the R^2 values of the Freundlich model are 0.939 and 0.902, respectively. These results indicate that both models describe this adsorption process well. However, the values for the maximum adsorbed quantity are significantly different from the experimental values. The Freundlich fitting of the adsorption of Pb(II) and Cu(II) on DPA-kaolin suggests that the adsorption is not uniform and that there is a distribution of surface-active sites with different adsorption energies [27].

Therefore, when considering the adsorption of Pb(II) onto Nat-kaolin and DPA-kaolin, as well as Cu(II) on Nat-kaolin, it appears that higher concentrations of adsorbate Pb to more favorable adsorption, as indicated by n values greater than 1. Conversely, the n value less than 1 for Cu(II) adsorption on DPA-kaolin suggests that favorable adsorption occurs at lower concentrations of adsorbate in solution.

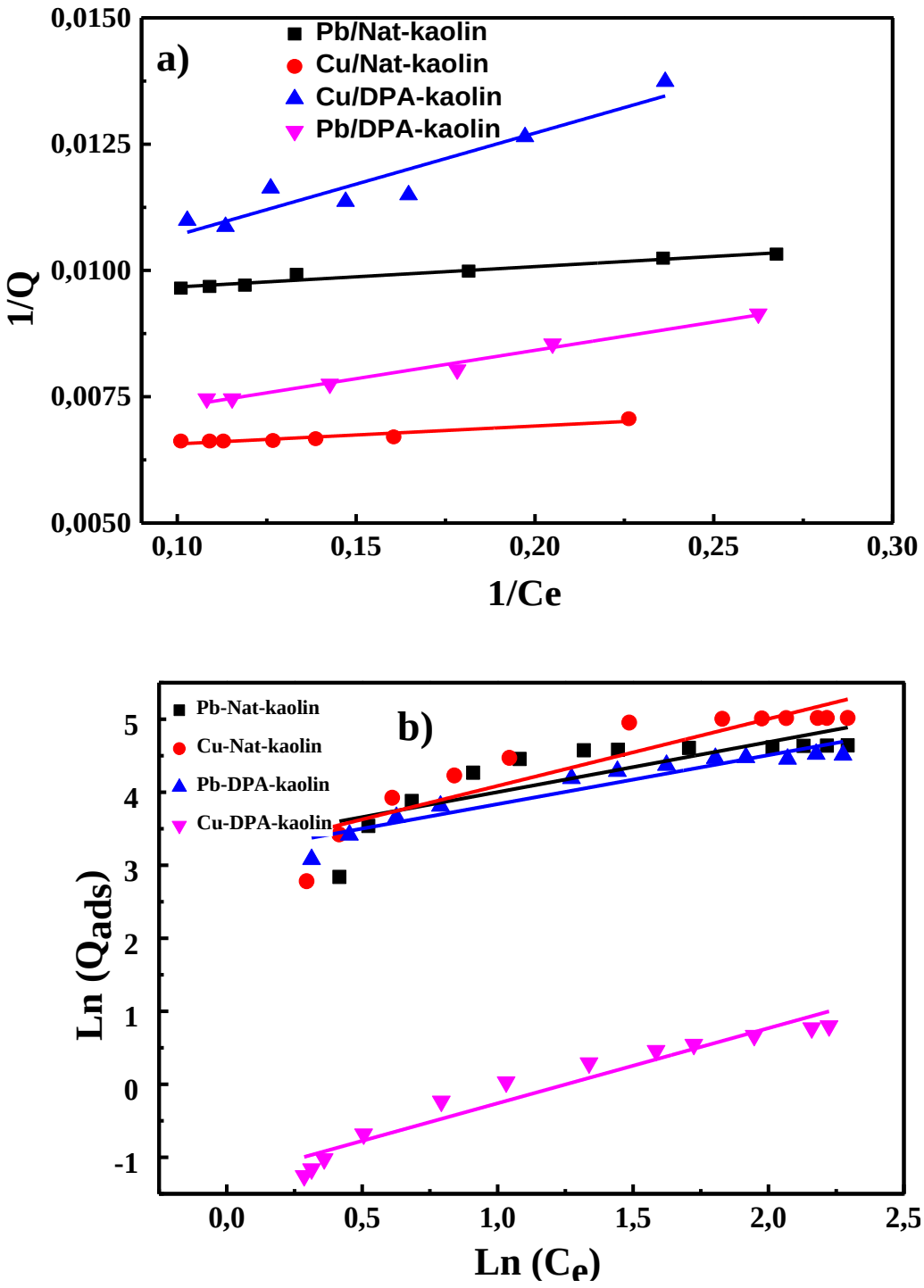

Figure IV.9: a) Langmuir isotherms b) Freundlich isotherms of Pb(II) and Cu(II) ions adsorption onto Nat-kaolin and DPA-kaolin.

Table IV.3: displays the constants calculated using the Langmuir and Freundlich models.

	Freundlich constants			Langmuir constants		
	K_F	N	R^2	Q_m	K_L	R^2
Cu/Nat-kaolin	27.58 ± 0.204	1.46 ±0.127	0.628	108±6.47E-05	2.29±6.71E-04	0.876
Pb/Nat-kaolin	23.77 ± 0.238	1.09 ± 0.154	0.823	161±7.24E-05	1.75±4.99E-04	0.892
Cu/DPA-kaolin	23.721 ± 0.109	1.49 ± 0.079	0.902	115±4.95E-04	0.429±0.00306	0.952
Pb/DPA-kaolin	0.27 ± 0.103	0.972 ±0.066	0.939	162 ±1.19E-04	0.551±6.71E-04	0.983

IV.1.8 Adsorption mechanism

The adsorption of Pb(II) and Cu(II) onto diphenylamine-modified kaolin is facilitated by a number of mechanisms, including electrostatic interactions [28, 16], ion exchange, complexation, and precipitation. The diphenylamine modification of kaolin increases the surface area and introduces functional groups, including amino and hydroxyl, which collectively enhance the binding of metals [29]. This results in the formation of stable coordination complexes between the metal ions and these functional groups. This complexation mechanism is particularly effective in enhancing the adsorption of Pb (II) due to its higher affinity for the diphenylamine functional groups in comparison to Cu (II).

The precipitation of Pb(II) and Cu(II) as hydroxides ($Pb(OH)_2$ and $Cu(OH)_2$) at higher pH levels facilitates the adsorption process. The functional groups on the modified kaolin promote complex formation with metal ions, enhancing the adsorption process. At lower pH values, electrostatic attraction dominates, while precipitation and complexation play a more significant role at higher pH values, making this adsorption mechanism highly pH-dependent.

IV.1.9 Desorption

Figure IV.10 illustrates the desorption isotherms of Pb(II) and Cu(II) on DPA-Kaolin as a function of time. For both Pb (II) and Cu (II), the desorption capacity on DPA-Kaolin exhibited a similar trend, increasing with time.

With regard to Cu desorption, an initial rapid increase in the desorption capacity from 2.5 % to 15 % was observed after approximately an hour, followed by a faster desorption until it reached 50 % after six hours. In contrast, Pb desorption increased slowly by 20 % during the first three hours and then remained constant by 20 % for approximately three hours. Consequently, the desorption of Cu from DPA-Kaolin is greater than that of Pb from DPA-Kaolin due to the adsorption capacity differences. Cu exhibits a stronger adsorption capacity on DPA-Kaolin in comparison to Pb, and Cu forms weaker bonds with DPA-Kaolin, which makes it more easily desorbed.

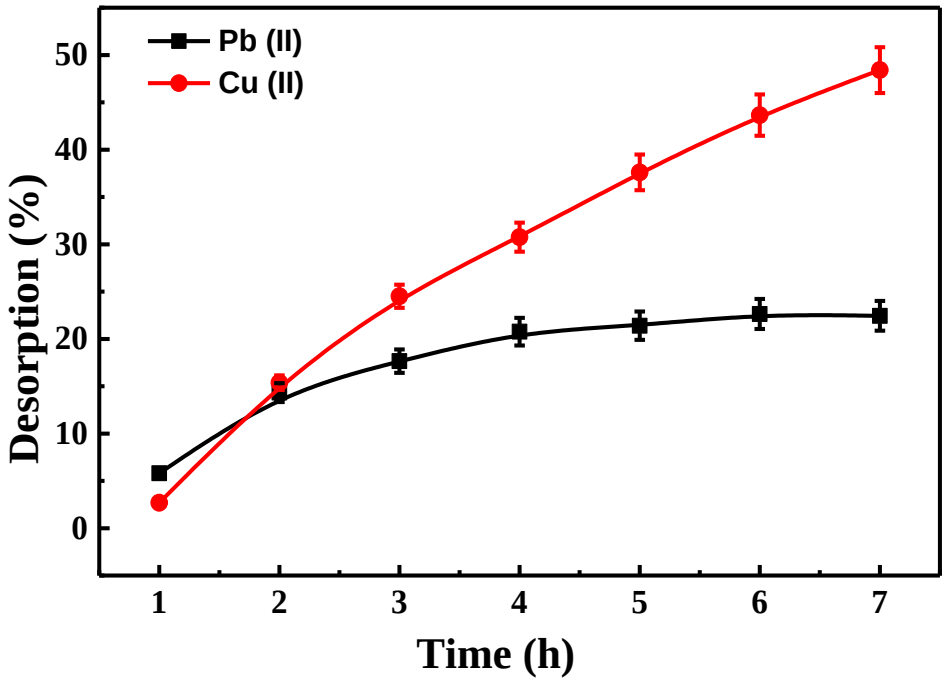

Figure IV.10: Desorption of Pb(II) and Cu(II) ions on DPA-kaolin.

IV.2 Mercury adsorption onto K, K-SLS, K-SDBS, K-M

IV.2.1 Mercury (II) adsorption isotherm

Considered a fundamental concept in the explanation of the process of metal adsorption on the surface of the adsorbent. These isotherms effectively illustrate the manner in which the metal and sorbent surfaces interact. Figure IV.11 presents the adsorption isotherms of mercury (II) on the four kaolin types K, K-SLS, K-SDBS and K-M at 25 °C. Figure IV.11 illustrates that the mercury adsorption capacity increases with increasing equilibrium Hg (II) concentrations, reaching an adsorption equilibrium of 17.77 $mg.g^{-1}$, 15.77 $mg.g^{-1}$, 13.45 $mg.g^{-1}$, and 12.77 $mg.g^{-1}$ for K-SLS, K-M, K-SDBS, and K, respectively. Natural kaolin (K), shows the lowest adsorption capacity among the samples with a saturation of around 12.77$mg.g^{-1}$. This indicated that the natural porosity, active sites, and surface chemistry of kaolin are not efficient enough to capture mercury ions optimally. Whereas the kaolin modified by sodium lauryl sulfate surfactant (K-SLS) shows the highest adsorption capacity at nearly 17.77$mg.g^{-1}$. The modification of kaolin by SLS creates new adsorption sites or increases the density of effective sites, enhancing the hydrophobicity of the kaolin surface, this promotes stronger and more numerous interactions with mercury ions, probably through hydrophobic bonds, thus improving the adsorption capacity [30].

Similar findings have been documented by *Harutyunyan et al.*, [31] With regards to the adsorption affinity rate of copper (II) on sodium dodecyl sulfate-modified bentonite, it is evident that this is higher than that of natural bentonite.

Mercury adsorption on K-SLS occurred through two distinct mechanisms, surface complexation and ion exchange. Throughout the ion exchange reaction, mercury ions are introduced into the inner layers of K-SLS via channels and pores. The exchange of these ions is facilitated by exchangeable cations. The diffusion rate of mercury ions is rapid within the pores, but then decreases as the ions pass through narrow channels, this is precisely when slow diffusion reactions occur at the interface between the channels and the surrounding environment [32]. The adsorption of metals ions such as Pb(II), Hg(II), and Cu(II) on anionic surfactant-modified clays is responsible for the formation of the cationic complexes on the clay surface [33].

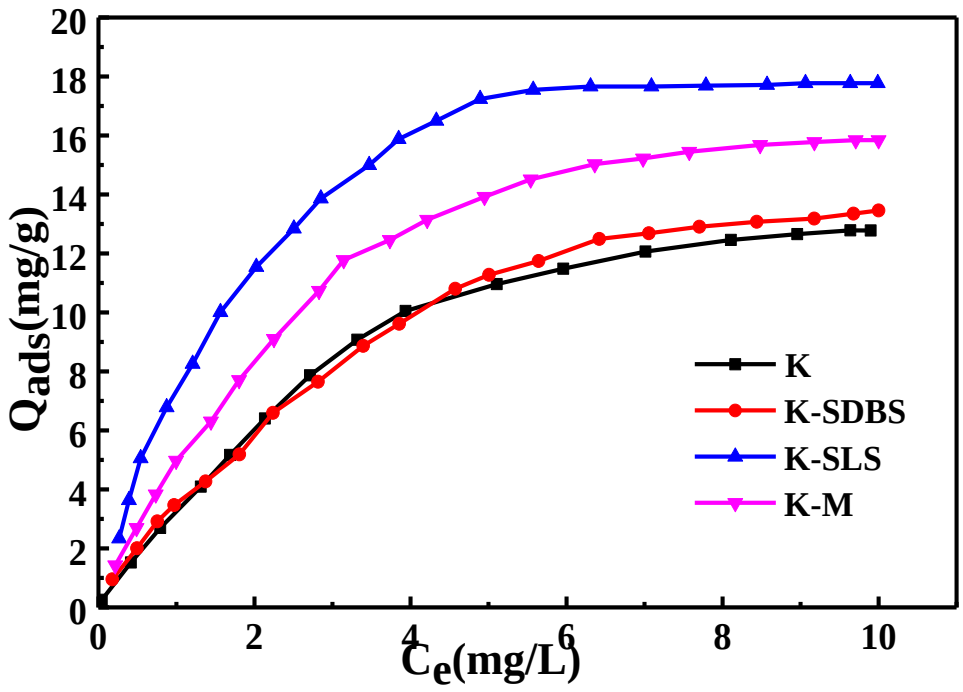

Figure IV.11: The adsorption isotherms of Hg(II) onto K, K-SLS, K-SDBS and K-M. (Mass of adsorbent = 0.5 g; Volume of solution = 100 ml; Stirring speed150 rpm.min; pH = 7; Temperature = 25°C).

IV.2.2 Effect of contact time

One crucial factor that can significantly affect the adsorption process is the duration of contact. The adsorption mechanism is comprised of two distinct phases: A rapid initial phase, followed by a slower subsequent phase.

Figure IV.12 illustrates the effect of the contact time on the adsorption capacity and removal efficiency of mercury by the four kaolin types K, K-SLS, K-SDBS and K-M.

As can be observed within initial 90-minute period, the removal efficiency of mercury by the four kaolin types increased rapidly with an increase in contact time until reaching a plateau with values of 8.74mg.g^{-1}, 9.30mg.g^{-1}, 10.1mg.g^{-1}, and 11.5mg.g^{-1} for K-M, K, K-SDBS, and K-SLS, respectively. This is explained by the fact that there are a greater number of adsorption sites accessible on the kaolin surface for mercury adsorption [34]. Subsequently, the rate of reduction slowed as the duration of the experiment exceeded 300 minutes. This was due to the occupation of available sites by mercury ions.

The higher adsorption of mercury on kaolin modified by the surfactant sodium lauryl sulfate (K-SLS) was observed as a consequence of the increase in surface area and pore volume that resulted from the modification [35], which led to increased availability of binding sites between the mercury ion and the kaolin surface. The negatively charged lauryl sulfate anions covered the kaolin surface, which encouraged an increase in the sorption of mercury ions [33].

Castro-Castro et al., [36], found that by increasing the contact duration from 5 to 30 minutes, the removal of Cr (VI) from organo bentonite improved quickly, thus the elimination of Cr (VI) rose considerably between 30 and 60 minutes, and the adsorption reached equilibrium after 90 minutes.

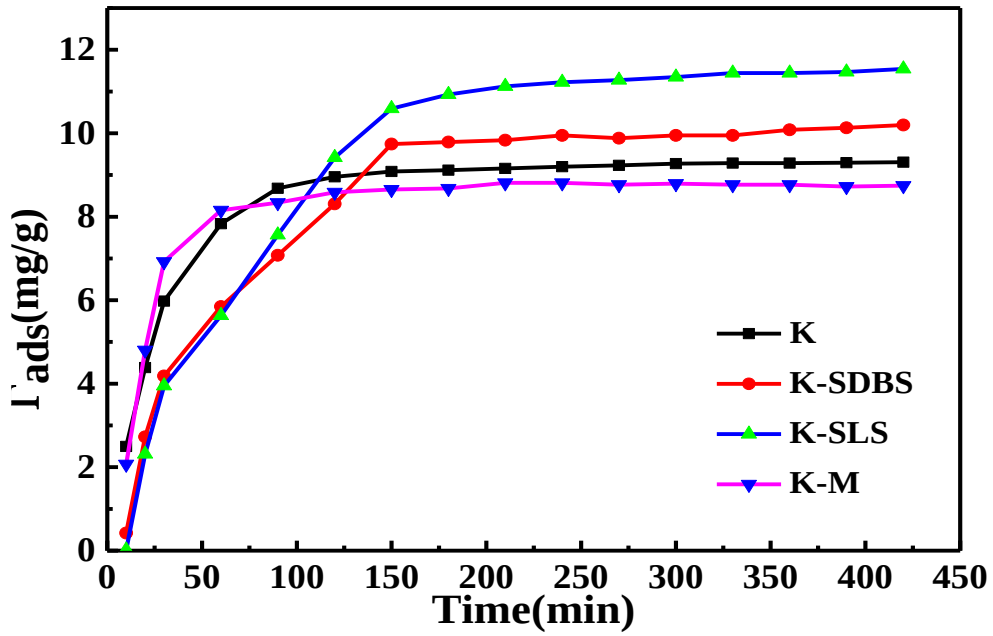

Figure IV.12: Effect of contact time on the adsorption of Hg(II) onto K, K-SLS, K-SDBS and K-M.(Mass of adsorbent = 0.5 g; Volume of solution = 100 ml; Stirring speed150 rpm.min; pH = 7; Temperature = 25°C;Time = 0-420 min).

IV.2.3 Kinetic Study

The examination of the adsorption rate and the adsorption mechanism plays an essential role in the design of adsorption systems. Various mathematical models can describe the kinetics of adsorption processes, with the pseudo-first-order and pseudo-second-order kinetic models being the most widely applied.

To investigate the adsorption system of mercury onto four types of kaolin (k, k-SLS, k-SDBS, and K-M) two kinetic models were used the pseudo-first-order model (Figure IV.13a) and the pseudo-second-order model (Figure IV.13b) with their parameters mentioned in Table IV.4.

According to correlation coefficients R^2 from Table IV.4, it is evident that the adsorption of mercury on four types of kaolin was more suitable in the pseudo-second-order model with R^2> 0.99 than in the pseudo-first-order model with R^2 between (0.77-0.96).This suggests that the pseudo-second-order model presupposes that the Chemisorption mechanisms are the step that restricts the rate of adsorption, specifically the sharing or exchange of electrons between Hg(II) and adsorbent, indicating the formation of chemical bonds X [37,38].

Mudzielwana et al., [38] evaluated the kinetic of As(III) and As(V) adsorption on kaolin modified with hexadecyltrimethylammonium bromide (HDTMA-Br) cationic surfactant. They found that the adsorption of As(V) was better explained by pseudo-second-order whereas the adsorption of As(III) was better explained by pseudo-first-order. This suggests that the adsorption of As(III) onto modified kaolin corresponds to physisorption while the adsorption of As(V) corresponds to chemisorptions.

Table IV.4: Parameters of the PFO, and PSO kinetic models from the adsorption of Hg(II) onto four types of kaolin (K, K-SLS, K-SDBS, and K-M).

	PFO			PSO		
	K_1	Q_e	R^2	K_2	Q_e	R^2
K	0.006± 3.54E-4	4.19±0.078	0.963	0.007±0.203	9.70±8.24E-4	0.999
K-SLS	0.006± 2.33E-4	11.01±0.051	0.979	0.001±0.466	11.6±0.001	0.993
K-SDBS	0.005± 4.15E-4	7.47±0.092	0.920	0.001±0.584	13.9±0.002	0.984
K-M	0.005± 8.07E-4	2.07±0.178	0.773	0.014±0.198	8.98±8.02E-4	0.999

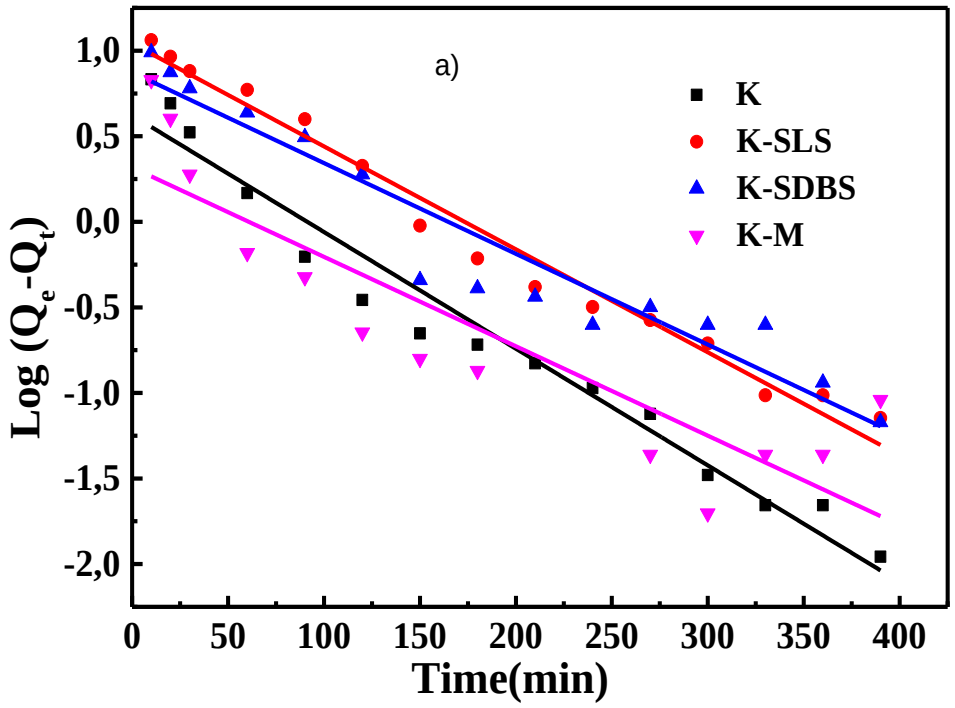

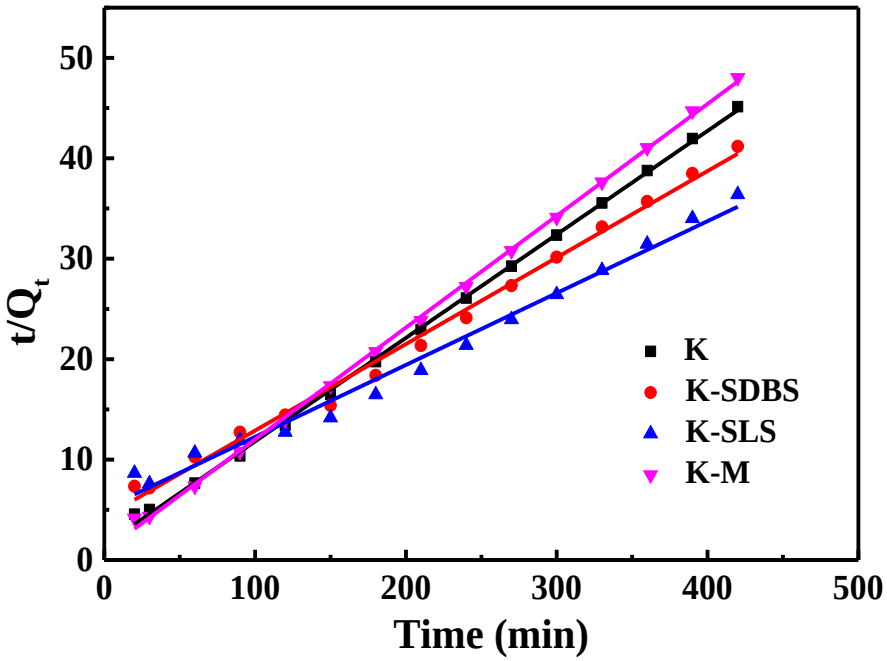

Figure IV.13: a)PFO Adsorption Kinetic and, PSO Adsorption Kinetic b) of Hg(II) ions adsorption by K, K-SLS, K-SDBS, and K-M.(Mass of adsorbent = 0.5 g; Volume of solution = 100 ml; Stirring speed150 rpm.min; pH = 7; Temperature = 25°C).

IV.2.4 Adsorption isotherm models

In order to examine the adsorption technique and the interaction between mercury ions and kaolin, the Langmuir, Freundlich, and Sips isotherm models were used in their nonlinear forms as shown in Figure IV.14a, b, and c respectively.

Equations (Eq. IV.4) represent the nonlinear Langmuir equation [39]:

$$\mathbf{Q_{ads} = \frac{Q_m K_L C_e}{1+\Gamma K_L}} \text{.....(Eq. IV.4)}$$

Where:

Q_{ads} represents the quantity of mercury ions adsorbed at time ($mg.g^{-1}$), C_e is the equilibrium concentration of mercury in the solution ($mg.L^{-1}$), Q_m is the maximum monolayer adsorbed amount in $mg.g^{-1}$, K_L is the equilibrium constant of Langmuir ($L.mg^{-1}$).

The following Equation (Eq. IV.5) apply to the nonlinear Freundlich isotherm [40], $\mathbf{Q_{ads} = K_F C_e^{\frac{1}{n}}}$ **……..…….. (Eq. IV.5)**

Where:

K_F (L.mg^{-1})and n are the Freundlich equilibrium constant, which indicates the adsorption capacity of the adsorbent and the adsorption intensity, respectively

The Sips nonlinear equation represented by equations (Eq. IV.6) below [41].

$\mathbf{Q_{ads} = \frac{Q_s K_s C_e^n}{1+K_s C_e^n}}$ **……..……..…….. (Eq. IV.6)**

Where:

Q_s is the highest possible adsorption level (mg.g^{-1}), C_e is the equilibrium concentration of the adsorbate (mg.L^{-1}), K_S is equilibrium binding constant (L.mg^{-1}), n is constant related to the heterogeneity of adsorbent without unit.

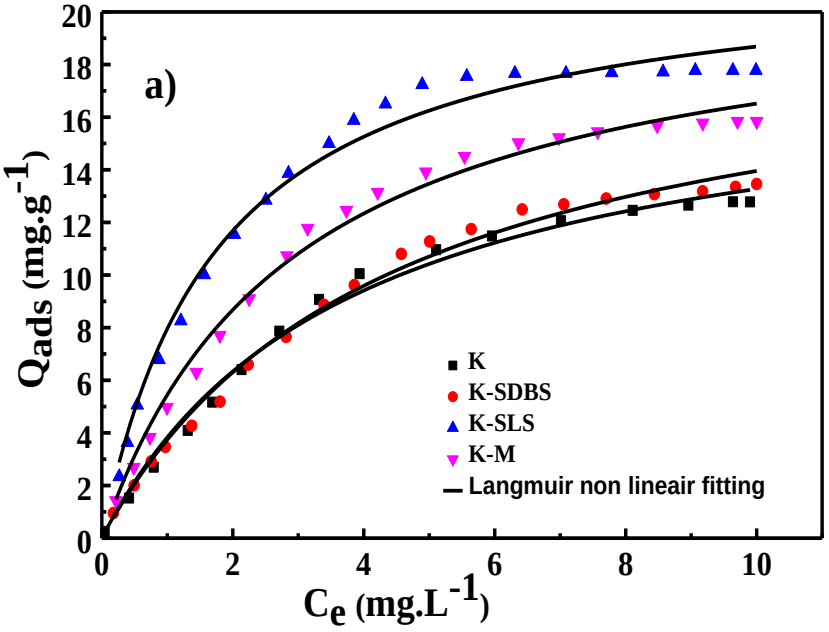

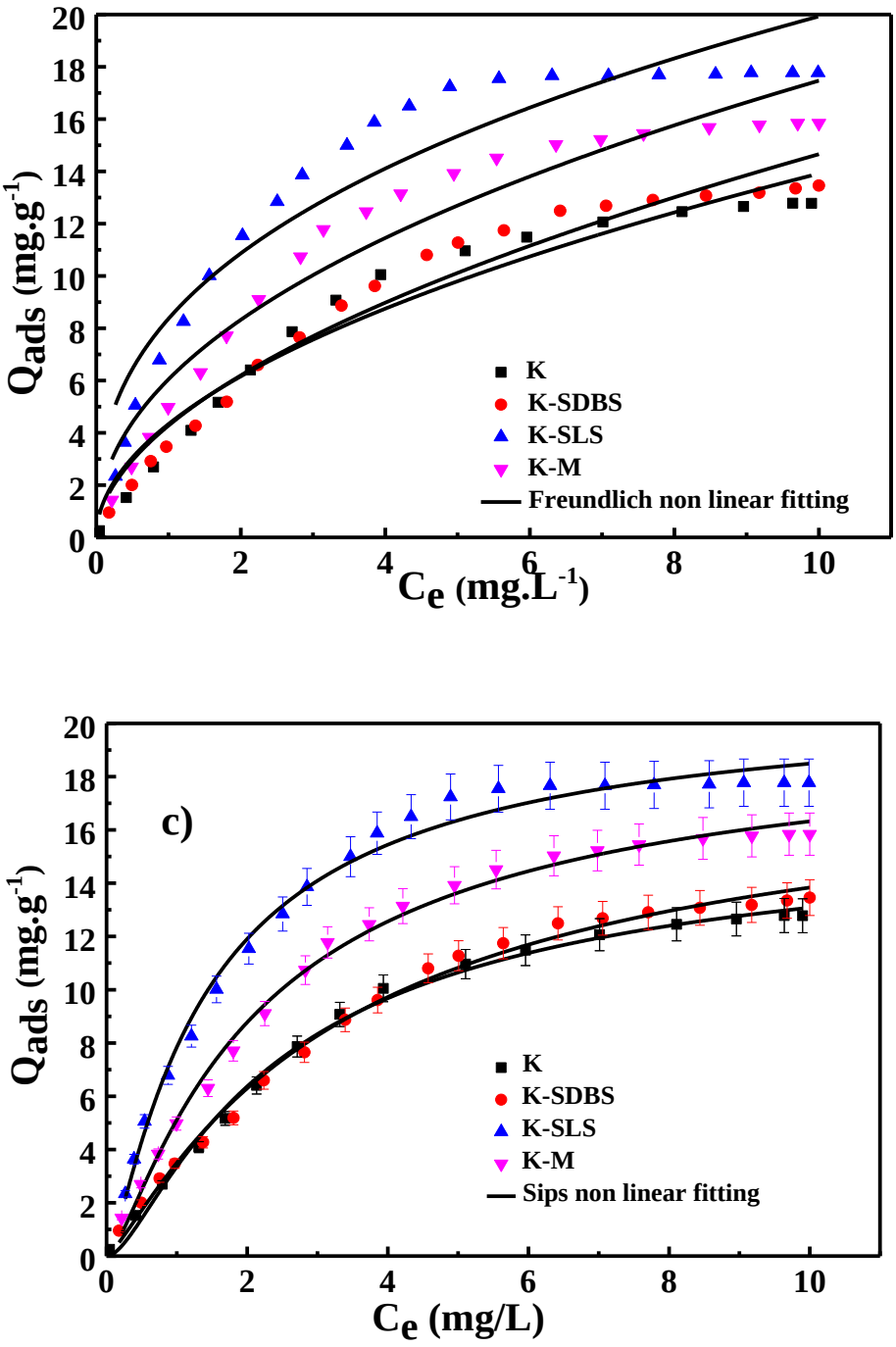

Figure IV.14: a) Langmuir isotherms, b) Freundlich isotherms, c) Sips isotherms of Hg(II) ions adsorption onto K, K-SLS, K-SDBS and K-M. .(Mass of adsorbent = 0.5 g; Volume of solution = 100 ml; Stirring speed150 rpm.min; pH = 7; Temperature = 25°C).

Table IV.5 presents the nonlinear adsorption isotherm parameters for the adsorption of mercury (II) on four distinct types of kaolin, as determined by the Langmuir, Freundlich, and Sips models. According to the correlation coefficient R^2 values shown in Table IV.5, we noticed that the Sips adsorption isotherms demonstrated superior fit compared to the Langmuir and Freundlich isotherms. The correlation coefficient R^2 for the Sips isotherms reached a value of 0.99 for all kaolin types. The R^2values for Langmuir are 0.99, 0.99, 0.98, and 0.99 for K, K-SDBS, K-SLS and K-M, respectively. In contrast, Freundlich's correlation coefficient R^2 values are 0.95, 0.96, 0.90, and 0.93 for K, K-SDBS, K-SLS, and K-M, respectively. The results confirmed that Sips isotherm can be used to predict the adsorption on heterogeneous surfaces [42]. This isotherm predicts the Langmuir model (monolayer adsorption) at high adsorbate concentrations, but at low adsorbate concentrations it is in accordance with the Freundlich model [43].

The highest possible adsorption level Q_m was found to be 16.4mg.g^{-1}, 18.7mg.g^{-1}, 21.1mg.g^{-1}, and 19.9mg.g^{-1}for the removal of mercury on K, K-SDBS, K-SLS, and K-M, respectively. This indicates that the adsorption of mercury is more effective on the Sips isotherm and the kaolin modified by the SLS surfactant was successful.

Table IV.5: The constants determined by the Langmuir, Freundlich, and Sips models.

	Langmuir constants			**Freundlich constants**			**Sips constants**			
	R^2	**K_L(L.mg^{-1})**	**Q_m(mg.g^{-1})**	**R^2**	**K_F(L.mg^{-1})**	**N**	**R^2**	**K_S(L.mg^{-1})**	**Q_S(mg.g^{-1})**	**n**
K	0.990	0.265 ±0.023	18.2± 0.662	0.954	4.33±0.344	1.97±0.164	0.995	0.816±0.271	16.4±0.458	1.98±0.466
K-SDBS	0.991	0.229 ±0.017	20.0± 0.655	0.962	4.27±0.278	1.86±0.120	0.992	0.386±0.114	18.7±0.782	1.31±0.213
K-SLS	0.986	0.567 ±0.041	21.9± 0.470	0.905	8.36±0.533	2.65±0.250	0.998	1.118±0.363	21.1±0.479	1.55±0.343
K-M	0.990	0.342 ±0.023	21.3± 0.543	0.939	6.04±0.405	2.17±0.171	0.993	0.739±0.199	19.9±0.491	1.59±0.282

IV.3 CONCLUSION

The present chapter provides a detailed investigation into the adsorption capabilities of both diphenylamine-modified kaolin (DPA-kaolin) and surfactant-modified kaolin for the removal of heavy metal ions. The results demonstrate that modifying kaolin with diphenylamine enhances its adsorption capacity due to increased surface area and the introduction of functional groups, while surfactant modifications significantly improve surface properties, porosity, and active adsorption site availability. The adsorption studies for lead and copper ions confirmed that DPA-kaolin follows a pseudo-second-order kinetic model, indicating chemisorption as the predominant mechanism, with thermodynamic analyses revealing an exothermic and spontaneous process. Similarly, surfactant-modified kaolin exhibited superior adsorption performance for mercury, with K-SLS achieving the highest adsorption capacity of 21.1 $mg.g^{-1}$. Isotherm modelling demonstrated that the Sips model best described mercury adsorption, reflecting a heterogeneous adsorption process, while kinetic studies supported a chemisorption-dominated mechanism. The influence of contact time emphasized the rapid initial phase followed by slower adsorption due to site saturation. Overall, these findings highlight the potential of both diphenylamine- and surfactant-functionalized kaolin as highly effective adsorbents for heavy metal removal.

IV.4 REFERENCES

[1] Musumba, G., Nakiguli, C., Lubanga, C., Mukasa, P., & Ntambi, E. (2020). Adsorption of Lead (II) and Copper (II) Ions from Mono Synthetic Aqueous Solutions Using Bio-Char from <i>Ficus natalensis</i> Fruits. Journal of Encapsulation and Adsorption Sciences, 10(04), 71–84. https://doi.org/10.4236/jeas.2020.104004.

[2] Hilal, R. H., & Nassif, R. A. (2023). Study on adsorption of some metals from waste solution by (unsaturated polyester-kaolin) composite. Kuwait Journal of Science, 50(3), 257–261. https://doi.org/10.1016/j.kjs.2023.01.010.

[3] Azam, M., Wabaidur, S., Khan, M., Al-Resayes, S., & Islam, M. (2022). Heavy Metal Ions Removal from Aqueous Solutions by Treated Ajwa Date Pits: Kinetic, Isotherm, and Thermodynamic Approach. Polymers, 14(5), 914. https://doi.org/10.3390/polym14050914.

[4] Janković, B. Ž., Janković, M. M., Marinović-Cincović, M. M., Todorović, D. J., & Šarap, N. B. (2018). Thermal analysis testing and natural radioactivity characterization of kaolin as building material. Journal of Thermal Analysis and Calorimetry, 133, 481–487. https://doi.org/10.1007/s10973-018-7159-1.

[5] Trikkaliotis, D. G., Christoforidis, A. K., Mitropoulos, A. C., & Kyzas, G. Z. (2020). Adsorption of copper ions onto chitosan/poly(vinyl alcohol) beads functionalized with poly(ethylene glycol). Carbohydrate Polymers, 234, 115890. https://doi.org/10.1016/j.carbpol.2020.115890.

[6] Manjuladevi, M., Anitha, R., & Manonmani, S. (2018). Kinetic study on adsorption of Cr(VI), Ni(II), Cd(II) and Pb(II) ions from aqueous solutions using activated carbon prepared from Cucumis melo peel. Applied Water Science, 8(1). https://doi.org/10.1007/s13201-018-0674-1.

[7] He, Y., Zhang, P., & Wang, L. (2023). Adsorption and Removal of Cr6+, Cu2+, Pb2+, and Zn2+ from Aqueous Solution by Magnetic Nano-Chitosan. Molecules, 28(6), 2607. https://doi.org/10.3390/molecules28062607.

[8] Kubilay, Ş., Gürkan, R., Savran, A., & Şahan, T. (2007). Removal of Cu(II), Zn(II) and Co(II) ions from aqueous solutions by adsorption onto natural bentonite. Adsorption, 13(1), 41–51. https://doi.org/10.1007/s10450-007-9003-y.

[9] Kamal, S., Kamal, A., Shahzad, T., Rehman, S., Azeem, M., & Bibi, I. (2017). Potential of kaolinite as adsorbent to remove anionic surfactant from simulated industrial wastewater. Desalination and Water Treatment, 88, 85–92. https://doi.org/10.5004/dwt.2017.21342.

[10] Emam, A. A., Ismail, L. F. M., Khalek, A., & Rehan, A. (2016). Adsorption study of some heavy metal ions on modified kaolinite clay. International Journal of Advanced Engineering Technology and Management Sciences (IJAETMAS), 3, 152–163.

[11] Maremeni, L. C., Modise, S. J., Mtunzi, F. M., Klink, M. J., & Pakade, V. E. (2018). Adsorptive removal of hexavalent chromium by Diphenylcarbazide-

GraftedMacadamiaNutshell Powder. Bioinorganic Chemistry and Applications, 2018, 1–14. https://doi.org/10.1155/2018/6171906.

[12] Punrattanasin, P., & Sariem, P. (2015). Adsorption of copper, zinc, and nickel using Loess as adsorbents. Polish Journal of Environmental Studies, 24, 1259–1266. https://doi.org/10.15244/pjoes/30264.

[13] Zerouali, M., Bouras, D., Daïra, R., Fellah, M., Boudjema, B., Barille, R., Sakher, E., Bellucci, S., & El-Hiti, G. A. (2024). Effect of Zn-doped CuO thin films on structural, morphological, optical, and electrical properties for photocatalysis application. Optical Materials, 152, 115495. https://doi.org/10.1016/j.optmat.2024.115495.

[14] Putra, W. P., Kamari, A., Yusoff, S. N. M., Ishak, C. F., Mohamed, A., Hashim, N., & Isa, I. M. (2014). Biosorption of Cu(II), Pb(II) and Zn(II) Ions from Aqueous Solutions Using Selected Waste Materials: Adsorption and Characterisation Studies. Journal of Encapsulation and Adsorption Sciences, 04(01), 25–35. https://doi.org/10.4236/jeas.2014.41004.

[15] Bouras, D., Fellah, M., Barille, R., Obrosov, A., Ikbal, A., Avramov, P. V., & El-Hiti, G. A. (2024). Multiple layers, porous surface, and their role in increasing the efficiency of photocatalytic coating on (DD3, DD3+ZrO2) ceramics and glass. Ceramics International, 50(21), 43854–43873. https://doi.org/10.1016/j.ceramint.2024.08.239.

[16] Bouras, D., Fellah, M., Barillé, R., Obrosov, A., & El-Hiti, G. A. (2024). Production of novel Zr–Mg nanoceramics based on kaolinite clay with strong antibacterial activity. Ceramics International, 50(16), 27949–27960. https://doi.org/10.1016/j.ceramint.2024.05.091.

[17] Bouras, D., Fellah, M., Habeeb, M. A., Aouar, L., Barille, R., & El-Hiti, G. A. (2024). Structural and antibacterial activity of developed nano-bioceramic DD3/ZrO2/ZnO/CuO powders. Journal of the Korean Ceramic Society, 61(5), 837–853. https://doi.org/10.1007/s43207-024-00398-6.

[18] Dahmani, M., Fellah, M., Hezil, N., Benoudia, M., Samad, M. A., Alburaikan, A., Khalifa, H. a. E., & Obrosov, A. (2023). Structural and mechanical evaluation of a new Ti-Nb-Mo alloy produced by high-energy ball milling with variable milling time for biomedical applications. The International Journal of Advanced Manufacturing Technology, 129(11–12), 4971–4991. https://doi.org/10.1007/s00170-023-12650-0.

[19] Liu, W., Zheng, J., Ou, X., Liu, X., Song, Y., Tian, C., Rong, W., Shi, Z., Dang, Z., & Lin, Z. (2018). Effective Extraction of Cr(VI) from Hazardous Gypsum Sludge via Controlling the Phase Transformation and Chromium Species. Environmental Science & Technology, 52(22), 13336–13342. https://doi.org/10.1021/acs.est.8b02213.

[20] Al-Essa, K. (2018). Heavy Metals Adsorption from Aqueous Solutions onto Unmodified and Modified Jordanian Kaolinite Clay: Batch and Column Techniques. American Journal of Applied Chemistry, 6(1), 25. https://doi.org/10.11648/j.ajac.20180601.14.

[21] El-Eswed, B., Alshaaer, M., Yousef, R. I., Hamadneh, I., & Khalili, F. (2012). Adsorption of Cu(II), Ni(II), Zn(II), Cd(II) and Pb(II) onto Kaolin/Zeolite Based- Geopolymers. Advances in Materials Physics and Chemistry, 02(04), 119–125. https://doi.org/10.4236/ampc.2012.24b032.

[22] Wahyuni, N. (2021). Adsorption capacity of CA2+ by hydrochloric acid activated kaolin. IOP Conference Series Earth and Environmental Science, 926(1), 012082. https://doi.org/10.1088/1755-1315/926/1/012082.

[23] Jaishankar, M., Tseten, T., Anbalagan, N., Mathew, B. B., & Beeregowda, K. N. (2014). Toxicity, mechanism and health effects of some heavy metals. Interdisciplinary Toxicology, 7(2), 60–72. https://doi.org/10.2478/intox-2014-0009.

[24] Pyrgaki, K., Messini, P., & Zotiadis, V. (2018). Adsorption of Pb and Cu from Aqueous Solutions by Raw and Heat-Treated Attapulgite Clay. Geosciences, 8(5), 157. https://doi.org/10.3390/geosciences8050157.

[25] Kypritidou, Z., & Argyraki, A. (2018). A multi-site mechanism model for studying Pb and Cu retention from aqueous solutions by Fe-Mg-rich clays. Clay Minerals, 53(2), 175–192. https://doi.org/10.1180/clm.2018.12.

[26] Dinh, V., Nguyen, P., Tran, M., Luu, A., Hung, N. Q., Luu, T., Kiet, H. T., Mai, X., Luong, T., Nguyen, T., Ho, H. T., Nguyen, D., Pham, D., Hoang, A., Le, V., & Nguyen, T. (2021). HTDMA-modified bentonite clay for effective removal of Pb(II) from aqueous solution. Chemosphere, 286, 131766. https://doi.org/10.1016/j.chemosphere.2021.131766.

[27] Slatni, I., Dhiffalah, A., Elberrichi, F. Z., Fardjaoui, N. E. H., Guendouzi, A., Duplay, J., Gasmi, B., & Maoui, A. (2022). Investigation of adsorption properties of modified DD kaolins to microporous material type 13X zeolite in treatment of textile industry effluent: experiments and theoretical approach. Euro-Mediterranean Journal for Environmental Integration, 7(3), 415–432. https://doi.org/10.1007/s41207-022-00324-4.

[28] Karkoosh, H., Reguyal, F., Vithanage, M., & Sarmah, A. K. (2024). Efficacy of anthocyanin, kaolinite and cabbage leaves-derived biochar for simultaneous removal of lead, copper and metoprolol from water. Environmental Pollution, 359, 124594. https://doi.org/10.1016/j.envpol.2024.124594.

[29] Kataria, N., Chauhan, A. K., Garg, V., & Kumar, P. (2022). Sequestration of heavy metals from contaminated water using magnetic carbon nanocomposites. Journal of Hazardous Materials Advances, 6, 100066. https://doi.org/10.1016/j.hazadv.2022.100066.

[30] Kayode, A. D., Sunday, A. S., Oluyemi, A. S., Abidemi, I. O., Folasade, A. A., Gbolahan, A. M., & Kayode, P. O. (2021). Ionic surfactant enhancement of clay properties for heavy metals adsorption: kinetics and isotherms. Indonesian Journal of Chemistry, 21(4), 825. https://doi.org/10.22146/ijc.59480.

[31] Harutyunyan, L. R., Tangamyan, L. S., & Harutyunyan, R. S. (2019). Sorption of Co^{2+}, Cu^{2+}, Zn^{2+}, Mn^{2+} metal ions from aqueous solutions on anionic surfactant-modified bentonite. Chemistry and Biology, 53, 81–85.

[32] Merrikhpour, H., Mobarakpour, S., & Azimi, S. B. (2022). Adsorption of Cd2+, Cu2+, and Ni2+ onto surfactant modified bentonite. Desalination and Water Treatment, 271, 157–165. https://doi.org/10.5004/dwt.2022.28768.

[33] Travis, C. C., & Etnier, E. L. (1981). A survey of sorption relationships for reactive solutes in soil. Journal of Environmental Quality, 10(1), 8–17. https://doi.org/10.2134/jeq1981.00472425001000010002x.

[34] Shiferaw, Y., Yassin, J. M., & Tedla, A. (2019). Removal of organic dye and toxic hexavalent chromium ions by natural clay adsorption. Desalination and Water Treatment, 165, 222–231. https://doi.org/10.5004/dwt.2019.24585.

[35] Kgabi, D. P., & Ambushe, A. A. (2024). Removal of Pb(II) ions from aqueous solutions using natural and HDTMA-modified bentonite and kaolin clays. Heliyon, 10(18), e38136. https://doi.org/10.1016/j.heliyon.2024.e38136.

[36] Castro-Castro, J. D., Macías-Quiroga, I. F., Giraldo-Gómez, G. I., & Sanabria-González, N. R. (2020). Adsorption of CR(VI) in aqueous solution using a Surfactant-Modified bentonite. The Scientific World JOURNAL, 2020, 1–9. https://doi.org/10.1155/2020/3628163.

[37] Liu, C., Wu, P., Zhu, Y., & Tran, L. (2015). Simultaneous adsorption of Cd2+ and BPA on amphoteric surfactant activated montmorillonite. Chemosphere, 144, 1026–1032. https://doi.org/10.1016/j.chemosphere.2015.09.063.

[38] Mudzielwana, R., Gitari, M. W., & Ndungu, P. (2019). Performance evaluation of surfactant modified kaolin clay in As(III) and As(V) adsorption from groundwater: adsorption kinetics, isotherms and thermodynamics. Heliyon, 5(11), e02756. https://doi.org/10.1016/j.heliyon.2019.e02756.

[39] Langmuir, I. (1918). The adsorption of gases on plane surfaces of glass, mica and platinum. Journal of the American Chemical Society, 40, 1361–1403.

[40] Freundlich, H. (1932). Of the adsorption of gases. Section II. Kinetics and energetics of gas adsorption. Introductory paper to section II. Transactions of the Faraday Society, 28, 195. https://doi.org/10.1039/tf9322800195.

[41] Sips, R. (1948). On the Structure of a Catalyst Surface. The Journal of Chemical Physics, 16(5), 490–495. https://doi.org/10.1063/1.1746922.

[42] Ayawei, N., Ebelegi, A. N., & Wankasi, D. (2017). Modelling and interpretation of adsorption isotherms. Journal of Chemistry, e3039817.

[43] Kosnan, M. A., Azam, M. A., Safie, N. E., Munawar, R. F., & Takasaki, A. (2022). Recent progress of electrode architecture for MXENE/MOS2 Supercapacitor: Preparation methods and characterizations. Micromachines, 13(11), 1837. https://doi.org/10.3390/mi13111837.

GENERAL CONCLUSION

GENERAL CONCLUSION

In our study, we synthesized and characterized kaolin-type mineral clay from Djebel Dabagh region, Guelma, northeastern Algeria, for the removal of heavy metals.

The first synthesis was performed with diphenylamine to efficiently remove lead (II) and copper (II) from aqueous solutions, while the second synthesis was modified with surfactants to efficiently remove mercury (II) from aqueous solutions.

Our main objective was to synthesize and characterize new kaolin-based adsorbents for the adsorption of heavy metals (Pb, Cu, Hg). Thus, we have successfully achieved the synthesis and characterization of four different types of adsorbents.

A range of characterization techniques used in this investigation (FTIR, XRD, SEM, EDX, and BET) have effectively demonstrated the alteration of kaolin by diphenylamine.

Following the addition of diphenylamine, the specific surface of natural kaolin rose from 66.69 to 71.35 $m^2.g^{-1}$. New vibration bands were detected in the DPA-kaolin's FTIR spectra at 1248 cm^{-1}, which matched the C-N of DPA. Furthermore, the stretching vibration of aromatic C-H was found to be the cause of the band at 3032 cm^{-1}. On the other hand, the phenyl ring C=C vibration was represented by the bands at 1528 cm^{-1}, 1597 cm^{-1}, and 1662 cm^{-1}, while the N-H bonds (amine group) of DPA were responsible for the band at 3360 cm^{-1}. These outcomes offer convincing proof of the kaolin alteration process's efficacy. The adsorption capacity of Pb on NAT-kaolin and DPA-kaolin was found to be 103 $\mu mol.g^{-1}$ and 151 $\mu mol.g^{-1}$, respectively. In comparison, the adsorption capacity of Cu on Nat-kaolin and DPA-kaolin was 91 $\mu mol.g^{-1}$ and 134 $\mu mol.g^{-1}$, respectively. Pb(II) and Cu(II) adsorption is improved by the chemical modification of DPA-kaolin in comparison to Nat-kaolin. Adsorption of Pb(II) and Cu(II) to kaolin is greatly enhanced by diphenylamine's affinity for these metals. The pH is the dominant factor in the adsorption process because the change in pH of a solution leads to the change in the surface of the adsorbents. In our study, we note that the adsorption of Pb(II) and Cu(II) is significantly better at pH 5, with an adsorption rate of about 83% and 52%, respectively. This is because as pH increases, the surface of DPA-kaolin becomes more negatively charged, which increases the electrostatic attraction between the positive charge of heavy metal ions and the

adsorbent. The latter is also favored by a decrease in temperature in the case of the adsorption of Pb(II) and Cu(II), and this for a DPA-kaolin type of clay. The adsorption process is therefore exothermic in nature. The experimental kinetics data were tested using pseudo-first-order, pseudo-second-order, and Weber-Morris Intraparticle models. The results showed that the pseudo-second-order model is the most suitable for determining the order of adsorption kinetics of Pb(II) and Cu(II) adsorption processes on DPA-kaolin, because its correlation coefficient R2 is close to unity 0.999 and 0.996, respectively. The Langmuir and Freundlich adsorption models are in good agreement with the experimental adsorption results, as evidenced by the high values of their correlation coefficients and the correlation between the calculated and experimentally adsorbed amounts of Pb (II) and Cu (II).

Research on the effective modification of kaolin using sodium lauryl sulfate (SLS), sodium dodecyl benzene sulfonate (SDBS), and a combination of the two surfactants is intriguing, especially in light of the potential improvements in characteristics.

An overview of the main findings from each characterization technique used to examine both natural and modified kaolin can be seen below.

The modified kaolin surface showed holes or pores and became rougher, according to the SEM data, indicating that the surfactants changed the particle arrangement.

According to the TG/DTA study, the thermal peaks of the modified kaolin may shift or change in intensity, indicating alterations with SDBS or SLS that alter thermal behavior.

Two new peaks appeared at roughly 2theta = 21.00° and 42.58° in the FTIR spectra of kaolin treated by SLS, along with variations in intensity. Furthermore, the SDBS surfactant-modified kaolin showed a new peak at 2theta = 8.85°.

These outcomes verify that the kaolin alteration was successful. For K-SLS, K-M, and K-SDBS, the specific surface area rose by roughly 38.3, 31.9, and 17.5%, respectively. Compared to kaolin modified with a combination of both surfactants (SLS+SDBS) and, lastly, kaolin treated with the anionic surfactant SDBS, the adsorption of mercury was higher on kaolin modified with the anionic surfactant SLS.